8-19-2016 12:00 AM

Characterizing the Role of the Neuropeptide Y-Y5R System in Breast Cancer

Jenna Kara
The University of Western Ontario

Supervisor
Dr. Paula Foster
The University of Western Ontario Joint Supervisor
Dr. Dwayne Jackson
The University of Western Ontario

Graduate Program in Medical Biophysics
A thesis submitted in partial fulfillment of the requirements for the degree in Master of Science

Abstract

Studies have demonstrated a correlation between stress and an increased risk of breast cancer. Neuropeptide Y (NPY) is up- regulated in chronic stress and induces proliferation and chemotaxis of 4T1 breast cancer cells via Y5 receptor (Y5R) activation. In the studies performed in this thesis, we characterize NPY-Y5R as a regulatory system that promotes breast cancer metastasis. We compared three cancer cell sublines derived from the same murine mammary fat pad tumour, that greatly differ in metastatic potential (67NR, 168FARN, and 4T1) in addition to a 4T1-Y5R knockdown established in our labs. In this thesis we demonstrate significance of up-regulation and cytoplasmic localization of Y5R to support an aggressively metastasizing breast cancer cell line. Using cellular MRI we characterized the knockdown of Y5R to alter breast carcinogenesis and metastasis. In this respect, NPY and its Y5 receptor could be therapeutic targets to combat breast cancer metastasis.

Keywords: Neuropeptide Y; Y5 receptor; stress; breast cancer; metastasis; 4T1-derived cell lines; cellular MRI; mouse model

Co-Authorship Statement

The work contained herein was carried out by the author, under the supervision of Dr. Paula Foster and Dr. Dwayne Jackson and the advice of Dr. Ann Chambers and Dr. Savita Dhanvantari. This included cell culture, immunocytochemistry, Western Blot analysis, MTS assay, operation of the 3T MRI system, mouse anesthesia, perfusions, tissue preparation, data analysis and manuscript preparation.

Julia Hrynkiewicz assisted with Western Blots and MTS assay. Dr. Phil Medeiros conducted the Y5R- targeted shRNA transfection of the 4T1 cell line. Ashley Makela conducted the orthotopic cell injections. Dr. Amanda Hamilton conducted Hematoxylin & Eosin tissue staining, Perl's Prussian Blue and Nuclear Fast Red tissue staining, and Y5R Immunohistochemistry on tumours and lungs. Dr. Paula Foster detected and assessed lung and lymph node metastases in MR images.

Acknowledgments

I would like to thank first and foremost my supervisor, Dr. Paula Foster. You have been an inspiration for me as a leader in scientific innovation. I am grateful for your time, dedication, and support you continuously provided in every facet of my degree.

Thank you to my co-supervisor Dr. Dwayne Jackson, for encouraging me to act diplomatically and analyze critically. I would also like to thank my advisory committee, Dr. Savita Dhanvantari and Dr. Ann Chambers for cultivating curiosity and independent thinking while providing invaluable direction and insight.

I want to extend my deepest gratitude to my dad and Meeta; you have supported me throughout this entire process. You have been by side to take on any obstacles and challenges I faced, you have been behind me to support my every decision, and been my safety nets in times I faltered. Thank you to my siblings, Jamal, Jasmine, and Jaden, for being my best friends and confidants.

I would like to thank the entire Foster lab that graciously took me into their lab. To Katie Parkins, Ashley Makela, Jeff Gaudet, Donna Murrell, Amanda Hamilton, and Matt Fox, thank you for the laughs, scientific banter, and being an instrumental support system. To all those that took the time to help me with the hoses, you are the real MVPs.

Table of Contents

List of Figures

List of Acronyms and Abbreviations

6-OHDA	6-Hydroxydopamine
APP	Aminopeptidase P
ATP	Adenosine Triphosphate
BBB	Blood Brain Barrier
BDNF	Brain-derive Neurotrophic Factor
bSSFP	Balanced-Steady State Free Precession
cAMP	cyclic Adenosine Monophosphate
DMEM	Dulbecco's Modified Eagle's Medium
DPPIV	Dipeptidyl Peptidase IV
EDTA	Ethylenediaminetetraacetic acid
EGFR	Epidermal Growth Factor Receptor
ER	Estrogen Receptor
ERK	Extracellular Signal-Regulated Kinases
FACS	Fluorescent-Activated Cell Sorting
Gd	Gadolinium

Gd-DTPA	Gadopentetic acid
GDP	Guanosine Diphosphate
GFP	Green Fluorescent Protein
GPCR	G- Protein Coupled Receptor
GTP	Guanosine Triphosphate
H&E	Hematoxylin and Eosin
HER-2	Human Epidermal Growth Factor Receptor 2
ICC	Immunocytochemistry
IHC	Immunohistochemistry
IL-1β	Interleukin-1β
IL-4	Interleukin 4
KD	Knockdown
Mn	Manganese
MPIO	Micron-size Superparamagnetic Iron Oxide nanoparticles
MRI	Magnetic Resonance Imaging
MTA-1	Metastasis Associated 1

NE	Norepinephrine
NFR	Nuclear Fast Red
NK	Natural Killer Cell
NPY	Neuropeptide Y
PBS	Phosphate Buffered Saline
PI3	Phosphoinositide 3
PPB	Perls' Prussian Blue
PR	Progesterone Receptor
RF	Radiofrequency
RIPA	Radioimmunoprecipitation Assay Buffer
RISC	RNA- Induced Silencing Complex
SDS-PAGE	Sodium Dodecyl Sulfate Polyacrylamide Gel Electrophoresis
siRNA	Small Interfering RNA
shRNA	Small hairpin RNA
SPIO	Standard magnetic iron oxide particles
T1wSE	T1-weighted spin echo

TAM	Tumour Associated Macrophages
TBST	Tris Buffered Saline- Tween
Th2	T-Helper 2
TNF-α	Tumour Necrosis Factor α
VEGF	Vascular Endothelial Growth Factor
USPIO	Ultra small iron oxide nanoparticles
Y1R	Neuropeptide Y1 Receptor
Y2R	Neuropeptide Y2 Receptor
Y4R	Neuropeptide Y4 Receptor
Y5R	Neuropeptide Y5 Receptor
Y6R	Neuropeptide Y6 Receptor

List of Appendices

Chapter 1- Background

1.1 Breast cancer and metastasis

Breast cancer is the second most common form of cancer death in females.[1] The 98.8% 5-year survival rate of localized breast cancer drops to 26.3% when the breast cancer is metastastic at diagnosis.[2] Breast cancer commonly metastasizes to the lung, liver, bone, and brain.[3]

Cancer metastasis is the dissemination of cells from the primary tumour via the lymphatics or hematogenously and proliferation at a distant site. Metastasis is an inefficient process supported by a high number of circulating cancer cells that do not result in the formation of a tumour.[4] This inefficiency is due to the conditions in the metastatic cascade that the cell must withstand prior to arresting in an alternate site. Cells must successfully intravasate from the primary site into the vasculature, withstand shear forces in the circulation, extravasate into an alternate site and successfully form micrometastases in this new microenvironment.[5] The primary characteristics that determine successful metastasis of a cancer cell fate require further investigation.

1.2 Stress and breast cancer

In a study of 1,601 breast cancer patients, 180 (11.2%) had triple negative breast cancer. Patients with triple negative breast cancer had an increased likelihood of distant recurrence and increased risk of death within 5 years of diagnosis.[6] In triple negative breast cancers, negative for the estrogen receptor (ER), progesterone receptor (PR) and human epidermal growth factor receptor 2 (HER-2), treatment with classic hormone therapy and HER-2 directed therapy is futile. The sole current therapy for triple negative breast cancer is cytotoxic chemotherapy. Therefore, a novel target for therapy to treat triple-negative breast cancer is required.

Studies have demonstrated a correlation between elevated stress levels and poor prognosis and survival in patients with breast cancer.[7–11] Independent of body mass index, weight change, alcohol use, smoking, and physical activity, there is a two-fold increase in breast cancer recurrence after a single stressful life event, such as a disruption of marriage due to divorce, separation, or death of a spouse, that do not seem to be mediated or altered by perceptions of one's daily stress, adverse personality, or pessimistic attitude.[12] In a retrospective study of 94 women with breast cancer recurrence or metastasis, planned comparisons revealed a significantly longer disease-free interval amongst women who had reported no traumatic or stressful life events compared to those who had experienced one or more, such as abandonment or close member of kin dying.[13]

1.3 Stress-induced release of Neuropeptide Y

Neuropeptide Y (NPY) is most widely expressed in the central and peripheral nervous systems and plays a major role in cognitive function, feeding patterns, and cardiovascular regulation.[14] NPY elicits its ubiquitous effects by binding to G- Protein Coupled Receptors, Y1R, Y2R, Y4R, Y5R, and Y6R, which have been cloned in mammals.[15] NPY is a sympathetic neurotransmitter that is released in greater quantities during chronic stress and in response to a life-threatening stressor from sympathetic nerves, adrenal medulla and platelets.[16,17] Cold exposure significantly stimulates the release of NPY in both humans and rodents.[18,19] Additionally, exposure of to an aggressor mouse stimulates the release of NPY in rodents.[17] In clinical trials, Y5R antagonist, MK-0577, proved insufficient as a monotherapy to treat obesity but displayed favourable clinical safety.[20]

The pleiotropic influence of NPY varies between males and females. Basal sympathetic nerve activity is lower in females compared to males.[21] Jackson et al. demonstrated that estrogen has

the capacity to blunt Y1R activation in skeletal muscle.[22] Local noradrenergic mechanisms are NPY-Y1R mediated and can be modulated by reproductive hormone activity. When estrogen and progesterone are elevated during the luteal phase, persistent vasoconstriction, is observed. Furthermore, when estrogen and progesterone are low during the follicular phase vasoconstriction is abolished. This mechanism is NPY mediated, validated by consistent vasomotor activity with α and β receptor blockade[23] Additionally, Glenn et al. demonstrated that peptidases, that enhance Y2R and Y5R binding, may be more active in females compared to males.[24]

NPY vasoactive effects are not limited to periods of chronic and intense stress. NPY contributes to maintaining baseline vasomotor tone and sympathetically induced vasoconstriction, supported by high circulating levels of NPY in patients with hypertension.[25] Additionally, the ratio of released NPY and norepinephrine (NE) from sympathetic nerves is consistent, independent of the degree of sympathetic stimulation, both contributing to basal vasomotor tone.[26]

1.4 Neuropeptide Y Receptors Trafficking and Localization

Neuropeptide Y1R-Y6R are G_i-protein coupled receptors with seven transmembrane loops with the capacity to induce a multitude of downstream cascading effects upon NPY binding. Post-activation, NPY receptors adopt a conformation causing the alpha subunit to convert guanosine diphosphoate (GDP) to guanosine triphosphate (GTP). As a result Neuropeptide Y receptors regulate transcription primarily via phosphoinositide 3 (PI3) kinase activity.[27] Downstream effector extracellular signal-regulated kinases (ERK) activity and mitogen-activated protein kinases (MAPK) are induced and cyclic adenosine monophosphate (cAMP)-dependent pathways are inhibited, dually contributing to transcriptional regulation. Independent of PI3 kinase activity, insulin growth factor receptor transactivation by NPY receptors is required to activate ERK.[27]

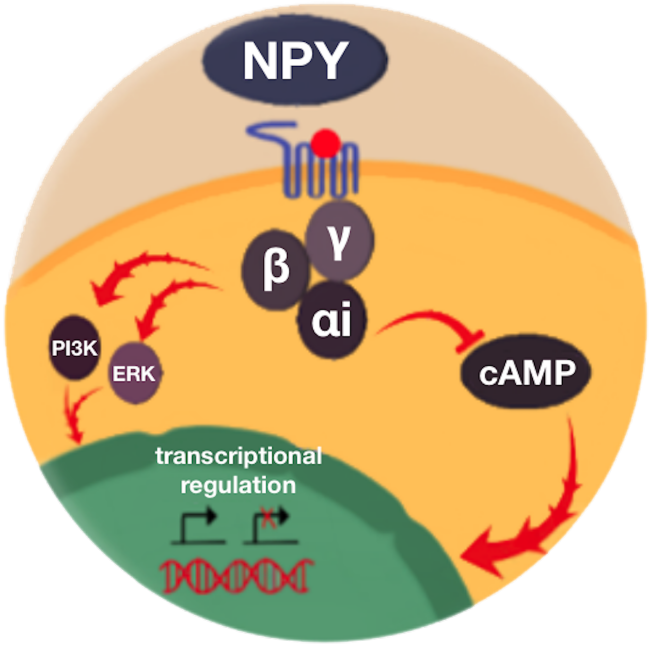

Figure 1.4.1. NPY-Y receptor Molecular Mechanism. Neuropeptide Y can activate Y1R- Y6R via binding to the seven transmembrane G_i-protein coupled receptors. Transcriptional regulation primarily occurs via PI3K and ERK activation and cAMP inhibition.

The affinity of NPY to receptors is regulated by the proteolytic cleavage of NPY by dipeptidyl peptidase IV (DPPIV) and aminopeptidase P (APP), the resulting cleaved form of NPY binds preferentially to Y2R and Y5R compared to Y1R.[28] Previous studies have shown that activated NPY Y1 and Y2 receptors internalize via clathrin-coated pits within the cytoplasm and close to the nucleus in human embryonic kidney cells[29]. These receptors return to the plasma membrane by cytosolic β-arrestins directly or transiently enter the rough endoplasmic reticulum.[30]. In contrast to Y1R and Y2R, Y5R internalizes less, slower, and requires greater agonist stimulation[29]. Of particular interest, human Y1R and Y5R are transcribed in opposite directions from a common promoter region on chromosome 4q31-q32.[31]

Y5R is expressed in a tissue-specific manner, primarily in the colon, ovaries, spleen, and testes. It is expressed as two isoforms, short and long, with the short form dominating in expression quantitatively. Therefore, it is suggested that alternative splicing of the 5'UTR could regulate the level of transcription of the receptor in a tissue specific –manner.[32] Y5R has a very long third intracellular loop compared to Y1R, Y2R, and Y4R.[29] Y5R has two binding sites with the potential to bind high or low affinity to its ligands, NPY, NPY3-36, PYY, PYY3-36, and PP. Sheriff et al. postulated that the activation of Y5R in normal physiological conditions occurs by binding the high affinity site and the activation of Y5R in pathophysiological conditions occurs by binding the low affinity site.[33]

1.5 Neuropeptide Y and the Immune System

NPY and the immune system modulate each other's activity bi-directionally. NPY secretion has been found to be increased in transgenic mice that over-express tumour necrosis factor (TNFα) and inhibited in human astrocytes by interleukin (IL)-1β.[29,30] NPY plays a prominent role in immune modulator release, Natural Killer Cell (NK) activity, T helper cell differentiation, B cell homeostasis, and leukocyte trafficking. NPY can elicit its effects by binding and activating Y1R, Y4R, or Y5R expressed by neutrophils and Y1R expressed by both T cells and granulocytes.[31,32] NPY suppresses NK cell activity in a dose-dependent manner *in vitro,* as well as in the rat spleen *in vivo.*[33,34] Additionally, NPY supports a shift to T-Helper 2 (Th2) cells through stimulation of IL-4 secretion, stimulating the conversion of macrophages to anti-inflammatory M2 cells, which stimulate tumour growth.[35,36] Furthermore, NPY induces increased chemotaxis of monocytes and preferential mobilization of leukocytes.[37,38] Therefore, previous studies have suggested indirect methods of how stress, molecularly transduced via NPY, can affect cancer progression via immunosuppression.

1.6 Neuropeptide Y5R in cancer

Neuropeptide Y5R is expressed in cancer cell lines including breast and brain xenograft models.[39-42] In neuroblastoma, Y5R is up-regulated via brain-derived neurotrophic factor (BDNF). Of particular interest, BDNF was found to induce internalization of Y5R, contributing to chemo-resistant properties. Furthermore, chemotherapeutic treatment-induced cellular stress and increased NPY release resulting in increased Y5R expression. Administration of a Y5R antagonist sensitized the cells to chemotherapy, permitting tumour cell death.[39] In Ewing sarcoma, hypoxia shifts the inhibitory actions of NPY, mediated via Y1R and Y5R, to proliferative, migratory, and angiogenic via Y2R and Y5R activation by increasing DPPIV activity.[40]

1.6.1 NPY-Y5R system and breast cancer

The lateral and anterior cutaneous branches of the second and sixth intercostal nerves sympathetically innervate the mammary gland, smooth muscle of the areola, skin, and breast blood vessels.[41] In this respect, the breast microenvironment is susceptible to the alterations in NPY flux induced by chronic stress. This susceptibility has the potential to have a negative impact on women with family histories of breast cancer, who have an increased basal release of sympathetic neurotransmitters in response to daily stressors.[42] In breast tumour tissue, the NPY precursor, pre-pro-NPY, is up-regulated accompanied with a down-regulation of NPY (1-36), however the DPPIV processed form of NPY (3-36) was not assayed.[43] Human breast carcinoma cell lines MCF-7, T47D, MDA MB-231, MDA MB-468, HS578T, BT-549 express significantly more Y5R than Y1R and Y2R.[33] Immunohistochemical observation has revealed the predominant expression of Y5R with respect to Y1R and Y2R in 4T1 cells grown in murine mammary fatpad.[44]

1.6.1.1 Proliferation

The rate of cancer cell proliferation is indicative of breast cancer aggression and has an increased potential to develop into clinically relevant tumours. NPY has been found to be a potent mitogen in both human breast and murine mammary cancer cells.[33,44] The Jackson lab previously evaluated the independent contributions of Y1R, Y2R, and Y5R on NPY-induced proliferation. Solely, Y5R-antagonism has the capacity to inhibit the NPY-induced proliferation of 4T1 cancer cells.[44] Sheriff et al. demonstrated the significant proliferative effects of NPY on BT-549 cells, which is inhibited by Y5R antagonism.[33]

1.6.1.2 Migration

The capacity of malignant cancer cells to migrate to neighbouring tissue and vasculature is a pre-requisite for metastasis. Sheriff et al. demonstrated that the triple negative human MDA-MB-231 cells have an increased propensity to migrate due to Y5R-mediated NPY stimulation.[33] Medeiros et al. demonstrated that NPY-induced chemotaxis of 4T1 cells is primarily via Y2R and Y5R stimulation in a concentration-dependent manner. This is supported by Y1R antagonism eliciting no effect on NPY-induced chemotaxis of 4T1 cells, in contrast to migratory inhibition via Y5R antagonism.[44]

1.6.1.3 Angiogenesis

Neuropeptide Y stimulates the expression of vascular endothelial growth factor (VEGF), one of the primary regulatory pro-angiogenic factors in the tumour microenvironment. At physiological concentrations of NPY-conditioned media from 4T1 and MDA-MB-231 human breast cancer cells, there was a significant increase in VEGF expression with the capacity to induce angiogenesis *in vitro* evaluated by an endothelial tube formation assay. Angiogenesis was specifically induced by Y5R agonist treatment, in contrast to Y1R and Y2R activation. This

experiment elucidated the paracrine mechanism of NPY to activate Y5R inducing the release of pro-angiogenic VEGF.[45]

1.6.1.4 Tumourigenicity and Metastasis

Neuropeptide Y is robustly expressed in MFP tumours supplied by sympathetic innervation. The Jackson lab has chemically-induced sympathectomy, via 6-hydroxydopamine (6-OHDA) treatment, and found a reduction in mammary fatpad tumour burden by up to 50%.[44] Furthermore, oral administration of 90mg/kg of a specific Y5R antagonist TAC557, significantly attenuated tumour growth and reduced metastatic lung lesion burden.[46]

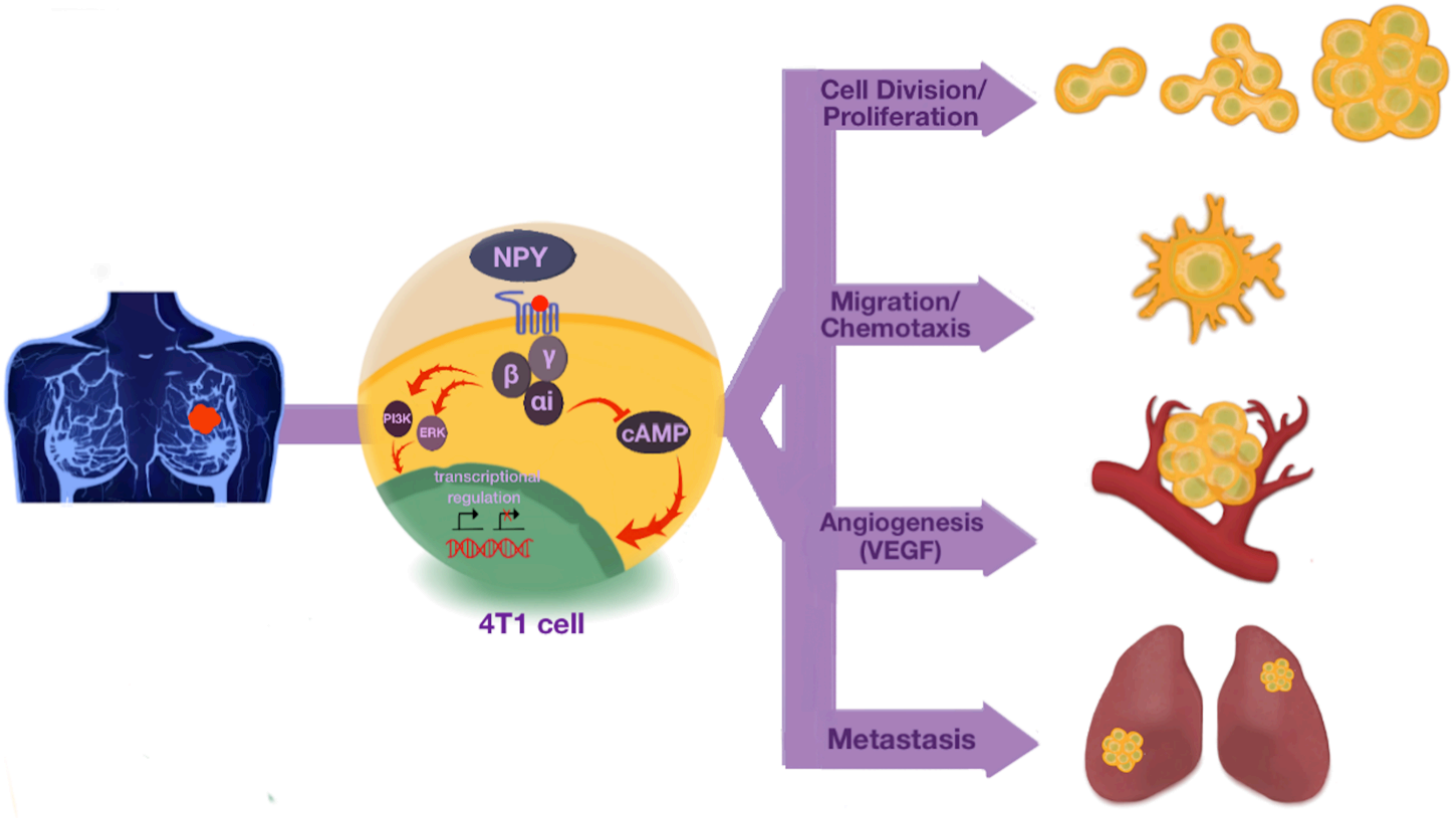

Figure 1.6.1 Role of NPY-Y5R in 4T1 murine mammary fat pad cancer cells. The Jackson lab has previously demonstrated how NPY can stimulate 4T1 cells to proliferate, migrate, metastasize, and induce angiogenesis. Using Y5R specific antagonism, it has been shown that these hallmarks of cancer are Y5R mediated. The contribution of Y5R to determine metastatic potential in various cell lines and its role in the metastatic cascade has yet to be elucidated.

1.7 4T1-derived Cell Lines

In addition to the study of cancer *in vitro,* cancer cell behaviour should be examined within a well-recapitulated tumour microenvironment. The 4T1-derived murine mammary carcinoma cell lines are syngeneic immune competent models and thereby permit this evaluation as opposed to human cell xenograft models in immune-compromised mice. Identification of specific biomarkers indicative of metastatic ability would be ideal to determine the fate and risk potential of cancer cells. The 67NR, 168 FARN, and 4T1 cell lines originate from the same murine mammary fat pad tumour but differ in metastatic potential.[47] The 67NR line was established by re-plating a monolayer of cells followed by subsequent passaging on gelatin substratum, resulting in a retained elongated spindle morphology over 40 passages.[48] The 168FARN line was established by re-plating the primary cells onto a non-gelatinized dish and were selected for their fibroblastic morphology that was retained for 20 passages. [48] The 4T1 cell line was formed by repeated and sequential selection of lung metastases from intravenous injection.[49]

67NR cells solely proliferate in the mammary fat pad and do not intravasate to the circulation to metastasize. 168FARN cells have the capacity to disseminate to the lymph node and do not metastasize to other parts of the body, in this sense intravasation is fulfilled without resulting in extravasation. 4T1 cells are able to aggressively metastasize from the primary mammary fatpad to the lungs, liver, bone and brain primarily hematogenously.[47]

The 4T1 cell line has been evaluated to effectively model the metastatic progression that is clinically observed, with a more accurate recapitulation of human metastasis compared to xenograft models.[50] Human stage IV breast cancer is classified by the presence of metastases in distant organs.[51] The features of human stage IV breast cancer can include: (1) the presence of edema and ulcerations of the skin in and around the primary tumor burden (2) the extension of

the primary tumor to the chest cavity lining, (3) the presence of metastatic cells in the draining lymph nodes.[51] All these features are observed when 4T1 primary tumours exceed 3mm in diameter.[50]

Despite originating from the same tumour, the cell lines vary morphologically in culture. 67NR cells form a network-like lattice, in contrast to 168FARN and 4T1 cells that possess a fibroblastic appearance in culture.[47] The cells innately differ in proliferation *in vitro*; 4T1 cells have a doubling time of 13.6±1.5h, 168FARN cells have a doubling time of 21±3.9h, and 67NR cells have a doubling time of 22.4±1.8h.[48,49] The growth of the latter two under the influence of NPY-stimulation is yet to be elucidated.

The inherent phenotypic properties of 67NR and 168FARN cells differ *in vitro*. 67NR cells possess comparable adherent capability to 168FARN cells, with diminished migratory potential, but enhanced invasive properties. Despite the enhanced invasive ability of 67NR cells *in vitro*, they do not metastasize *in vivo*.[53]

1.8 shRNA knockdown

shRNA knockdown is achieved through successful vector transfection, transcription of shRNA, and subsequent sequestration and degradation of the target mRNA.[54] Vector transfection permits exploitation of the cellular transcription machinery to transcribe the shRNA. Knockdown can also be achieved via exogenously introduced and processed siRNA. shRNA is more efficient as it integrates into the endogenous miRNA pathway and has enhanced loading onto the RNA-induced silencing complex (RISC).[55] shRNA results in a knockdown of the targeted mRNA expression as opposed to a knockout, which alters the genomic sequence.[56] Knockout of genomic

DNA has the potential to cause detrimental cellular defects due to off-target sequence deletions.[57]

Down-regulation of key proteins and receptors can elucidate their contribution to carcinogenesis and metastasis. shRNA has been employed to degrade HER2/*neu* protein levels, resulting in suppression of migration and invasion of breast cancer cells *in vitro* without alteration of cell viability.[58] shRNA has also been used to reduce the expression of epidermal growth factor receptor (EGFR) in human breast adenocarcinoma MDA-MB-231 cells by 60% and inhibit mammary fat pad tumour growth and VEGF secretion *in vivo*.[59] Furthermore, shRNA can be used to reveal cellular mechanisms in response to therapy. shRNA against metastasis associated-1 (MTA-1) recovered the expression of estrogen receptor (ER) alpha, permitting sensitization of MDA-MB-231 cells to estrogen therapy.[60]

In this thesis, we investigate the role of Y5R in aggressively metastasizing 4T1 cells by knocking down Y5R expression facilitated by shRNA. Using this knockdown, we evaluate the contribution of Y5R to breast cancer cell proliferation and metastasis.

1.9 MRI for evaluating tumour development and metastasis

Magnetic Resonance Imaging (MRI) relies on the properties of hydrogen atoms (protons) to generate an image. A strong magnetic field causes proton alignment within a subject. A radiofrequency (RF) transmitter is subsequently turned on then off, causing the protons to be energized then relaxed, respectively. Energy is emitted from protons when they relax to their state of equilibrium. The emitted energy produces a signal that is detected and translated by advanced computer processing. Image contrast exploits the variable relaxation rates of protons in biological tissue. T1-, T2-and T2*-*weighted* images are common image contrasts.

MRI has been widely used to study preclinical mouse models of cancer.[61–66] Cancer tissue has different relaxation rates in contrast with normal tissue, permitting MRI to play a significant role in the detection, staging and characterization of cancer.[67] Tumors may appear as either hypo-or hyper-intense regions relative to normal tissue, depending on the composition and pulse sequence used. MRI provides excellent three dimensional anatomic detail and sensitivity to permit tumour size quantification and location, in addition to edema, hemorrhage, and necrosis.[65]

In vivo MRI permits non-invasive observation of tumors and metastases longitudinally and in three dimensions and all spatial orientations. 3D MRI permits *in vivo* tumour size quantification, in comparison to histological tissue sections, which must account for shrinkage and deformation due to the chemical processing, or caliper measurements that assume symmetrical tumour volume. MRI permits comprehensive analysis of tumour growth rate, tumour development and metastasis, in contrast to traditional histology.

Contrast agents are employed to enhance regions of interest by shortening both the T1 and T2 times of surrounding tissues, in general affecting one relaxation more than the other. Paramagnetic contrast agents induce T1 shortening and include gadolinium-(Gd) based and manganese (Mn) based agents that are detected as bright signals on T1-weighted images. Superparamagnetic contrast agents all consist of iron-oxide cores and induce T2-shortening resulting in signal loss or hypointensity.

MRI post-Gd is often used to assess the integrity of the blood-brain-barrier (BBB) and in cancer imaging the blood-tumour-barrier. Gd is a small-sized contrast agent that is administered intravenously that provides enhancement of highly perfused tissue and vessel permeability. The Foster lab has investigated how the BBB permeability is dynamic in accordance with the

progression of breast cancer metastasis. Gd-enhanced contrast MRI is widely recognized as the most accurate diagnostic tool in the detection of brain metastases, however the Foster lab found many metastases detected did not exhibit Gadopentetic acid (Gd-DTPA) enhancement and were only detectable using bSSFP.[64,65] The Foster lab was the first to use 3T MRI and employ bSSFP to monitor the development of melanoma brain metastases longitudinally. They found bSSFP imaging permits detection of brain metastases at early time points that can be undetected on T1-weighted spin echo (T1wSE) images.[64]

Post-Gd MRI has also been used to enhance contrast in mouse models of breast cancer. Gd MRI can be used to identify aggressive tumours, due to high angiogenic activity required to maintain blood supply to highly proliferative tumour cells. Gd enhancement also permits differentiation between ER positive luminal breast tumours and triple negative basal breast tumours.[69] Gd MRI has provided insight in the alterations of tumour vasculature with estradiol deprivation in luminal tumours in a murine orthotopic xenograft model, while basal tumours remain unaffected by estradiol deprivation.[70] Angiogenesis can be indicative of a developed tumour, however the fluid-filled core of an aggressively metastasizing large tumour can inhibit Gd transport.[71]

1.10 Iron oxide labeling of cells for MRI

Cellular MRI can be achieved by pre-labeling cells with iron oxide nanoparticles prior to their administration. Iron oxide contrast agents create negative contrast in T2-or T2*-weighted proton MR images. The presence of intracellular iron causes a distortion in the local magnetic field resulting in abnormal signal hypointensity in iron-sensitive images. Therefore, iron-labeled cells appear as regions of signal loss, or black holes in the MR images. The reduced transverse (T2) and effective transverse (T2*) relaxation times of nearby nuclei extends to signal loss that occupies more space than the contrast agent itself resulting in a "blooming artifact."

Iron oxide nanoparticles are classified on the basis of size; ultra small superparamagnetic iron oxide nanoparticles (USPIO), standard magnetic superparamagnetic iron oxide particles (SPIO), or micron-size superparamagnetic iron oxide nanoparticles (MPIO). USPIO particles are 10-20nm in diameter, SPIO particles are 50-100nm in diameter, and MPIO particles are approximately 1-5μm in diameter.[72]

A variety of cell types can be easily loaded with iron oxide nanoparticles by simple co-incubation. Nanoparticle uptake is mediated by scavenger receptors, receptor-independent macropinocytosis, and clathrin–mediated uptake leading to iron oxide storage in endosomes.[73] Cancer cells readily uptake MPIOs, for example B16F10 melanoma cells have an uptake efficiency of 100% with an average iron content of 35pg of Fe/cell.[65] Studies show that there is minimal impact on cell function or phenotype at a wide range of iron loading levels.[74,75] Specifically, MPIO or SPIO cancer cell labeling has no discernable effect on viability, *in vitro* proliferation, cell apoptosis, necrosis, or *in vivo* metastasis compared to unlabeled cells.[62,65,76] Heyn *et al.* have demonstrated that even single iron-labeled cells can be detected *in vivo*. Single cell detection was permitted due to the aforementioned blooming artifact whereby cancer cells of approximately 20μm in diameter elicited a signal void of 300μm diameter in the MR image.[62]

1.11 Cancer Cell Imaging with MRI

Very few groups have used cellular MRI to study cancer cells because the iron label is diluted over time in proliferative cells, leading to label loss and therefore loss of cell detection. The Foster lab reported that intracellular iron disappeared after 5 days, when visualized with photomicrographs, corresponding to the sixth generation of daughter cells.[65] Similarly, using flow cytometry and Perls' Prussian Blue (PPB) staining, Economopoulos et al. found that less

than 50% of cells retained detectable quantities of iron four days post-labeling and only 1-2.5% remained labeled by day 10.[61]

However, the dilution of iron by cancer cells can be exploited to provide insight in regards to their proliferative status. The Foster lab has demonstrated that cancer cells that are non-proliferative, or slowly-cycling, will retain the iron label and the fate of these cells can be tracked with MRI.[61] The Foster lab was the first to identify non-proliferative cancer cells in the brain using iron oxide labeling techniques. Using this effective cell tracking technique, human breast cancer MDA-MB-231 cells were characterized as proliferative (1.5%), transiently proliferative (94%), and non-proliferative (4.5%) of the original tumour imaged at day 0.[62] Non-proliferative cells are considered dormant in a state of cell cycle arrest with the potential to form metastases and are likely the culprit of recurrence.

Magnitzsky et al. exploited iron label retention in slowly proliferative melanoma cells subcutaneously implanted and found a positive correlation with a biomarker, JARID1B. When the tumours reached $1cm^3$ after 5-6 weeks, MR imaging demonstrated that iron-retaining cells were localized close to the tumour vasculature elucidating the localization of slowly proliferative cells.[63]

Townson et al. used cellular MRI to monitor iron-labeled metastatic melanoma cells.[80] B16F1 cells were iron-labeled and injected via the mesenteric vein. Mice were treated with either doxorubicin or vehicle. MRI was used to quantify both the number of liver metastases and persisting iron-labeled cells. Doxorubicin decreased metastatic growth but did not decrease the existing metastatic cell populations. This important work showed the ability to assess the effect of treatment on both proliferative and non-proliferative cell populations and pointed to the lack

of effect on non-proliferating cells as a factor, which may be responsible for failure rates in treatment of metastatic disease.[77]

Economopolous et al. used cellular MRI to monitor the development of iron-labeled primary MDA-MB-231 mammary fat pad tumours and metastasis to the lymph nodes.[64] Over time, the signal loss associated with the iron-labeled cancer cells was redistributed throughout the tumour as the cancer cells proliferated. After 4 weeks some iron-labeled MDA-MB-231 cells persisted in the primary tumour indicating that some of the cells were non-proliferative. Of particular interest was the observation of iron-labeled MDA-MB-231 cells in lymph nodes. MRI showed signal loss in axillary or brachial lymph nodes at 3 or 4 weeks post mammary fat pad cell implantation. The presence of iron-positive MDA-MB-231 cells in nodes was validated by confocal microscopy; indicating that nonproliferative, or slowly-dividing, cancer cells can leave a primary tumour and metastasize to the lymph node.[61] This paper showed that the proliferative status of cancer cells can be evaluated by the retention of iron nanoparticles with cellular MRI.

In this thesis we will employ similar techniques to investigate the use of 3D cellular MRI for *in vivo* monitoring of the development of 4T1 and 4T1 Y5R-KD primary mammary fat pad tumors, proliferative status and the incidence of metastases.

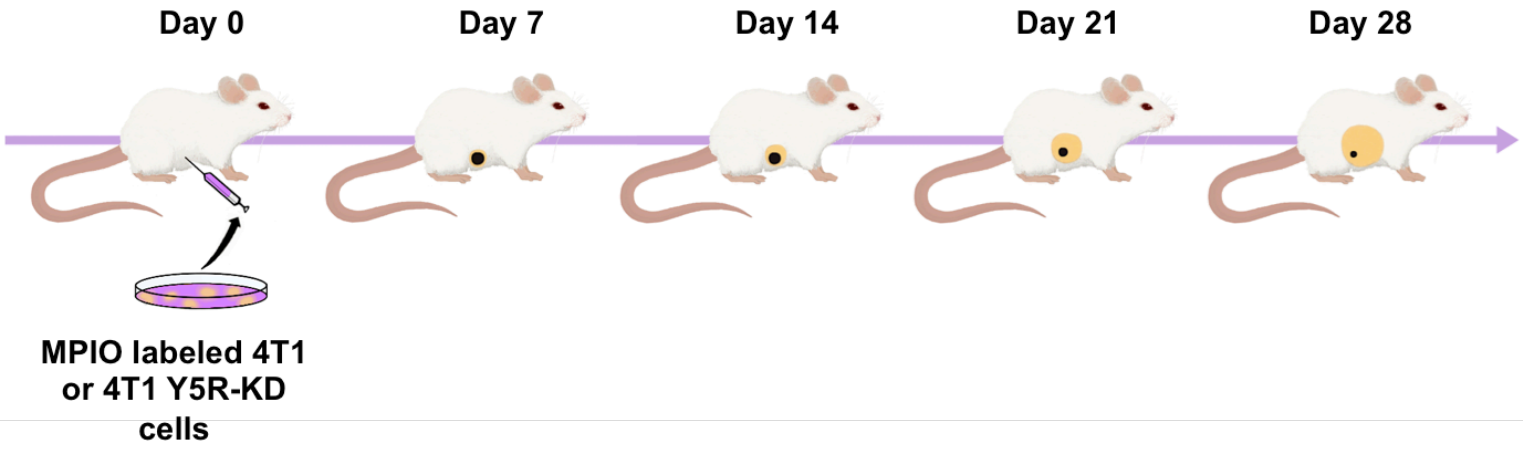

Figure 1.11.1 Cellular MRI of 4T1 and 4T1 Y5R-KD models. Schematic showing the proposed application of 3D cellular MRI to monitor 4T1 and 4T1 Y5R-KD orthotopically implanted cells. Cells are grown *in vitro* followed by co-incubation and labeling with MPIOs. After 24 hours, cells are injected into the thoracic mammary fat pad. At weekly time points, the mice will be imaged and tumour growth will be quantified. The proliferation of cells will result in the dilution of iron permitting assessment of tumour growth and cellular proliferative status.

1.12 Objectives, Specific Aim and Hypotheses

The overall objective of this thesis was to elucidate the impact of the NPY-Y5R as a system that mediates breast cancer development and to develop an *in vivo* model in which the contributions of Y5R could be functionally studied.

1.12.1 Specific Aims

1. Evaluate the heterogeneity of expression of Y5R of breast cancer cell lines of various levels of aggression.

2. Investigate the proliferative potential of the breast cancer cell lines induced by various concentrations of NPY. Understand the specific role of Y5R in proliferation via receptor blockade.

3. Establish and validate a 4T1- Y5R knockdown to assess resulting phenotypic alterations that contribute to breast cancer carcinogenesis.

4. Utilize cellular MRI for the *in vivo* evaluation of the influence of Y5R on primary tumour growth, proliferation and metastasis.

1.12.2 Overall Hypothesis

Neuropeptide Y-Y5R is a factor that promotes breast cancer tumourigenicity and metastasis.

1.12.2.1 Specific Hypotheses

1. The metastatic potential coordinates with the Y5R expression of the respective cell lines. Therefore, metastatic strains of breast cancer with express more Y5R.

2. NPY stimulates the proliferation of breast cancer cell lines. Y5R antagonism will inhibit Neuropeptide Y- stimulated proliferation.

3. Knockdown of Y5R will mitigate the proliferative stimulation of NPY.

4. Knockdown of Y5R will reduce the metastatic burden and inhibit proliferation.

1.13 References

1. Canada, S. Canadian Cancer Statistics Special topic : Skin cancers. *Can. Cancer Soc.* **2014,** 1–132 (2014).

2. Institute, N. C. SEER Stat Fact Sheets: Female Breast Cancer. *SEER* Survival by Stage (2012).

3. Lee, Y. T. Breast carcinoma: pattern of metastasis at autopsy. *J. Surg. Oncol.* **23,** 175–180 (1983).

4. MacDonald, I. C., Groom, A. C. & Chambers, A. F. Cancer spread and micrometastasis development: Quantitative approaches for in vivo models. *BioEssays* **24,** 885–893 (2002).

5. Chambers, A. F. *et al.* Steps in tumor metastasis: new concepts from intravital videomicroscopy. *Cancer Metastasis Rev.* **14,** 279–301 (1995).

6. Dent, R. *et al.* Triple-Negative Breast Cancer: Clinical Features and Patterns of Recurrence. *Clin. Cancer Res.* **13 ,** 4429–4434 (2007).

7. Fawzy, F. I. *et al.* Malignant Melanoma: Effects of an Early Structured Psychiatric Intervention, Coping, and Affective State on Recurrence and Survival 6 Years Later. *Arch. Gen. Psychiatry* **50,** 681–689 (1993).

8. Cooper, C. L. & Faragher, E. B. Psychosocial stress and breast cancer: the inter-relationship between stress events, coping strategies and personality. *Psychol. Med.* **23,** 653–662 (1993).

9. Funch, D. P. & Marshall, J. The role of stress, social support and age in survival from breast cancer. *J. Psychosom. Res.* **27,** 77–83 (1983).

10. Levy, S., Herberman, R., Lippman, M. & d'Angelo, T. Correlation of stress factors with sustained depression of natural killer cell activity and predicted prognosis in patients with breast cancer. *J. Clin. Oncol.* **5,** 348–353 (1987).

11. Chorot, P. & Sandin, B. Life events and stress reactivity as predictors of cancer, coronary heart disease and anxiety disorders. *Int. J. Psychosom.* **41,** 34–40 (1994).

12. Lillberg, K. *et al.* Stressful life events and risk of breast cancer in 10,808 women: a cohort study. *Am. J. Epidemiol.* **157,** 415–423 (2003).

13. Palesh, O. *et al.* Stress history and breast cancer recurrence. *J. Psychosom. Res.* **63,** 233–239 (2007).

14. Brothers, S. P. & Wahlestedt, C. Therapeutic potential of neuropeptide Y (NPY) receptor ligands. *EMBO Mol. Med.* **2,** 429–439 (2010).

15. Michel, M. C. *et al.* XVI. International Union of Pharmacology recommendations for the nomenclature of neuropeptide Y, peptide YY, and pancreatic polypeptide receptors. *Pharmacol. Rev.* **50,** 143–150 (1998).

16. Abe, K., Kuo, L. & Zukowska, Z. Neuropeptide Y is a mediator of chronic vascular and metabolic maladaptations to stress and hypernutrition. *Exp. Biol. Med. (Maywood).* **235,** 1179–1184 (2010).

17. Kuo, L. E. *et al.* Neuropeptide Y acts directly in the periphery on fat tissue and mediates stress-induced obesity and metabolic syndrome. *Nat. Med.* **13,** 803–811 (2007).

18. Zukowska-Grojec, Z., Konarska, M. & McCarty, R. Differential plasma catecholamine and neuropeptide Y responses to acute stress in rats. *Life Sci.* **42,** 1615–1624 (1988).

19. Morris, M. J. *et al.* Increases in plasma neuropeptide Y concentrations during sympathetic activation in man. *J. Auton. Nerv. Syst.* **17,** 143–149 (1986).

20. Erondu, N. *et al.* Neuropeptide Y5 receptor antagonism does not induce clinically meaningful weight loss in overweight and obese adults. *Cell Metab.* **4,** 275–282 (2006).

21. Hart, E. C. *et al.* Sex differences in sympathetic neural-hemodynamic balance implications for human blood pressure regulation. *Hypertension* **53,** 571–576 (2009).

22. Jackson, D. N., Ellis, C. G. & Shoemaker, J. K. Estrogen modulates the contribution of neuropeptide Y to baseline hindlimb blood flow control in female Sprague-Dawley rats. *Am. J. Physiol. Regul. Integr. Comp. Physiol.* **298,** R1351–7 (2010).

23. Hodges, G. J., Jackson, D. N., Mattar, L., Johnson, J. M. & Shoemaker, J. K. Neuropeptide Y and neurovascular control in skeletal muscle and skin. *Am. J. Physiol. - Regul. Integr. Comp. Physiol.* **297,** R546–R555 (2009).

24. Glenn, T. C. & Krause, D. N. Vascular responses to neuropeptide Y are greater in female than male rats:effect of age. *Aging Clin. Exp. Res.* **6,** 111–118 (1997).

25. Lettgen, B., Wagner, S., Hanze, J., Lang, R. E. & Rascher, W. Elevated plasma concentration of neuropeptide Y in adolescents with primary hypertension. *J. Hum. Hypertens.* **8,** 345–349 (1994).

26. De Potter, W. P., Kurzawa, R., Miserez, B. & Coen, E. P. Evidence against differential release of noradrenaline, neuropeptide Y, and dopamine-beta-hydroxylase from adrenergic nerves in the isolated perfused sheep spleen. *Synapse* **19,** 67–76 (1995).

27. Lecat, S., Belemnaba, L., Galzi, J.-L. & Bucher, B. Neuropeptide Y receptor mediates activation of ERK1/2 via transactivation of the IGF receptor. *Cell. Signal.* **27,** 1297–1304 (2015).

28. Zukowska-Grojec, Z. Neuropeptide Y. A novel sympathetic stress hormone and more. *Ann. N. Y. Acad. Sci.* **771,** 219–233 (1995).

29. Böhme, I., Stichel, J., Walther, C., Mörl, K. & Beck-Sickinger, A. G. Agonist induced receptor internalization of neuropeptide Y receptor subtypes depends on third intracellular loop and C-terminus. *Cell. Signal.* **20,** 1740–1749 (2008).

30. Ouedraogo, M. *et al.* Distinct motifs of neuropeptide y receptors differentially regulate trafficking and desensitization. *Traffic* **9,** 305–324 (2008).

31. Herzog, H. *et al.* Overlapping Gene Structure of the Human Neuropeptide Y Receptor Subtypes Y1 and Y5 Suggests Coordinate Transcriptional Regulation. *Genomics* **41,** 315–319 (1997).

32. Rodriguez, M. *et al.* Molecular identification of the long isoform of the human neuropeptide Y Y5 receptor and pharmacological comparison with the short Y5 receptor isoform. *Biochem. J.* **369,** 667–673 (2003).

33. Sheriff, S. *et al.* Neuropeptide Y Y5 receptor promotes cell growth through extracellular signal-regulated kinase signaling and cyclic AMP inhibition in a human breast cancer cell line. *Mol. Cancer Res.* **8,** 604–614 (2010).

34. Barnea, A., Roberts, J., Keller, P. & Word, R. A. Interleukin-1beta induces expression of neuropeptide Y in primary astrocyte cultures in a cytokine-specific manner: induction in human but not rat astrocytes. *Brain Res.* **896,** 137–145 (2001).

35. Rethnam, S., Raju, B., Fristad, I., Berggreen, E. & Heyeraas, K. J. Differential expression of neuropeptide Y Y1 receptors during pulpal inflammation. *Int. Endod. J.* **43,** 492–498 (2010).

36. von Horsten, S. *et al.* Brain NPY Y1 receptors rapidly mediate the behavioral response to novelty and a compartment-specific modulation of granulocyte function in blood and spleen. *Brain Res.* **806,** 282–286 (1998).

37. Mantovani Alberto, Sica Antonio & Locati, M. Macrophage Polarization Comes of Age. *Immunity* **23,** 344–346 (2005).

38. Bedoui, S. *et al.* Differential effects of neuropeptide Y (NPY) on leukocyte subsets in the blood: mobilization of B-1-like B-lymphocytes and activated monocytes. *J. Neuroimmunol.* **117,** 125–132 (2001).

39. Czarnecka, M. *et al.* Neuropeptide Y receptor Y5 as an inducible pro-survival factor in

neuroblastoma: implications for tumor chemoresistance. *Oncogene* **34,** 3131–3143 (2015).

40. Tilan, J. U. *et al.* Hypoxia shifts activity of neuropeptide Y in Ewing sarcoma from growth-inhibitory to growth-promoting effects. *Oncotarget* **4,** 2487–2501 (2013).

41. Fischer, J. E. & Bland, K. I. *Mastery of surgery*. (Philadelphia: Wolters Kluwer/Lippincott Williams & Wilkins., 2007).

42. James, G. D., Berge-Landry Hv, H. van, Valdimarsdottir, H. B., Montgomery, G. H. & Bovbjerg, D. H. Urinary catecholamine levels in daily life are elevated in women at familial risk of breast cancer. *Psychoneuroendocrinology* **29,** 831–838 (2004).

43. Zhang, J. *et al.* Differential processing of neuropeptide proprotein in human breast adenocarcinoma. 745–752 (2013). doi:10.3275/8935

44. Medeiros, P. J. *et al.* Neuropeptide Y stimulates proliferation and migration in the 4T1 breast cancer cell line. *Int. J. cancer* **131,** 276–286 (2012).

45. Medeiros, P. J. & Jackson, D. N. Neuropeptide Y Y5-receptor activation on breast cancer cells acts as a paracrine system that stimulates VEGF expression and secretion to promote angiogenesis. *Peptides* **48,** 106–113 (2013).

46. Medeiros, P. J. The Impact of the Neuropeptide Y System on the Progression of Breast Cancer. (University of Western Ontario, 2012). doi:Paper 1065

47. Aslakson, C. J. & Miller, F. R. Selective Events in the Metastatic Process Defined By Analysis of the Sequential Dissemination of Subpopulations of a Mouse Mammary-Tumor. *Cancer Res.* **52,** 1399–1405 (1992).

48. Dexter, D. L. *et al.* Heterogeneity of Tumor Cells from a Single Mouse Mammary Tumor of Tumor Cells from a Single Mouse Mammary Tumor1. *Cancer Res.* **38,** 3174–3181 (1978).

49. Miller, B., Miller, F., Wilburn, D. & Heppner, G. Analysis of tumour cell composition in

tumours composed of paired mixtures of mammary tumour cell lines. *Br. J. Cancer* **56,** 561–569 (1987).

50. Pulaski, B. A. & Ostrand-Rosenberg, S. in *Current Protocols in Immunology* (John Wiley & Sons, Inc., 2001). doi:10.1002/0471142735.im2002s39

51. Harris, J., Morrow, M. & Norton, L. *In Cancer, Priniciples, and Practive of Oncology*. (1997).

52. Simões, R. V *et al.* Metabolic Plasticity of Metastatic Breast Cancer Cells: Adaptation to Changes in the Microenvironment(). *Neoplasia* **17,** 671–684 (2015).

53. Eckhardt, B. L. *et al.* Genomic analysis of a spontaneous model of breast cancer metastasis to bone reveals a role for the extracellular matrix. *Mol Cancer Res* **3,** (2005).

54. Paddison, P. J., Caudy, A. A., Bernstein, E., Hannon, G. J. & Conklin, D. S. Short hairpin RNAs (shRNAs) induce sequence-specific silencing in mammalian cells. *Genes Dev* **16,** (2002).

55. McAnuff, M. A., Rettig, G. R. & Rice, K. G. Potency of siRNA versus shRNA mediated knockdown in vivo. *J. Pharm. Sci.* **96,** 2922–2930 (2007).

56. Davis, E. & Ph, D. Knockout by TALEN or CRISPR vs . Knockdown by shRNA or siRNA. *GenecCopoeia* 1–3 (2013).

57. Fu, Y. *et al.* High-frequency off-target mutagenesis induced by CRISPR-Cas nucleases in human cells. *Nat Biotech* **31,** 822–826 (2013).

58. Jang, J.-Y., Jeon, Y.-K. & Kim, C.-W. Degradation of HER2/neu by ANT2 shRNA suppresses migration and invasiveness of breast cancer cells. *BMC Cancer* **10,** 391 (2010).

59. Nickerson, N. K. *et al.* Decreased Autocrine EGFR Signaling in Metastatic Breast Cancer Cells Inhibits Tumor Growth in Bone and Mammary Fat Pad. *PLoS One* **7,** e30255 (2012).

60. Jiang, Q., Zhang, H. & Zhang, P. ShRNA-mediated gene silencing of MTA1 influenced

on protein expression of ER alpha, MMP-9, CyclinD1 and invasiveness, proliferation in breast cancer cell lines MDA-MB-231 and MCF-7 in vitro. *J. Exp. {&} Clin. Cancer Res.* **30,** 1–11 (2011).

61. Economopoulos, V., Chen, Y., McFadden, C. & Foster, P. J. MRI Detection of Nonproliferative Tumor Cells in Lymph Node Metastases Using Iron Oxide Particles in a Mouse Model of Breast Cancer. *Transl. Oncol.* **6,** 347–354 (2013).

62. Heyn, C. *et al.* In vivo MRI of cancer cell fate at the single-cell level in a mouse model of breast cancer metastasis to the brain. *Magn. Reson. Med.* **56,** 1001–1010 (2006).

63. Magnitsky, S., Roesch, A., Herlyn, M. & Glickson, J. D. In vivo and Ex vivo MR Imaging of Slowly Cycling Melanoma Cells. *Magn. Reson. Med.* **66,** 1362–1373 (2011).

64. Henry, M. N., Chen, Y., McFadden, C. D., Simedrea, F. C. & Foster, P. J. In-vivo longitudinal MRI study: an assessment of melanoma brain metastases in a clinically relevant mouse model. *Melanoma Res.* **25,** (2015).

65. Foster, P. J. *et al.* Cellular Magnetic Resonance Imaging: In Vivo Imaging of Melanoma Cells in Lymph Nodes of Mice. *Neoplasia* **10,** 207–216 (2008).

66. Srinivas, M. *et al.* Customizable, multi-functional fluorocarbon nanoparticles for quantitative in vivo imaging using 19F MRI and optical imaging. *Biomaterials* **31,** 7070–7077 (2010).

67. Damadian, R. Tumor detection by nuclear magnetic resonance. *Science* **171,** 1151–1153 (1971).

68. Percy, D. B. D. B. In vivo characterization of changing blood-tumor barrier permeability in a mouse model of breast cancer metastasis: a complementary magnetic resonance imaging approach. *Invest. Radiol.* **46,** 718–725 (2011).

69. Schnitt, S. J. Classification and prognosis of invasive breast cancer: from morphology to molecular taxonomy. *Mod. Pathol.* **23 Suppl 2,** S60–S64 (2010).

70. Huuse, E. M. *et al.* In vivo MRI and histopathological assessment of tumor microenvironment in luminal-like and basal-like breast cancer xenografts. *J. Magn. Reson. Imaging* **35,** 1098–1107 (2012).

71. Nofiele, J. T. & Cheng, H. L. M. Establishment of a lung metastatic breast tumor xenograft model in nude rats. *PLoS One* **9,** 1–7 (2014).

72. Modo, M. M. J. & Bulte, J. W. M. Molecular and cellular MR imaging. **4,** 143–164 (2007).

73. Arbab, A. S. *et al.* Characterization of biophysical and metabolic properties of cells labeled with superparamagnetic iron oxide nanoparticles and transfection agent for cellular MR imaging. *Radiology* **229,** 838–846 (2003).

74. Arbab, A. S. *et al.* Labeling of cells with ferumoxides-protamine sulfate complexes does not inhibit function or differentiation capacity of hematopoietic or mesenchymal stem cells. *NMR Biomed.* **18,** 553–559 (2005).

75. Muhammad, G., Jablonska, A., Rose, L., Walczak, P. & Janowski, M. Effect of MRI tags : SPIO nanoparticles and 19F nanoemulsion on various populations of mouse mesenchymal stem cells. 144–159 (2015).

76. Ribot, E. J. *et al.* In vivo single scan detection of both iron-labeled cells and breast cancer metastases in the mouse brain using balanced steady-state free precession imaging at 1.5 T. *J. Magn. Reson. Imaging* **34,** 231–238 (2011).

77. Townson, J. L. *et al.* Three-dimensional imaging and quantification of both solitary cells and metastases in whole mouse liver by magnetic resonance imaging. *Cancer Res.* **69,** 8326–8331 (2009).

Chapter 2- Neuropeptide Y-Y5R as a Mediating Factor of Breast Cancer

2.1 Introduction

In Canada, one in nine females is expected develop breast cancer in her life time.[1] The 98.8% 5- year survival rate of localized breast cancer drops to 26.3% when the breast cancer has metastasized.[2] Common sites of breast cancer metastasis are the lungs, liver, bone, and brain.[3] In triple negative breast cancers, negative for the estrogen receptor (ER), progesterone receptor (PR) and human epidermal growth factor receptor 2 (HER-2), treatment with classic hormone therapy is futile. Therefore, a therapy for a novel target to treat triple-negative breast cancer is required.

Behavioural and emotional stress has been implicated in breast cancer progression and metastasis. Studies have demonstrated a correlation between elevated stress levels and poor prognosis and survival in patients with breast cancer.[4–8] Furthermore, there has been documented support of prolonged survival in breast cancer patients who receive therapeutic emotional support.[6,9,10] Swim stress, surgical stress, social confrontation, and hypothermia in animal stress models have been shown to promote lung metastasis from injected breast cancer cells.[11–14]

Neuropeptide Y is a sympathetic neurotransmitter peripherally released from sympathetic nerves, adrenal medulla and platelets.[15] The lateral and anterior cutaneous branches of the second and sixth intercostal nerves sympathetically innervate the mammary gland, smooth muscle of the areola, skin, and breast vessels.[16] NPY is released in greater quantities during chronic stress and in response to a life-threatening stressor. In this respect, the breast microenvironment is susceptible to the alterations in NPY flux induced by stress. This susceptibility has the potential

to negatively impact women with family histories of breast cancer who have an increased basal release of sympathetic neurotransmitters in response to daily stressors.[17]

NPY elicits its effects by binding and activating G_i- protein coupled receptors (GPCR), Neuropeptide Y1R-Y6R. Neuropeptide Y5R is expressed in cancer cell lines including breast and brain xenograft models.[12-15] The Jackson lab has studied the influence of Neuropeptide Y in the murine 4T1 breast cancer cell line. The 4T1 cell line aggressively metastasizes to lungs, liver, bone and brain primarily hematogenously.[20] They have shown that NPY supports proliferation, migration, angiogenesis, and metastasis of 4T1 cells. Furthermore, they have shown that Y5R activation significantly contributes to these NPY supported cancerous processes.[21,22] Although the contribution of the NPY and Y5R has been well characterized in the 4T1 cell line, the influence of this system has yet to be characterized in cell lines of various metastatic potentials.

In this thesis, we aim to expand on the previous findings from the Jackson lab to further elucidate the impact of the NPY-Y5R as a system that mediates breast cancer metastasis and to develop an *in vivo* model in which the contributions of Y5R can be functionally studied. To meet this objective, we have investigated three cell lines with various metastatic capacities and investigated the role of Y5R and NPY-stimulated proliferation. Furthermore, we investigated the role of Y5R in aggressively metastasizing 4T1 cells by knocking down Y5R expression facilitated by shRNA. Using this knockdown, we evaluate the contribution of Y5R to breast cancer cell proliferation *in vitro* and metastasis *in vivo*. To study this in vivo we used cellular MRI to monitor tumour growth and metastasis and track the fate of iron oxide pre-labeled cancer cells

If a direct link can be established between the physiological stress response and breast cancer progression, NPY and its Y5 receptor could be potential therapeutic targets to combat breast cancer metastasis.

2.2 Methods

2.2.1 IN VITRO EXPERIMENTS

In vitro experiments were conducted to characterize the expression of Y5R in three cell lines of various metastatic potential; 67NR, 168 FARN, and 4T1. The proliferation of each cell line was investigated under the stimulation of NPY and Y5R blockade, to elucidate the specific contribution of the receptor.

2.2.1.1 Cell Culture

4T1 cells were a gift from Dr. Fred Miller (Wayne State University, Michigan USA), 168FARN and 67NR cells, were a gift from Dr. Ann Chambers (London Health Sciences Centre, London, Canada). The 67NR, 168 FARN, and 4T1 cell lines originate from the same murine mammary fat pad tumour with different metastatic potentials.[49] 67NR cells solely proliferate in the mammary fat pad and do not intravasate into vessels to metastasize. 168FARN cells have the capacity to disseminate to the lymph node but do not metastasize to other parts of the body. 4T1 cells are able to aggressively metastasize from the primary mammary fatpad to the lungs, liver, bone and brain.

Cells were cultivated in high glucose Dulbecco's Minimal Essential Medium (DMEM) supplemented with 10% sterile FBS. Cells were incubated at 37^{o}C and 5% carbon dioxide. At approximately 80% confluency, cells were washed with PBS and passaged using 0.25% trypsin-EDTA treatment for dissociation.

2.2.1.2 Development of a 4T1-Y5R Knockdown Cell Line

A 4T1 Y5R-Knockdown (KD) cell line was established to directly study the role of Y5R in an aggressively metastasizing breast cancer cell line. $3x10^5$ 4T1 cells were plated in a 6 well plate and grown to 50% confluence. Y5R specific shRNA green fluorescent protein positive (GFP+) expression plasmids (OriGene NM 006174) were suspended in 50µl of ddH_2O to a final concentration of 100ng/µl. 1µg of shRNA was diluted in 250µl of Opti-MEM I (Gibco 51985). 3µl of Lipofectamine™ 3000 (ThermoFisher Scientific, Waltham, MA, USA) was added to diluted shRNA and incubated for 15 minutes at room temperature. Cells were incubated with the shRNA mixture at 37°C and 5% CO_2 for 72h. These transfection steps toward establishing the 4T1 Y5R-KD cell line were completed by Dr. Phil Medeiros, a previous PhD student in the Jackson lab.

Cells that had previously been transfected with Y5R specific shRNA GFP+ expression plasmids were thawed, re-suspended and analyzed for GFP. Cells were re- suspended in 1% FBS in PBS and were then analyzed for live GFP+ containing cells by fluorescent-activated cell sorting (FACS). To determine viability, cells were stained with 7-Aminoactinomycin D (7AAD) viability dye (ThermoFisher Scientific, Waltham, MA, USA) for 10 minutes on ice prior to sorting. FACS was conducted on a FACSAriaIII system (BD Biosciences, Mississauga, ON, Canada) using a 100µm filter and parental 4T1 cells were used as a negative control.

One cell was seeded per well in four 96 well- plates using a FACSAriaIII to develop clonal colonies. Fluorescent colonies were trypsinized and expanded for GFP positive purity analysis and sorting. Purity greater than 95% prior to sort was deemed as stable transfection. FACS data was analyzed using BD FACSDiva Shortware version 8.0.1.

2.2.1.3 Immunocytochemistry

To determine the presence and localization of Y5R, immunocytochemistry was conducted on 67NR, 168FARN, 4T1 and 4T1 Y5R-KD cells. 10^5 cells of each strain were grown on sterile glass coverslips for 48hr, then fixed in ice-cold 4% paraformaldehyde for 15 min. Cells were washed in ice- cold phosphate-buffered saline (PBS; 2.68mM KCL, 1.46mMKH_2PO_4, 137mM Nal and 6.48mM Na_2HPO_4) and permeabilized in 0.25% (v/v) Triton-X 100 (in PBS) for 20 min at room temperature followed by PBS washes. Following 10 min blocking in 1.5% normal goat serum (in PBS), excess blocking reagent was removed, and replaced with 2ml of diluted (1:1000) primary antibody specific to NPY Y5R (Cat no. ab133757 Abcam, San Francisco, CA, USA) for 1hr at room temperature. Cells were washed, incubated in secondary antibody (biotinylated goat anti-rabbit secondary, 4μg/ml in 0.1% blocking serum in PBS) for 30 minutes at room temperature, washed and incubated in 1:1 avidin:biotin complex (ABC) (Vectastain Elite ABC® Kit (Standard), Cat. no. PK-6100, Vector Laboratories Inc., Burlingame, CA) solution for 30 min. After washing, cells were incubated in 3,3 diaminobenzidine (DAB Peroxidase Substrate Kit, 3,3'-diaminobenzidine, Cat. no. SK-4100, Vector Laboratories Inc., Burlingame, CA) for 8 minutes, rinsed, cleared and mounted.

2.2.1.4 Western Blot Analysis

To quantify and compare the expression of Y5R between 67NR, 168FARN, 4T1, and 4T1 Y5R-KD cell lines, Western Blot analysis was conducted. Cultured cells from a 75cm^2 flask were washed in ice cold PBS and then lysed in 1.5ml RIPA lysis buffer containing protease inhibitors (104mM AEBSF, 80 μM aprotinin, 2.1 mM leupeptin, 3.6 mM bestatin, 1.5 mM pepstatin A, 1.4 mM E-64). Cells were scraped and then lysed using a 27- gauge needle with syringe. Cells were centrifuged for 10 minutes at 14,000 rpm at 4^oC. Supernatant was collected

and stored at -20^{o}c until protein concentration was determined.

A Bradford assay (Bradford, 1976) was performed to determine total protein concentration of samples. Fifteen micrograms of protein from each sample were loaded on a 4% to 12% gradient gel and separated by SDS- PAGE. After electrophoresis, proteins were transferred at a constant voltage to polyvinylidene fluoride membranes. Membranes were blocked in 5% Bovine Serum Albumin (BSA) in Tris- Buffered Saline + Tween 20 (0.5%) (TTBS) for 1 hr. Membranes were then incubated in primary monoclonal antibody specific to NPY Y5R (Cat no. ab133757 Abcam, San Francisco, CA, USA) in 5% BSA- TTBS at a concentration of 1:1000 at 4^{o}C overnight. Membranes were washed three times in TTBS then incubated in secondary antibody conjugated to horseradish peroxidase (goat anti-rabbit IgD, 1:20000) in 2% BSA-TTBS for 1hr. Membranes were washed three times and bands were detected using an Immun- Star WesternC© chemilluminescent kit (Bio- Rad, Hercules, CA, USA) and imaged with the ChemiDoc XRS System (Bio-Rad, Hercules, CA, USA). Membranes were washed, stained for total protein using Coomassie Brilliant Blue and imaged using the ChemiDoc XRS. Densitometric band quantification was performed with Quantity One 1-D Analysis Software (Bio-Rad, Hercules, CA, USA). Y5R band intensity was normalized to the respective average lane signal intensity from Coomassie Brilliant Blue staining.

2.2.1.5 Cell Proliferation

In vitro MTS assays were conducted to investigate the effect of NPY on 67NR, 168 FARN and 4T1 cell line proliferation. One thousand two hundred and fifty viable cells were seeded per well of 96- well plates for 24 hrs in DMEM supplemented with 10% FBS. After 24hrs media was replaced with experimental medium (DMEM + 2% FBS) containing 10^{-11} to 10^{-6}M NPY (Tocris, Minneapolis, MN, USA) or scrambled 10^{-6}M NPY. The proliferative effect of

NPY was tested using an MTS (3- (4,5-dimethylthiazol-2-yl)-5-(3-carboxymethoxyphenyl)-2-(4-sulfophenyl)-2H tetrazolium) based assay (CellTiter 96 AQ_{ueous} One Solution, Madison, WI, USA). Absorbance of the wells at 490nm was measured after 24hr of NPY treatment. These experiments were conducted on 67NR, 168FARN and 4T1 cells in triplicate (per concentration) and repeated three times.

Receptor antagonist experiments were conducted to confirm Y5R- mediated proliferation induced by NPY. Twenty- four hours after cells were seeded, experimental media containing NPY (10^{-6}M) and Y5R- specific antagonist, L-152 804 (10^{-4}M), was added and cell proliferation was measured at 24hrs. Drugs were reconstituted in PBS and all treatments were compared to control cells that were incubated in media without the addition of drugs.

2.2.1.6 Statistics

Statistical analysis was performed using GraphPad software, data are presented as mean ± SEM. Non-linear regression analysis was performed on proliferation assays. Statistical differences between cell lines for Western blots and between treatments for proliferation assays were evaluated by one-way ANOVA, followed by Tukey's HSD test. The level of statistical probability was set at $p < 0.05$.

2.2.2 IN VIVO EXPERIMENTS

In vivo experiments were conducted on the aggressively metastasizing 4T1 strain and the 4T1 Y5R-KD strain in order to elucidate the role of Y5R in tumourigenicity and metastasis longitudinally in a biologically relevant murine model.

2.2.2.1 Iron- Oxide Cell Labeling for Imaging

To allow cancer cells to be visualized by MRI, $2x10^6$ 4T1 or 4T1 Y5R KD cells were plated in $75cm^2$ flask in 10ml of high glucose DMEM supplemented with 10% sterile FBS and were incubated for 24 hours at 37^oC and 5% carbon dioxide. Cells were then incubated with the same media containing 50µg/ml flash red fluorescent micron-sized superparamagnetic iron oxide particles (MPIO) (Bangs Laboratories Inc., Fishers, IN) for 24h. Cells were washed three times with 10ml of 37^oC HBSS and trypsinized with 0.25% trypsin-EDTA. Cells were centrifuged for 5 minutes at 1000RPM, the supernatant was aspirated and cells were re-suspended in 12 ml of HBSS three times. Cells were concentrated to $6x10^6$/ml for injection.

To verify cell labeling, $3x10^5$ cells were cytospun onto a slide and fixed in 3:1 methanol: glacial acetic acid. Cells were stained with 1% potassium hexacyano-ferrate (III) trihydrate in 1% HCl for 30 minutes. Cells were washed in dH_2O prior to counterstain with Nuclear fast red. Cells were washed and dehydrated in increasing concentrations of 75%, 95%, and 100% ethanol and xylene prior to being mounted.

2.2.2.2 Animal Model

To establish orthotopic tumours, 3×10^5 MPIO labeled 4T1 cells (n=8) or 4T1 Y5R KD GFP positive cells (n=9) were injected into the inguinal mammary fat pad of female 6-8 week BALB/c mice (Charles River Laboratory).

2.2.2.3 Magnetic Resonance Imaging

All imaging was performed on 3T MRI scanner (General Electric Medical Scanner, Milwaukee, WI) using a custom- built gradient coil insert with an inner diameter of 17.5cm, maximum gradient strength of 500mT/m and a peak slew rate of 3,000T/m/s, and a custom

solenoidal whole- mouse body radiofrequency (RF) coil 4cm in length and 3cm in diameter. Mice were anaesthetized with isoflurane (2% in oxygen) and placed prone in the coil, a warm saline bag was kept near the RF coil to maintain body temperature, and the mice were wrapped with gauze and tape for consistent positioning to minimize motion artefact due to respiration.

Images were acquired using bSSFP pulse sequence with 200μm isotropic spatial resolution. The scan parameters for bSSFP were as follows: repetition time (TR) =6.3ms, echo time (TE)=3.15ms, flip angle=35^{o}, bandwidth= +/- 31.25kHz, matrix=250x250, field of view (FOV) was 5x2.5cm (30 minutes), 0.2mm slice thickness, 2 signal averages (NEX)=2, RF phase cycles=8.

2.2.2.4 Image Analysis

Mouse body three dimensional (3D) bSSFP images were assessed for the appearance of primary tumours and metastases. Images were observed in all three orientations (axial, sagittal and coronal). Osirix image analysis software was used to make all measurements from images acquired in the study. To calculate the volume of the mammary fat pad tumour from MRI, manual segmentation was conducted in each acquired image using the closed polygon tracing tool and repulsor tool. Each tumour was segmented as a region of interest (ROI) and total tumour volume was calculated by using the ROI volume calculation tool in the software package.

To calculate the volume of the region of signal hypointensity within the tumours the mean signal intensity of the hypointense region was measured and a threshold value (mean signal + 2 standard deviations) was applied to the whole tumor volume. This value was normalized to the total tumour volume. All volume data was statistically compared using Graph Pad Prism analysis software (GraphPad Software, La Jolla, CA).

Primary tumour colour maps were generated by assigning colours to three signal intensity values; blue was assigned to voxels with values equal to the mean signal hypointensity $\pm$2SD, yellow was assigned to voxels with values equal to the mean signal hyperintensity $\pm$2SD, and green was assigned to the remainder of the tumour voxels.

2.2.2.5 Histology and Microscopy

All mice injected with 4T1 cells were euthanized at day 28. Two mice injected with 4T1 Y5R-KD cells were euthanized on each of days 14 and 21 and five were euthanized at day 28. Mice were cardiac perfused with 4% paraformaldehyde. Lungs and tumours were removed and immersed in 4% paraformaldehyde for 24 hours followed by increasing concentrations of 10%, 20%, and 30% sucrose to cryoprotect tissues. Lungs and tumours were embedded in Optimal Cutting Temperature medium in a cryomold. Frozen sections were cut with a cryostat (Leica Microsystems) with a thickness of 10μm. Tumour sections were cut with 1mm separation between samples, starting from what was discerned as the center of the tumour to yield three regions of interest. Lung sections were cut through a pair of lungs with 1mm separation between samples, starting from what was discerned as an edge of the lung to a midpoint, yielding two regions of interest. Three samples were taken at each region of interest for tumours and lungs to be stained with Hematoxylin and Eosin (H&E), Perl's Prussian Blue (PPB) and Nuclear Fast Red (NFR), and Immunohistochemistry (IHC).

2.2.2.6 Hematoxylin and Eosin staining

Tumour and lung slides were washed in xylene prior to washes in decreasing concentrations of ethanol, 100%, 95%, and 70%. Tissues were washed with dH_2O and stained with hemaxtoxylin. Tissues were washed with dH_2O, acid ethanol, and H_2O prior to eosin

staining. Tissues were washed and dehydrated in increasing concentrations of 75%, 95%, and 100% ethanol and xylene prior to being mounted.

2.2.2.7 Perls' Prussian Blue and Nuclear Fast Red staining

Tumour and lung slides were stained with 1% potassium hexacyano-ferrate (III) trihydrate in 1% HCl for 30 minutes. Tissues were washed in dH_2O prior to counterstain with Nuclear fast red. Tissues were washed and dehydrated in increasing concentrations of 75%, 95%, and 100% ethanol and xylene prior to being mounted.

2.2.2.8 Immunohistochemistry

Tumour and lung slides were rehydrated in 1X TBS-T (0.05M Tris Base, 1.8% NaCl, 0.05% Tween 20, pH 8.4). Tissues were blocked in for 30 minutes at room temperature in Protein Block Serum-Free solution (Product no. X0909, Dako, Agilent Technologies, Glostrup, Denmark). Tissues were then incubated in primary polyclonal antibody specific to NPY Y5R (Cat no. ab137204, Abcam, San Francisco, CA, USA) diluted to 1:50 in 1% bovine serum albumin, 1% normal goat serum, in TBS-T for 2hrs at room temperature. Adjacent slices were incubated in TBS-T as a negative control. Tissues were washed three times and incubated in goat anti-rabbit IgG (H+L) secondary antibody, Alexa Fluor® 568(Cat no. A-11011, Life Technologies, Carlsbad, CA) diluted to 1:500 in 1% bovine serum albumin, 1% normal goat serum, in TBST. Slides were washed prior to mounting and visualized with a fluorescence microscope.

2.2.2.9 Statistics

Statistical analysis was performed using GraphPad software, data are presented as mean ± SEM. Non-linear regression analysis was performed on mean 3D tumour volume growths and

signal void volumes to compare the cell lines. Statistical differences between treatments were evaluated by two-way ANOVA, followed by Tukey's HSD test. The level of statistical probability was set at $p < 0.05$.

2.3 Results

2.3.1 Y5R Presence and Localization in 67NR, 168FARN, and 4T1

Immunocytochemistry revealed receptor expression for Y5R in the 67NR, 168FARN, and 4T1 cell lines (Figure 2.1). Primarily, nuclear staining was found in the 67NR and 168FARN cell lines (Figure 2.1A&B). The 4T1 cell line displayed predominantly membranous and cytoplasmic staining in addition to nuclear staining (Figure 2.1C).

A. Conjugate and Chromagen Control

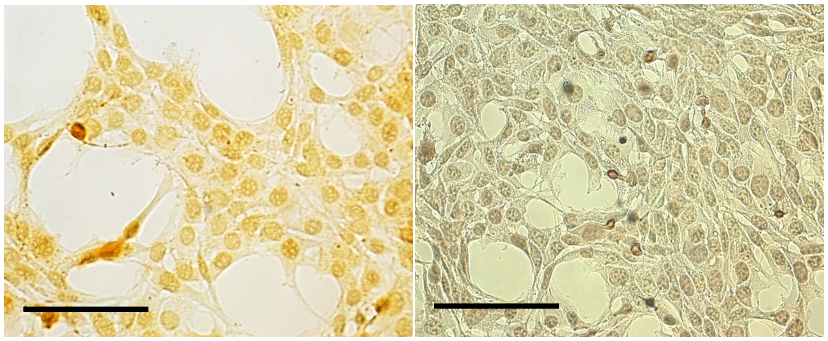

B.

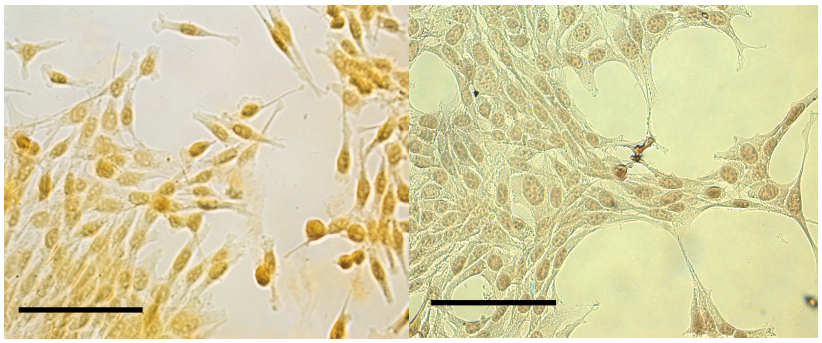

C.

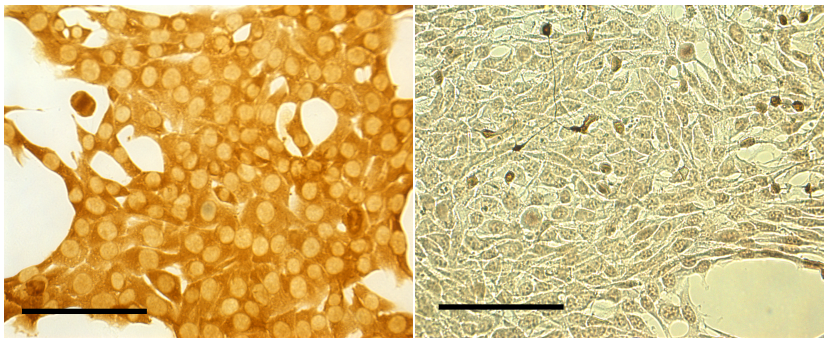

Figure 2.1 Y5R Immunocytochemistry of 67NR, 168FARN and 4T1 Cells (A. 67NR) Positive Y5R staining localized primarily in the nucleus (**B. 168FARN)** Positive Y5R staining localized primarily in the nucleus (**C. 4T1)** Positive Y5R staining localized primarily in the cytoplasm, membrane, and filapodia (Scale bars= 100μm). Conjugate and chromagen control was conducted for each cell strain without incubation of the primary Y5R antibody, demonstrating minimal background staining.

2.3.3 Y5R Expression Quantified in 67NR, 168FARN, and 4T1

Western blots revealed significantly enhanced expression of Y5R in 4T1 cells compared to 168FARN and 67NR cells (Figure 2.2). 4T1 expressed nine to twelve times greater levels of Y5R than the 67NR and 168FARN cell lines, respectively.

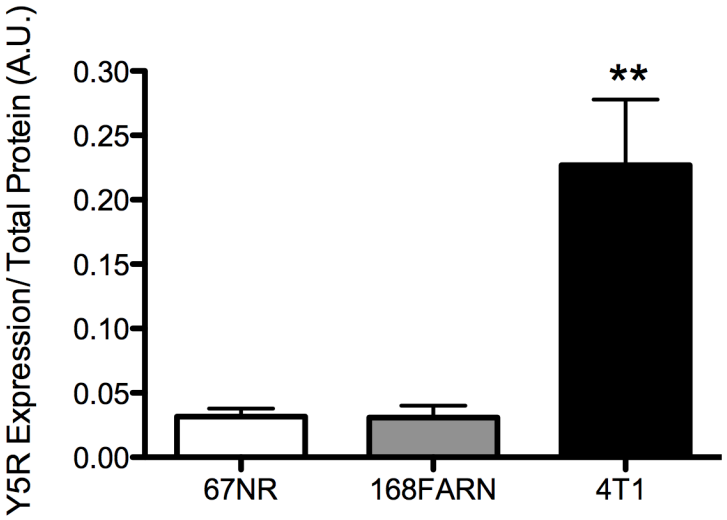

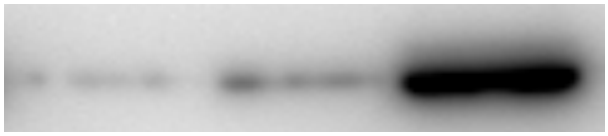

Figure 2.2 Basal Y5R Expression of Murine Mammary Fat Pad Carcinoma Cell Lines. Western Blot densitometry quantification of respective cell lysates normalized to total protein depicting the significantly enhanced Y5R expression of 4T1 cells compared to 168FARN and 67NR cells. Densitometric data are presented as Y5R expression normalized to total protein expression. Data are presented as mean$\pm$ SE (n=3, ** represents a significant difference from 67NR cells $p<0.01$, One- way ANOVA).

2.3.3 Effect of NPY on Proliferation of 67NR, 168FARN, and 4T1

The MTS proliferation assay demonstrated that NPY has a stimulatory effect on proliferation of the three cell lines, despite variable basal Y5R expression. Without normalization of NPY-stimulated proliferation to the respective basal cell strain proliferation, the cell lines had a significantly different proliferative response to NPY ($p<0.001$) (Appendix A). The un-stimulated proliferation of each cell line differed, supporting the normalization of experimental proliferation to basal growth to appropriately investigate the effect of NPY-stimulated proliferation. Experimental proliferation was normalized to basal growth by dividing experimental proliferation by un-stimulated proliferation of the respective cell line, resulting in a control growth of 1 for each cell line (Figure 2.3). Stimulated growth can be observed by values greater than 1.0, denoted by the dashed line. When normalized to the control, the proliferation of each cell line in response to NPY was not significantly different from each other ($p>0.05$, Two-way ANOVA). NPY concentration had a significant effect on the proliferation of the cell lines ($p<0.0001$, Two- way ANOVA).

67NR and 168FARN cell proliferation was stimulated by NPY at 10^{-10}M, 10^{-9}, and 10^{-7}M (Appendix A). The proliferation appears to drop at concentrations greater than 10^{-7}M. As expected, the administered scrambled sequence of NPY, as a negative control, did not stimulate proliferation of 67NR and 168FARNcells (Appendix A). The proliferation appears to plateau at 10^{-10}M of NPY. 4T1 cell proliferation was strongly stimulated by all tested concentrations of NPY, except 10^{-8}M, with no apparent plateau in cell growth (Appendix A). The administered scrambled sequence of NPY, as a negative control, did not stimulate proliferation of 4T1 cells.

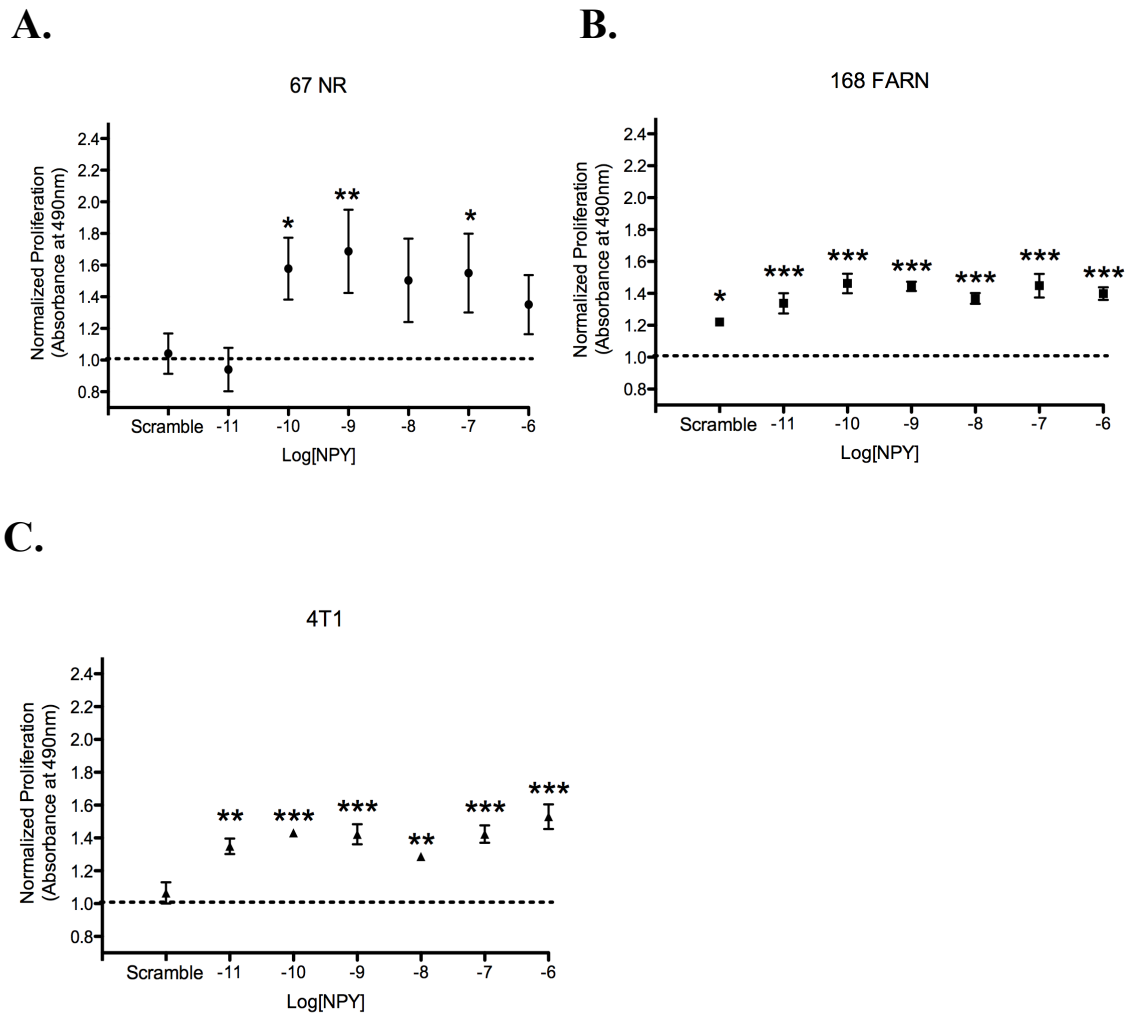

Figure 2.3 NPY stimulates proliferation of 67NR, 168FARN, and 4T1 cell lines. NPY treatment stimulated an increase in proliferation of all three cell lines at various concentrations (NPY 10^{-11}M-10^{-6}M). **(A. 67NR)** A proliferative effect was stimulated by NPY at 10^{-10}M, 10^{-9}, 10^{-7}M. **(B. 168 FARN)** A proliferative effect was stimulated by all tested concentrations of NPY and a subtle stimulation by the scrambled form of NPY. **(C. 4T1)** A proliferative effect was stimulated by all tested concentrations of NPY. (All values were statistically compared to respective control cell growth, * denotes $p<0.05$, ** denotes $p<0.01$, *** denotes $p<0.001$, One-way ANOVA).

2.3.4 Effect of Y5R blockade on proliferation on 67NR, 168FARN, 4T1

To determine the specific contribution of Y5R activation in NPY-stimulated proliferation, the effect of Y5R blockade by a Y5R- specfic antagonist (L-152804) was examined by the MTS proliferation assay. Cells were incubated with media containing NPY (10^{-6} M) and L-152804 (10^{-4} M). The data were compared to the proliferation of the cells at their peak proliferation. 67NR and 168FARN cell proliferation was stimulated most at 10^{-9} M NPY and 4T1 cell proliferation was stimulated most at 10^{-6} M NPY. The Y5R antagonist restored the growth of the cells to basal level in all three cell lines as depicted in Figure 2.4.

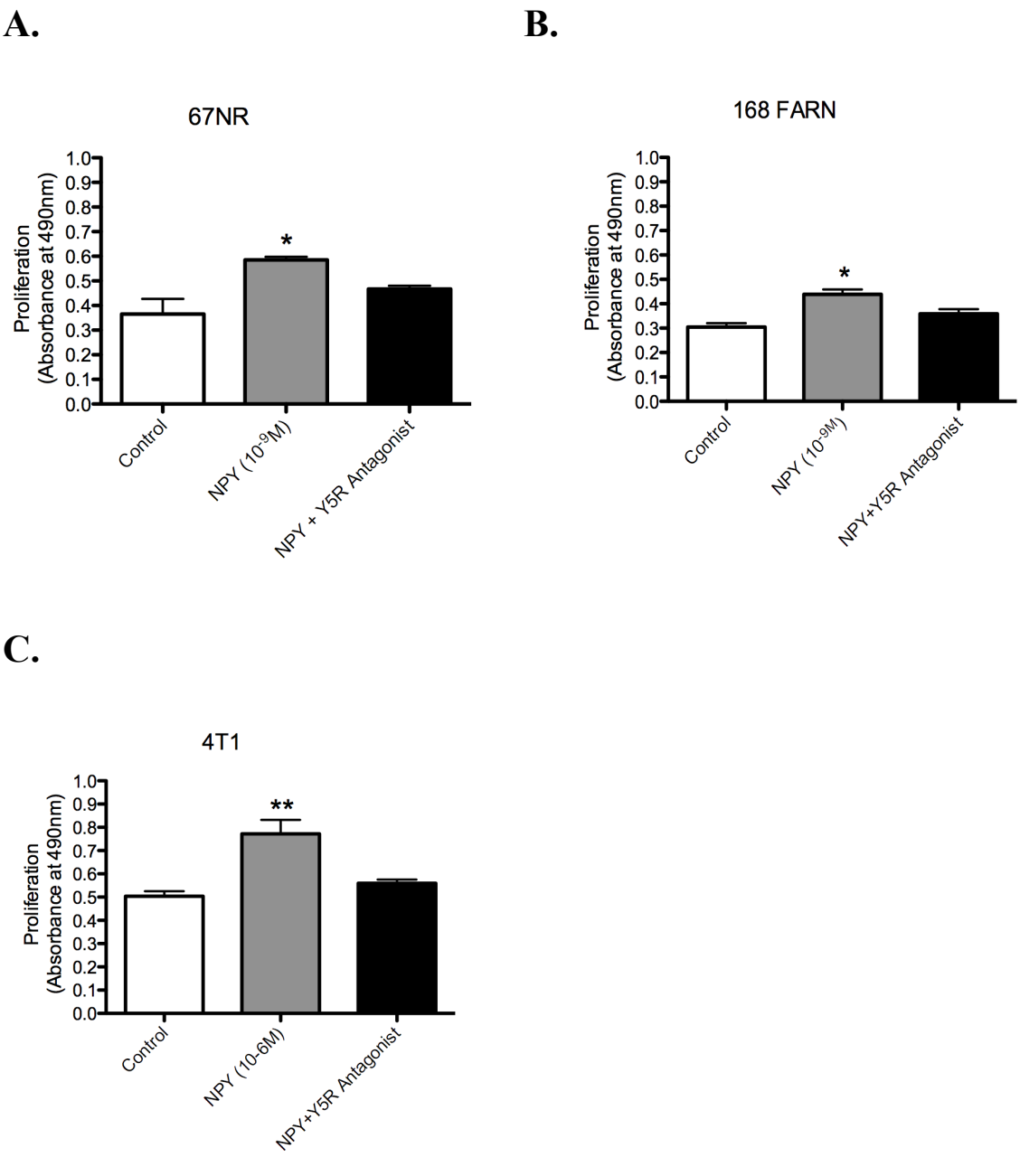

Figure 2.4 Y5R Blockade inhibits NPY stimulated proliferation of 67NR, 168FARN, and 4T1 cell lines. (A. 67NR) proliferation was significantly stimulated by 10^{-9}M NPY ($p<0.05$). NPY in conjunction with L-152 804 (10^{-4} M) restored proliferation to control. **(B. 168FARN)** proliferation was significantly stimulated by 10^{-9}M NPY ($p<0.05$). NPY in conjunction with L-152 804 (10^{-4} M) restored proliferation to control**. (C. 4T1)** proliferation was significantly stimulated by 10^{-6}M NPY ($p<0.05$). NPY in conjunction with L-152 804 (10^{-4} M) restored proliferation to control. (All values were statistically compared to respective control cell growth, * denotes $p<0.05$, ** denotes $p<0.01$, One- way ANOVA).

2.3.5 Establishing and validating 4T1 Y5R-Knockdown

A 4T1 Y5R-Knockdown (KD) was established previously as described above via shRNA. Positive vector transfection was selected using flow cytometry to select for GFP+ cells. 7-AAD viability gating was applied to analyze solely viable cells. Side scatter gate was applied to analyze solely single cells. Forward scatter gate was applied to confirm that cells were analyzed and not debris of the same size. GFP+ gate was applied to analyze cells that expressed GFP. Prior to the final flow cytometry sort, the GFP purity was evaluated at 98.1%. Post flow cytometry sort, the GFP purity was evaluated at 98.7%. GFP+ purity with applied gates post final sort is shown in Figure 2.5A.

Western blotting was conducted to confirm the knockdown and revealed a reduction of 51.67% in the expression of Y5R in the 4T1 Y5R-KD (n=6) compared to the 4T1 (n=6) cell line as shown in Figure 5B. Figure 5C shows reduced Y5R expression in the 4T1 Y5R-KD cell line in the membrane and cytoplasm compared to the 4T1 cell line.

A.

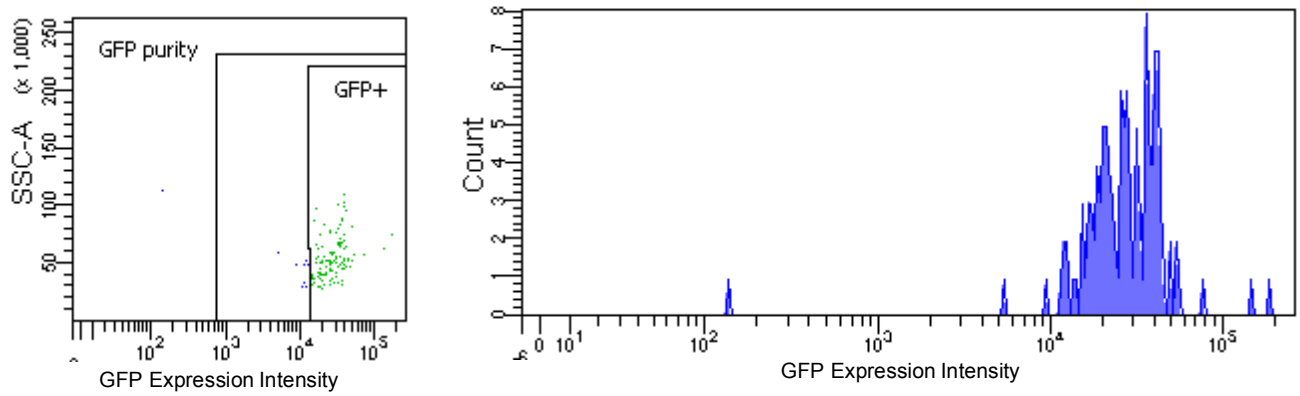
GFP purity
GFP+
SSC-A (x 1,000)
GFP Expression Intensity
Count
GFP Expression Intensity

B.

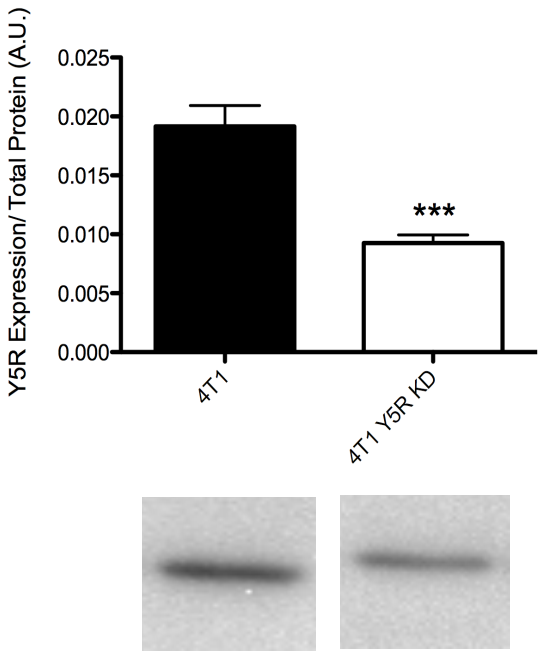
Y5R Expression/ Total Protein (A.U.)
0.025
0.020
0.015
0.010
0.005
0.000
***
4T1
4T1 Y5R KD

C. 4T1 4T1 Y5R-KD

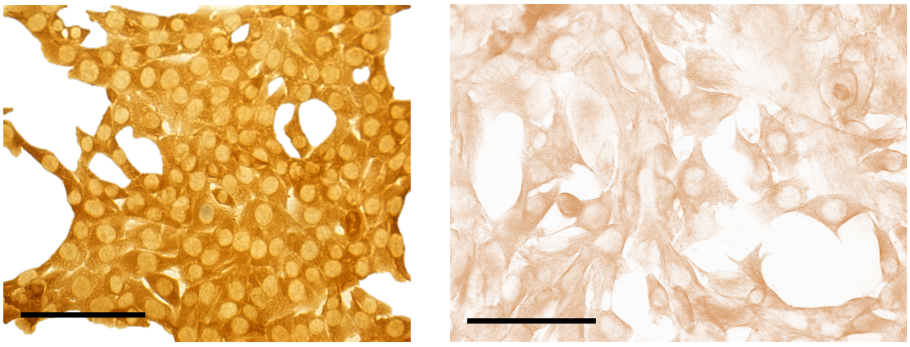

Figure 2.5 shRNA Y5R Specific Knockdown Decreased Y5R Expression (A. Flow Cytometry) 4T1 Y5R KD achieved via shRNA sorted via flow cytometry with a purity of 98.7% GFP+. 7-AAD viability gate, side-scatter gate, forward scatter gate and final GFP+ gate applied. **(B. Western Blot)** Densitometry quantification of 4T1 and 4T1 Y5R KD cell lysates normalized to total protein depicting the significantly reduced Y5R expression of 4T1 Y5R KD cell line compared to the 4T1 cell line. Densitometric data are presented as Y5R expression normalized to total protein expression discerned from Coomassie blue staining average lane intensity. Data are presented as mean$\pm$ SE (n=6, *** represents a significant difference from 4T1 cell line $p<0.001$, un-paired t-test). **(C. Immunocytochemistry of 4T1 and 4T1 Y5R KD)** Immunocytochemistry of 4T1 and 4T1 Y5R KD cells with decreased cytoplasmic Y5R expression (Scale bar=100µm).

2.3.6 Effect of NPY on Proliferation of 4T1 and 4T1 Y5R-KD

An MTS assay was conducted on the 4T1 and 4T1 Y5R-KD cell line to elucidate the proliferative effect that NPY would have on the newly developed strain with a diminished Y5R expression. The MTS Assay revealed 4T1 and 4T1 Y5R-KD cell strains proliferate at similar rates in the absence of NPY as shown by the control in Figure 6A. As a negative control, a scrambled sequence of NPY was applied to both 4T1 and 4T1 Y5R-KD cell lines. The scrambled NPY sequence did not induce proliferation of the 4T1 and 4T1 Y5R-KD cell lines as shown in Figure 2.6A. This is expected as scrambled NPY does not activate targeted NPY receptors. 4T1 and 4T1 Y5R-KD cells responded significantly different to NPY stimulation ($p<0.05$, Two- way ANOVA). 4T1 cells achieved a plateau of proliferation at 10^{-10} M NPY as shown in Figure 2.6B. In contrast, the 4T1 Y5R-KD cell line requires a greater concentration of 10^{-7} M NPY, for cell proliferation to plateau as shown in Figure 2.6C. There is a significant difference in proliferation between 4T1 and 4T1 Y5R KD cells at concentrations of 10^{-10} M ($p<0.05$), 10^{-9} M ($p<0.05$), 10^{-8} M ($p<0.05$), and 10^{-6} M ($p<0.05$) as shown in Figure 2.6A($p<0.05$, Two way ANOVA). 4T1 Y5R-KD cell proliferation is stimulated solely at 10^{-7} M ($p<0.05$) as shown in Figure 2.6C, compared to 4T1 cells that proliferate at 10^{-10} M ($p<0.05$), 10^{-9} M ($p<0.05$), 10^{-7} M ($p<0.01$), and 10^{-6} M ($p<0.01$) as shown in Figure 2.6B. Therefore, 4T1 Y5R-KD requires more NPY to enhance proliferation compared to 4T1 cells.

A.

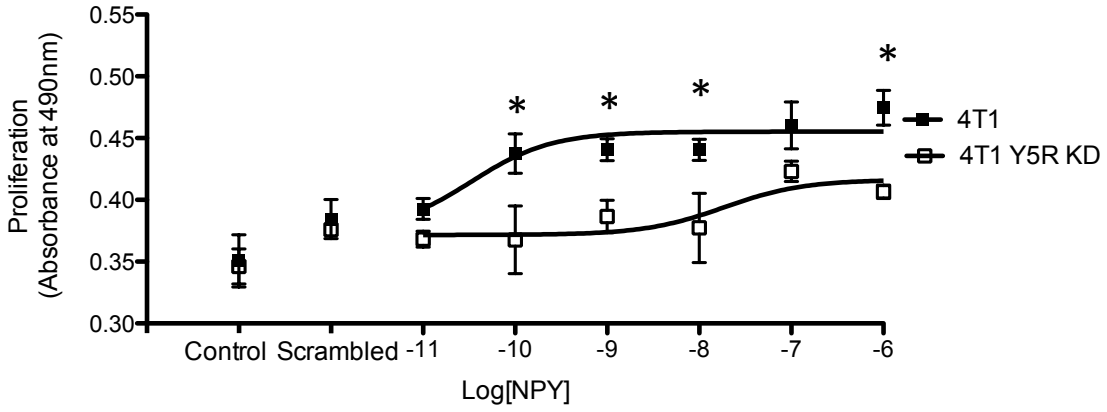
Proliferation (Absorbance at 490nm)
0.55
0.50
0.45
0.40
0.35
0.30
Control
Scrambled
-11
-10
-9
-8
-7
-6
Log[NPY]
4T1
4T1 Y5R KD
*

B.

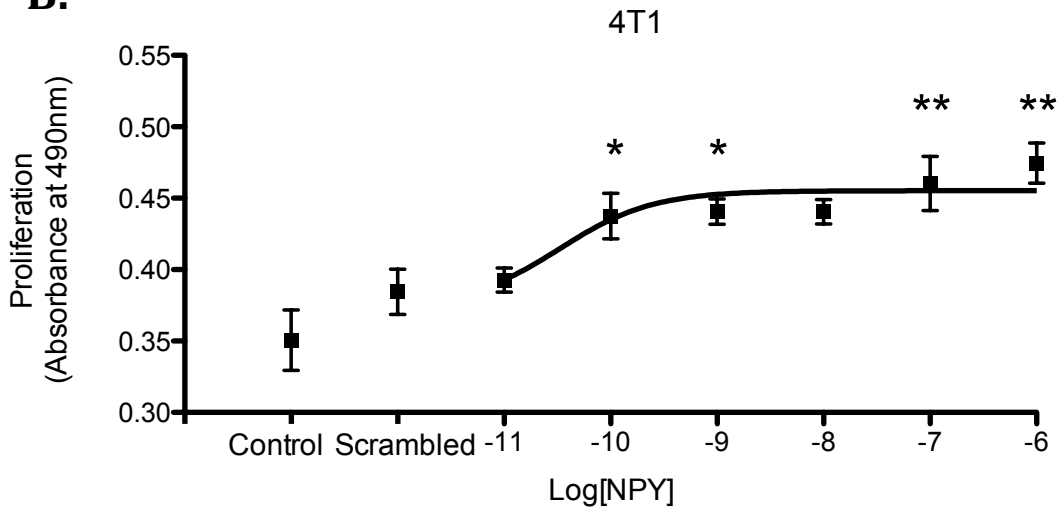
4T1
Proliferation (Absorbance at 490nm)
0.55
0.50
0.45
0.40
0.35
0.30
Control
Scrambled
-11
-10
-9
-8
-7
-6
Log[NPY]
*
**

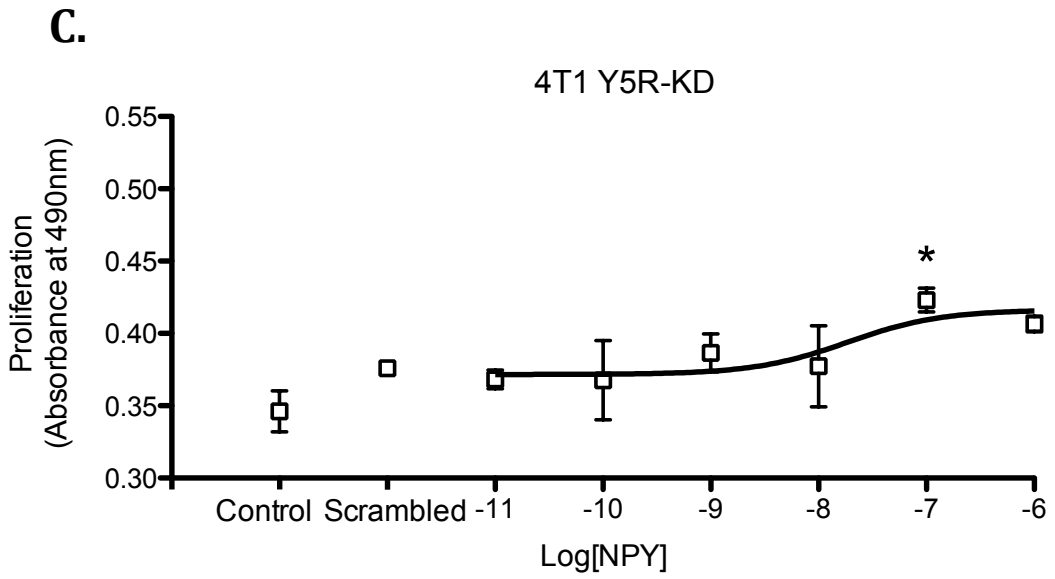

Figure 2.6 MTS Assay of 4T1 and 4T1 Y5R-KD with NPY stimulation (10^{-11}-10^{-6}M) (A. 4T1 and 4T1 Y5R-KD proliferation) MTS Proliferation Assay demonstrated that without NPY stimulation, there is no significant difference in proliferation between 4T1 and 4T1 Y5R KD cells. 4T1 and 4T1 Y5R-KD cells proliferate significantly differently in response to NPY ($p<0.05$). The cell line accounted for 40.81% of variation of proliferation in response to NPY ($p<0.05$, Two way ANOVA with repeated measures, n=3). Concentration accounted for 26.91% of variation of proliferation in response to NPY ($p<0.01$, Two way ANOVA with repeated measures, n=3). There was a significant difference in proliferation between 4T1 and 4T1 Y5R KD cells at concentrations of 10^{-10} M ($p<0.05$), 10^{-9} M ($p<0.05$), 10^{-8} M ($p<0.05$), and 10^{-6} M ($p<0.05$, Two way ANOVA with repeated measures, n=3). **(B. 4T1)** MTS Proliferation Assay demonstrated that NPY has a stimulatory effect on proliferation 4T1 cells at concentrations of 10^{-10} M ($p<0.05$), 10^{-9} M ($p<0.05$), 10^{-7} M ($p<0.01$), and 10^{-6} M ($p<0.01$) of NPY compared to un-stimulated 4T1 cells (One-way ANOVA with repeated measures, n=3). **(C. 4T1 Y5R-KD)** NPY stimulated proliferation of 4T1 Y5R-KD cells solely at a concentration of 10^{-9} M compared to un-stimulated 4T1 Y5R-KD cells (One-way ANOVA with repeated measures, n=3).

2.3.7 Effect of Y5R blockade on proliferation on 4T1 and 4T1 Y5R-KD

The effect of Y5R blockade by a Y5R- specfic antagonist (L-152804) was examined by the MTS proliferation assay. Cells were incubated with media containing NPY (10^{-6} M) and L-152804 (10^{-4} M). The Y5R antagonist restored the growth of the cells to basal level in 4T1 cells as shown in Figure 2.7A. There was no significant difference in the proliferation of 4T1 Y5R-KD cells between control, maximal NPY- stimulated proliferation and maximal NPY in conjunction with L-152804 as shown in Figure 2.7B.

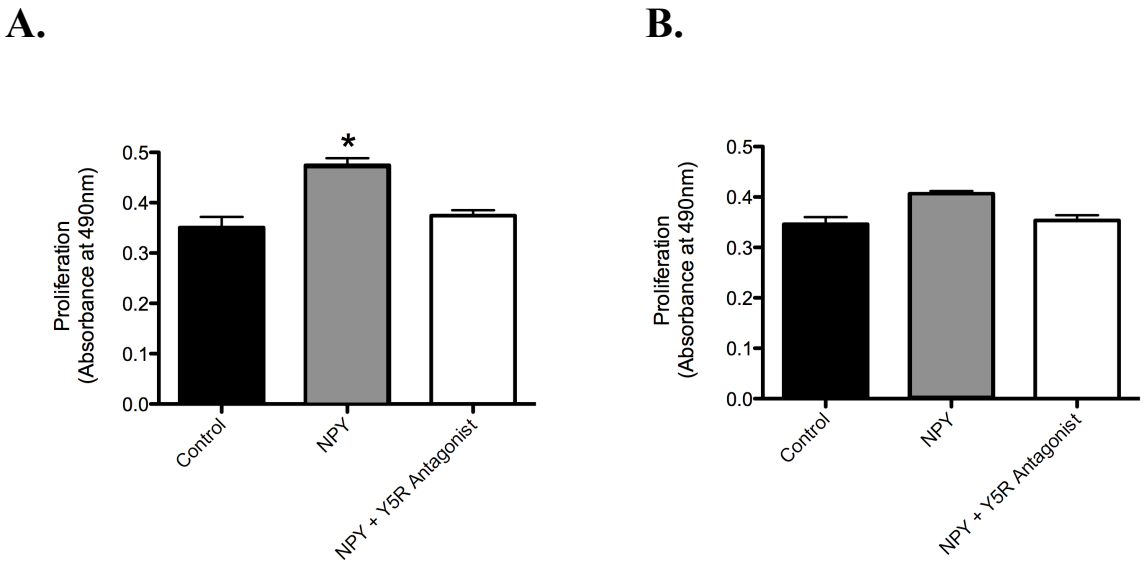

Figure 2.7 MTS Assay of 4T1 and 4T1 Y5R-KD with NPY and Y5R Antagonism. (A. 4T1) Proliferation was significantly stimulated by 10^{-6}M NPY ($p<0.05$). NPY in conjunction with L-152 804 (10^{-4} M) restored proliferation to control. **(B. 4T1 Y5R-KD)** There was no significant difference between treatments in 4T1 Y5R-KD cells (All values were statistically compared to respective control cell growth, * denotes $p<0.05$, One- way ANOVA).

2.3.8. Iron oxide labeling of 4T1 and 4T1-Y5R KD cells for injection

Prior to orthotopic injection, 4T1 and 4T1 Y5R-KD cells were pre-labeled with MPIOs to track proliferative status via iron dilution. The large iron oxide nanoparticle size permits single cell tracking with MRI. Figure 2.8 shows iron oxide nanoparticles stained with Perls' Prussian Blue and cell nuclei stained with Nuclear Fast Red of 4T1 cells (Figure 2.8A) and 4T1 Y5R-KD cells (Figure 2.8B). Qualitatively, as seen in Figure 2.8, it appears that both 4T1 and 4T1 Y5R-KD cells were nearly all labeled, prior to injection.

A. **B.**

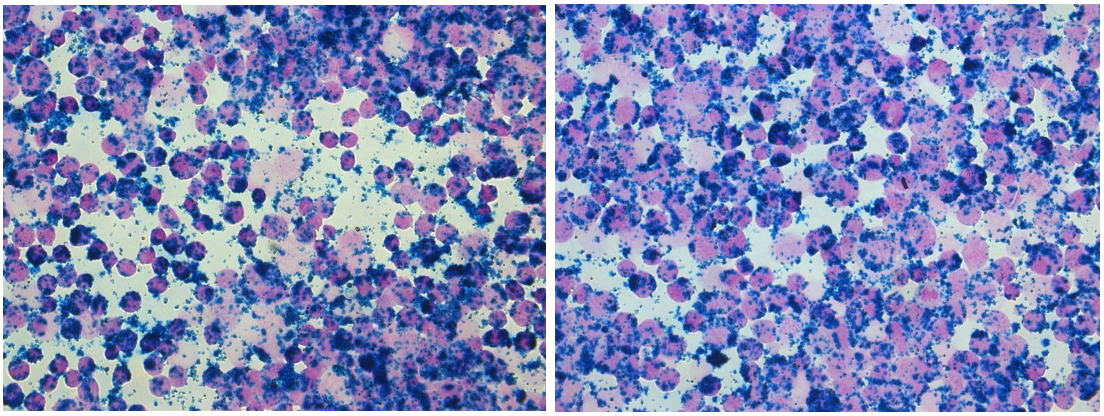

Figure 2.8 PPB and NFR Staining of 4T1 and 4T1 Y5R-KD Cells (A. 4T1) Nuclei stained with Nuclear Fast Red and iron oxide nanoparticles stained with Perl's Prussian Blue of cells injected for MR imaging **(B. 4T1 Y5R-KD)** Nuclei stained with Nuclear Fast Red and Iron oxide nanoparticles stained with Perl's Prussian Blue of cells injected for MR imaging.

2.3.9 *In vivo* mammary fat pad tumour appearance and volumes

BALB/c mice were imaged on days 7, 14, 21 and 28 with the bSSFP imaging sequence. 4T1 and 4T1 Y5R-KD cells were pre-labeled with MPIOs to allow for tracking cells and monitoring proliferation *in vivo;* as cells proliferate the iron is diluted between daughter cells to a level below the sensitivity of MRI. The fraction of iron at each time point can be compared between the two cell lines to estimate patterns and degree of *in vivo* cell proliferation.

Figure 2.9 shows representative MR images of the mouse body at day 14 post 4T1 cell injection. The locations of the mammary fat pad tumour are outlined in green. Isovolumetric voxels permit visualization of the tumour in the sagittal, coronal and axial orientations without distortion. Figure 2.10 shows similar images for a mouse that received 4T1 Y5R KD cells. In both subject groups, signal loss appears within the primary tumour.

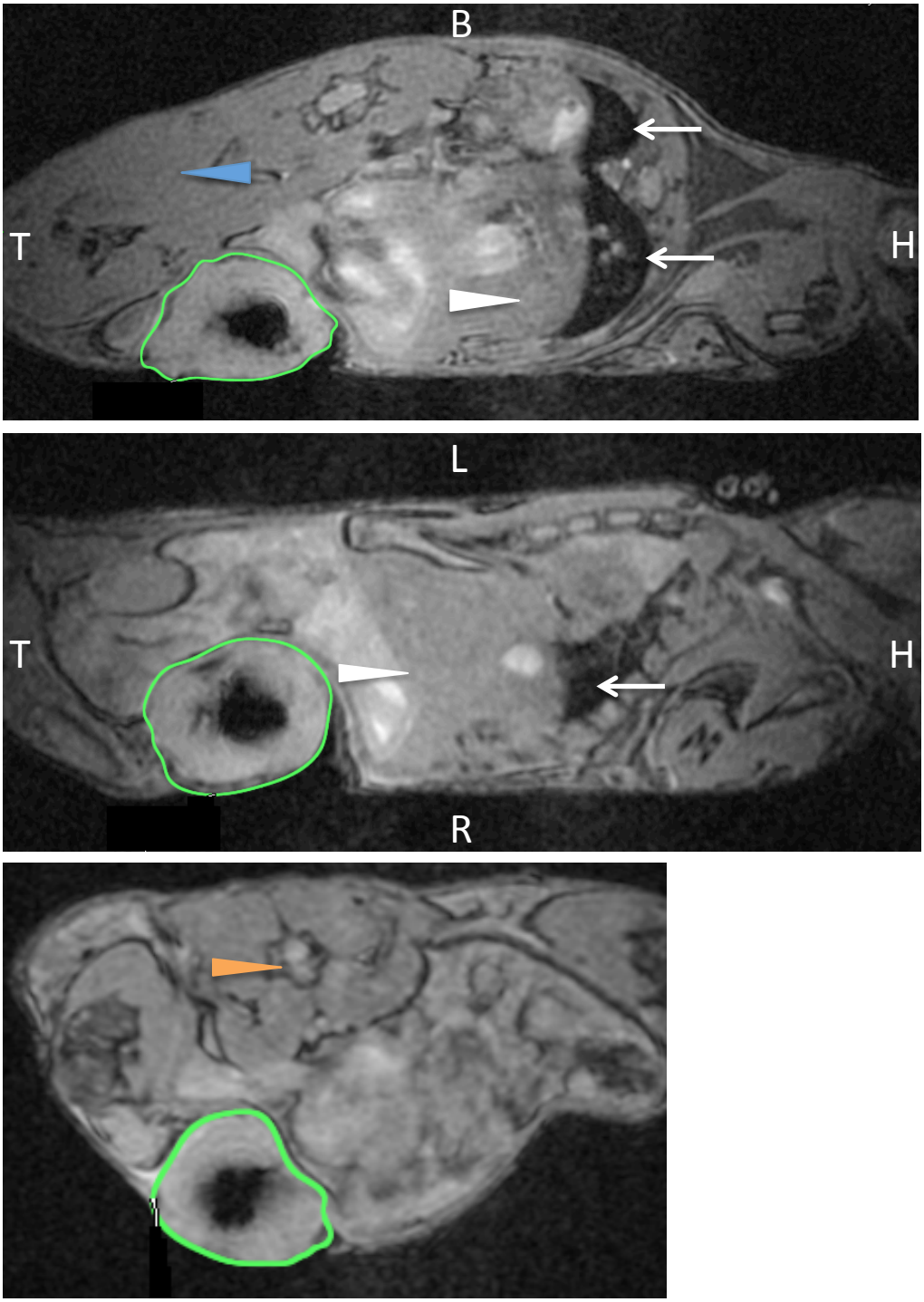

Figure 2.9 MR Appearance of 4T1 MPIO Pre-labelled Mammary Fat pad Tumour at Day 14. (A. Sagittal view) H-head, T-tail, B-back, white arrows- lungs, white arrow head- liver, blue arrow- muscle. **(B. Coronal view)** H-head, T-tail, L-left, R-right, white arrow- lung, white arrow head- liver. **(C. Axial view)** Orange arrow head-spine. Tumour is outlined in green in all images.

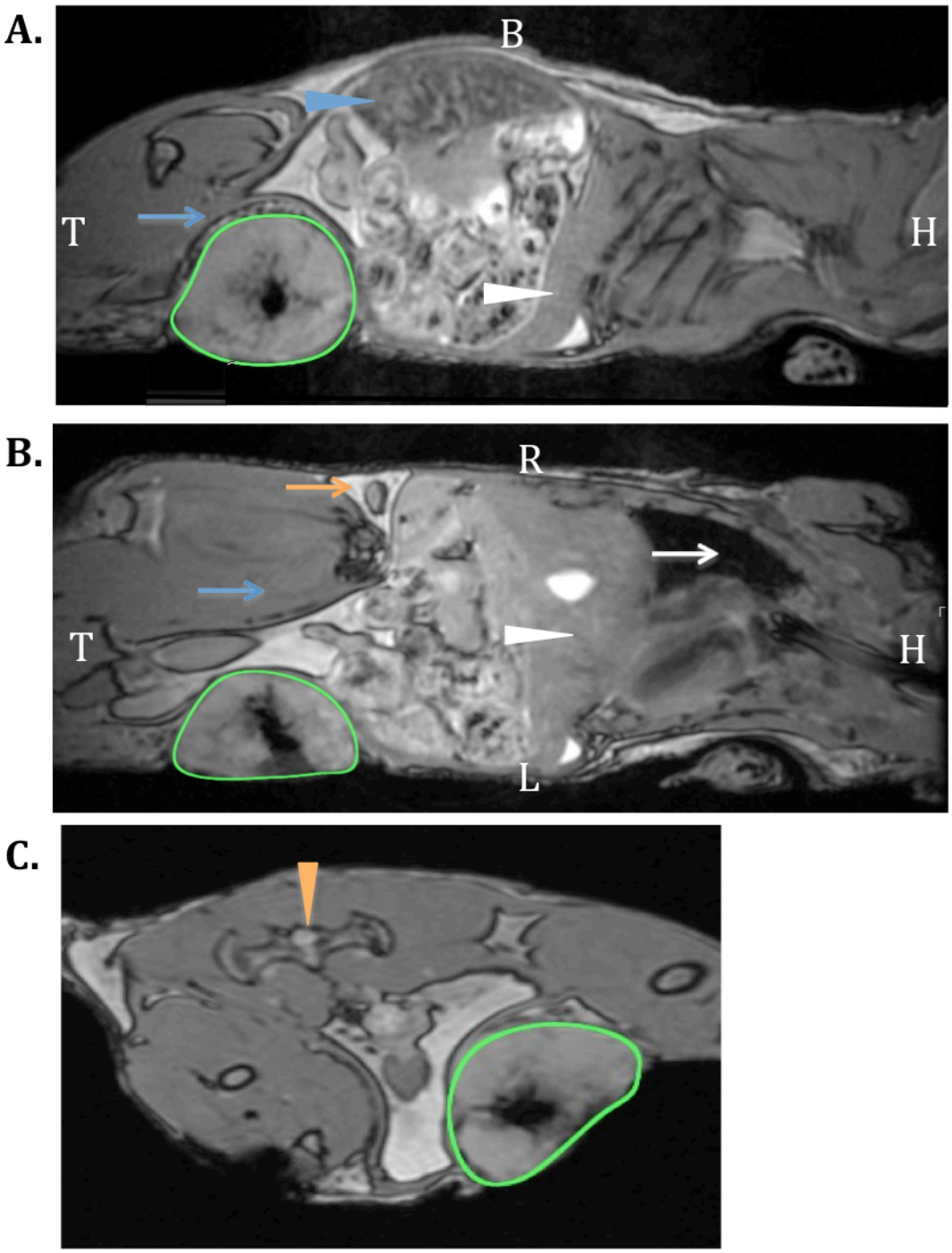

Figure 2.10 MR Appearance of 4T1 Y5R-KD MPIO Pre-labeled Mammary Fat Pad Tumour at Day 14. (A. Sagittal view) H-head, T-tail, B-back, white arrow head- liver, blue arrow- muscle, blue arrow head-spleen. **(B. Coronal view)** H-head, T-tail, L-left, R- right, white arrow- lung, white arrow head- liver, blue arrow-muscle, orange arrow- lymph node. **(C. Axial view)** Orange arrow head-spine. Tumour is outlined in green in all images.

2.3.10 Longitudinal MRI of primary tumour

Figure 2.11 and 2.12 show representative cropped images of the 4T1 and 4T1 Y5R-KD primary mammary fat pad tumours, respectively, at each imaging time point and the corresponding signal intensity colour maps. In the colour maps, blue represents regions of signal hypointensity (due to iron oxide particles), yellow represents regions of hyperintense signal (due to fluid accumulation) and green represents intermediate signal intensities (tumour mass). In all mice the tumour size increased over time.

For all mice with 4T1 tumours (Figure 2.11), a large region of low signal intensity was observed in the central part of the tumour at day 7. Iron appears with low signal intensity in bSSFP images, therefore, this observation suggests the presence of iron retaining cells in the tumour. Over time, as the tumour increased in size this region of central signal loss decreased in size. In images acquired on day 28 subtle regions of signal hyperintensity were apparent in all tumours. Fluids appear bright in bSSFP images, therefore, these regions suggest that there is accumulation of fluid, possibly due to necrosis, in tumours at this timepoint.

Images of 4T1 Y5R-KD tumours showed some differences compared to 4T1 tumours (Figure 2.12). Signal loss was again observed in images of the 4T1 Y5R-KD tumours at day 7, however, the signal loss was not restricted to the central zone of the tumour. Instead signal loss was observed distributed throughout the tumour mass. In addition, the total volume of signal loss was less in 4T1 Y5R-KD tumours compared to 4T1. Over time, this pattern of signal loss persisted. As with 4T1 tumours the region of signal loss decreased over time. In one of the five 4T1 Y5R-KD mice no signal loss could be detected in the day 28 image of the tumour. In images acquired on day 28 regions of signal hyperintensity became apparent. A larger amount of the 4T1

Y5R-KD tumours were occupied by signal hyperintensity as compared to 4T1 tumours (Figure 2.13).

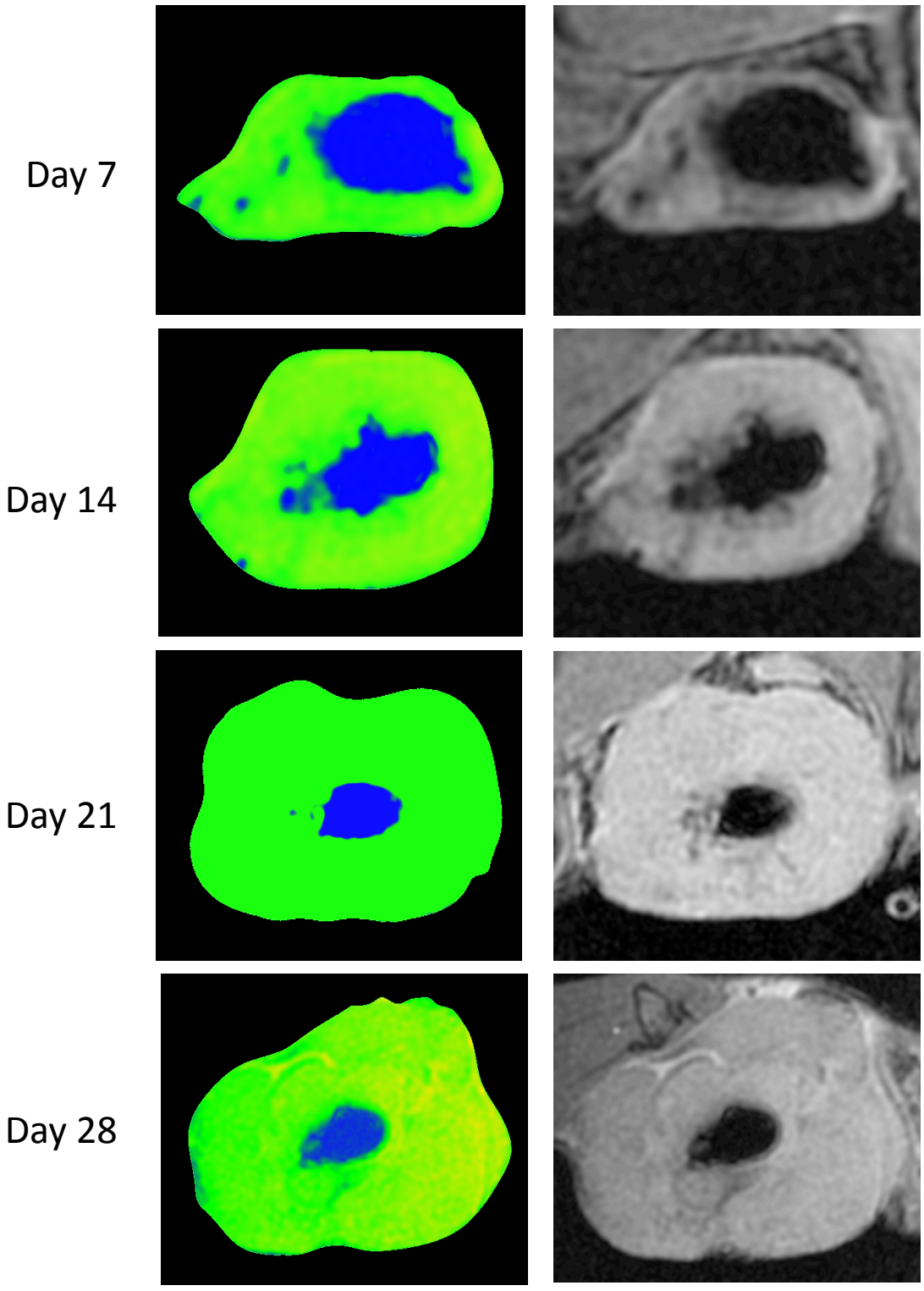

Figure 2.11 4T1 Mammary Fat Pad Tumours. MR image and colour map, respectively, of a MPIO pre-labeled tumour at days 7, 14, 21, and 28.

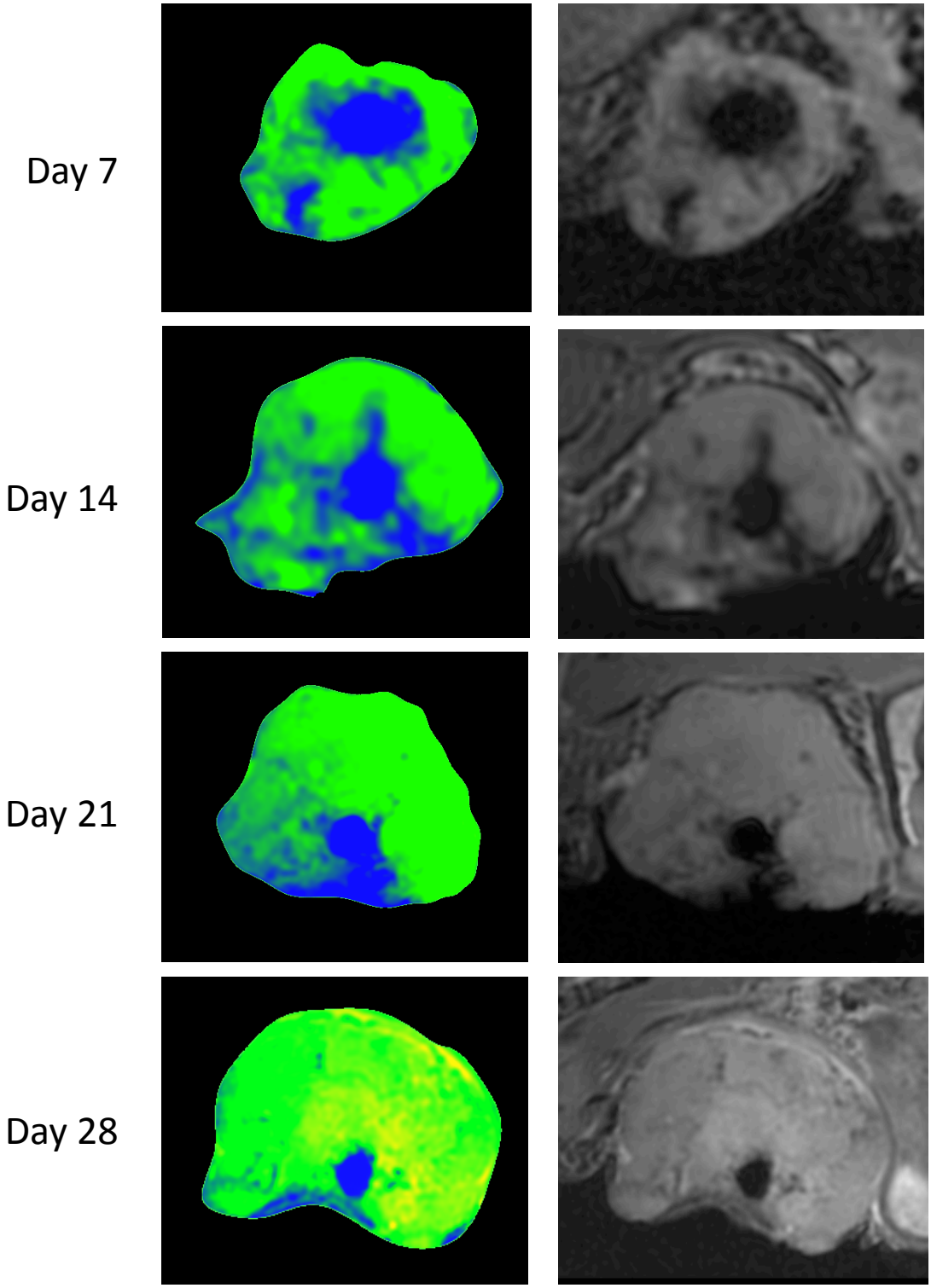

Figure 2.12 4T1 Y5R KD Mammary Fat Pad Tumours. MR image and colour map, respectively, of a MPIO pre-labeled tumour at days 7, 14, 21, and 28.

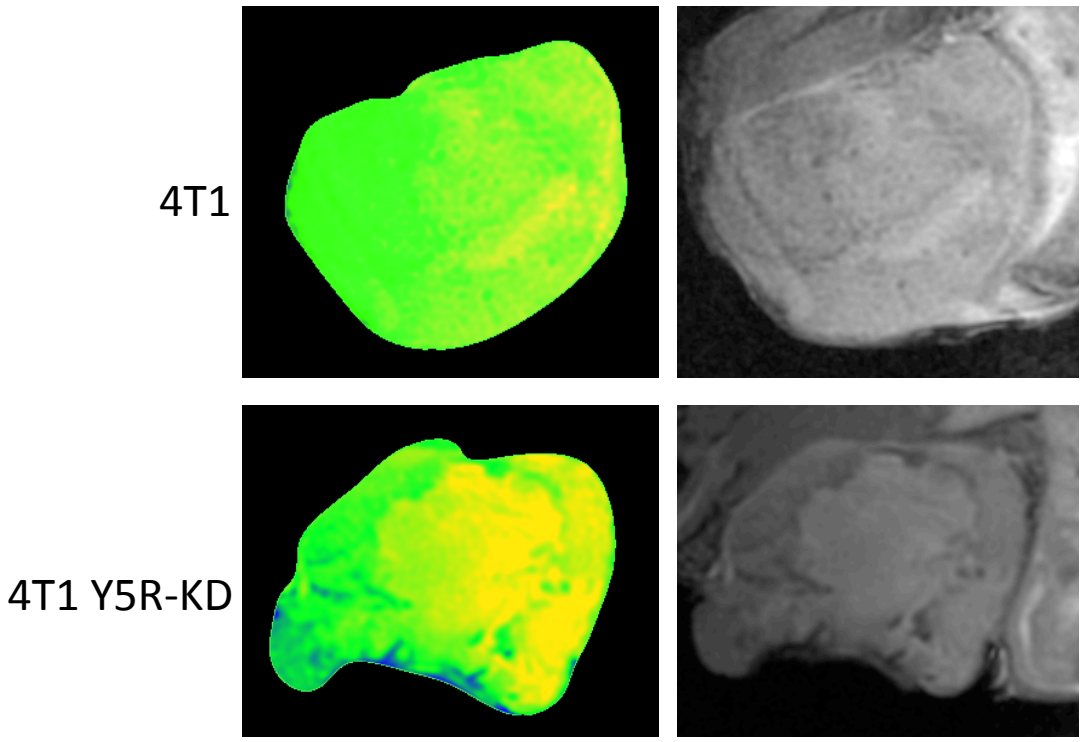

Figure 2.13 Representative 4T1 and 4T1 Y5R-KD tumours at Day 28 Highlighting Differences in Amount of Signal Hyperintensity. At day 28, the 4T1 Y5R-KD tumours has larger regions of signal hyperintensity compared to 4T1 tumours. Regions of hyperintensity are represented with yellow. Green represents intermediate signal intensity and blue represents signal hypointensity.

2.3.11 Volumes of the primary tumour and signal void regions

bSSFP images were collected in 3D, permitting measurement of tumour volume (Figure 2.14). The tumour volumes measured for the 4T1 and the 4T1 Y5R-KD cell lines were not significantly different at days 7, 14, and 21 between cell lines. At day 28 post- cell injection, the mean 4T1 tumour volume was significantly greater than the mean 4T1Y5R KD tumour volume ($p<0.001$, Two way ANOVA). This suggests that the tumourigenicity of the two cell lines is significantly different ($p<0.05$, Two way ANOVA). The tumour growth was modeled with an exponential equation ($Y=Y_0 * e^{k-x}$) for the 4T1 cell line ($Y_0=0.05261$, $k=0.1113$) and the 4T1 Y5R-KD cell ($Y_0=0.04209$, $k=0.1112$).

At day 7, the percentage of the tumours occupied by signal loss was significantly greater in 4T1 tumours (16.56 ± 7.89) compared to 4T1 Y5R-KD tumours (8.29 ± 2.48) ($p<0.001$). This was not significantly different at days 14, 21, and 28 (Figure 2.15). The change in signal loss over time between the two cell lines is significantly different ($p<0.01$, Two way ANOVA). A one-phase decay ($Y=Y_0 - plateau*e^{-kx} + plateau$) was fit to the 4T1 cell line signal void volume normalized to tumour volume ($Y_0=86.35$, plateau=1.19, K=0.2446, $R^2=0.7704$) and the 4T1 Y5R-KD cell line signal void volume normalized to tumour volume ($Y_0=20.11$, plateau=0.7975, K=0.1354, $R^2=0.7116$).

Figure 2.14 Mean 3D Tumour volume from MRI. The average tumour volume for the 4T1 and the 4T1 Y5R-KD cell lines were not significantly different at days 7, 14, and 21. 4T1 Y5R KD tumours were significantly smaller than 4T1 tumours at day 28 ($p<0.001$, Two way ANOVA). Tumourigenicity of the two cell lines is significantly different ($p<0.05$, Two way ANOVA). Tumour growth was modeled with an exponential equation ($Y=Y_0 * e^{k-x}$) for the 4T1 cell line ($Y_0=0.05261$, $k=0.1113$) and the 4T1 Y5R-KD cell ($Y_0=0.04209$, $k=0.111$)

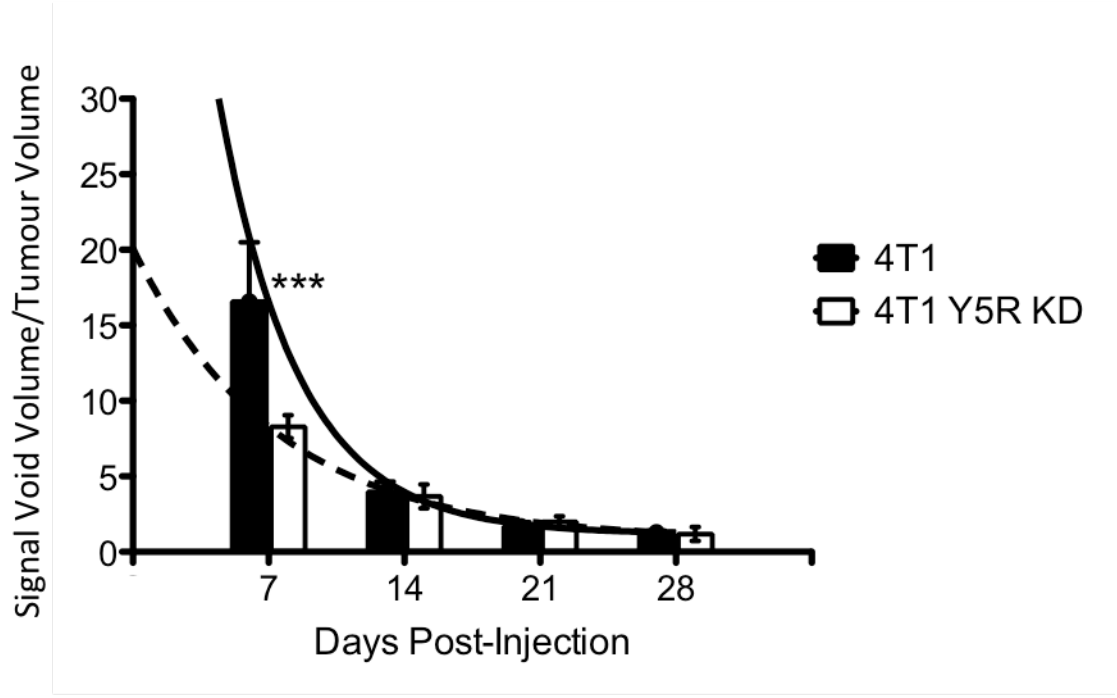

Figure 2.15 Signal Void Volume Normalized to Tumour Volume. Signal void volume normalized to tumour volume was significantly greater in 4T1 tumours than 4T1 Y5R-KD tumours at day 7. The iron void volume normalized to tumour volume of the 4T1 cell line and the 4T1 Y5R-KD cell line was not significantly different at days 14, 21, and 28 (Figure 12). The dilution of iron between the two cell lines is significantly different ($p<0.01$, Two way ANOVA). A one-phase decay ($Y=Y_0 - \text{plateau}*e^{-kx} + \text{plateau}$) was fit to the 4T1 cell line iron void volume normalized to tumour volume ($Y_0=86.35$, plateau=1.19, K=0.2446, $R^2=0.7704$) and the 4T1 Y5R-KD cell line iron void volume normalized to tumour volume ($Y_0=20.11$, plateau=0.7975, K=0.1354, $R^2=0.7116$).

2.3.12 Images of Metastases

Both lung and lymph node metastases were observed using MRI. Lung metastases were observed in both 4T1 and 4T1 Y5R-KD mice. MRI detectable lung metastases were observed as early as 21 days post cell implantation in 4T1 mice and in images acquired on day 28 in 4T1 Y5R-KD mice. Lung metastases were visible as regions of signal hyperintensity in the lung, which normally appears black in MR images because of air. At day 21, 3 of 4 4T1 mice had MRI detectable lung metastases. By day 28, all 4T1 mice had visible lung metastases. At day 28, 3 of 5 4T1 Y5R-KD mice had MRI detectable lung metastases. Lung metastases appeared larger in 4T1 mice. Representative images of lung metastases are shown in Figure 2.16.

Metastases in lymph nodes were only observed in mice that received the 4T1 Y5R-KD cells. Nodal metastases were detected in images of 3 of the 5 mice (Figures 2.17-2.19). Metastases were detected in either the contralateral or ipsilateral axillary node and in the ipsilateral inguinal node. In Figure 2.17 an axillary node metastasis is shown on the contralateral side to the primary tumour (yellow arrow). Images are shown in all three orientations. In Figure 2.18 an axillary node metastasis is shown on the ipsilateral side to the primary tumour (yellow arrow). This metastasis has two lobes. In Figure 2.18 an inguinal node metastasis is visible near the primary tumour. This metastasis is of particular interest since it contains a distinct region of signal void. Unfortunately in this study the nodes were not recovered for histological assessment.

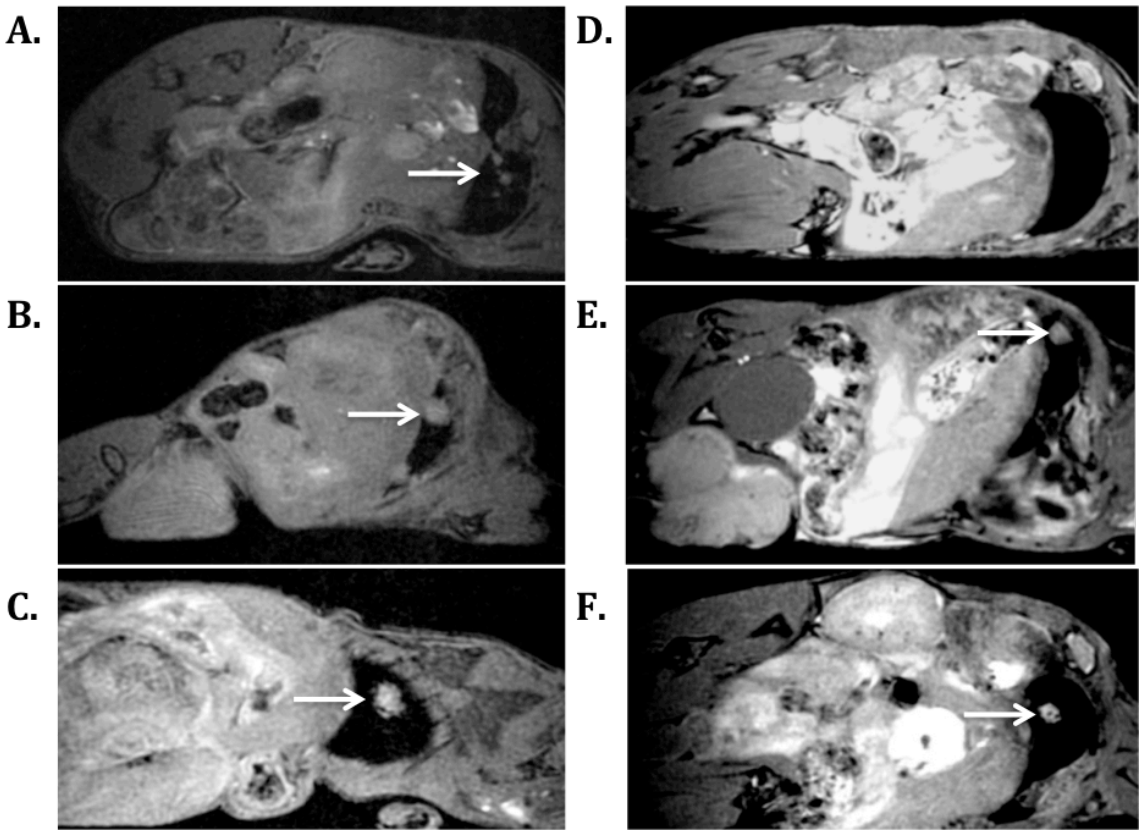

Figure 2.16 MR Images of Representative Lung Metastases. Sagittal image slices of mice bodies showing MRI detectable lung metastases (white arrow) as regions of signal hyperintensity on black lungs **(A. 4T1, day 21)** Representative lung metastases found in 3 of 4 4T1 mice at day 21. **(B and C. 4T1, Day 28)** Representative lung metastases found in all 4 4T1 mice at day 28. **(D. 4T1 Y5R-KD, day 21)** Representative lung images demonstrating lack of metastases at day 21 in 4T1 Y5R-KD mice. **(E and F. 4T1 Y5R-KD, Day 28)** Representative lung metastases found in 3 of 5 4T1 mice at day 28.

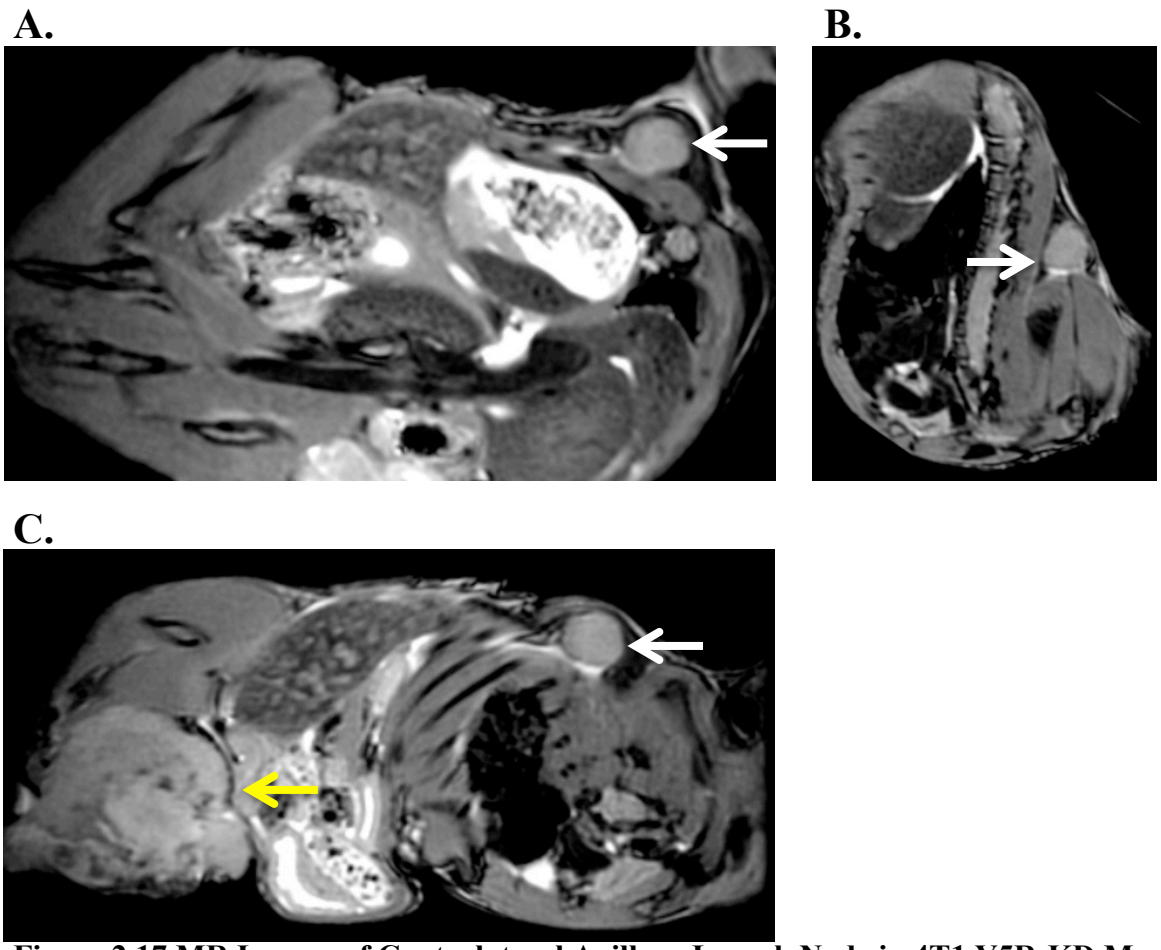

Figure 2.17 MR Images of Contralateral Axillary Lymph Node in 4T1 Y5R-KD Mouse at Day 28. (A. Coronal view) Enlarged axillary lymph node (white arrow) **(B. Axial view)** Enlarge axillary lymph node (white arrow) **(C. Sagittal view)** Enlarged contralateral axillary lymph node (white arrow) with heterogeneous mammary fat pad 4T1 Y5R-KD primary tumour (yellow arrow) with speckled signal voids and necrotic core.

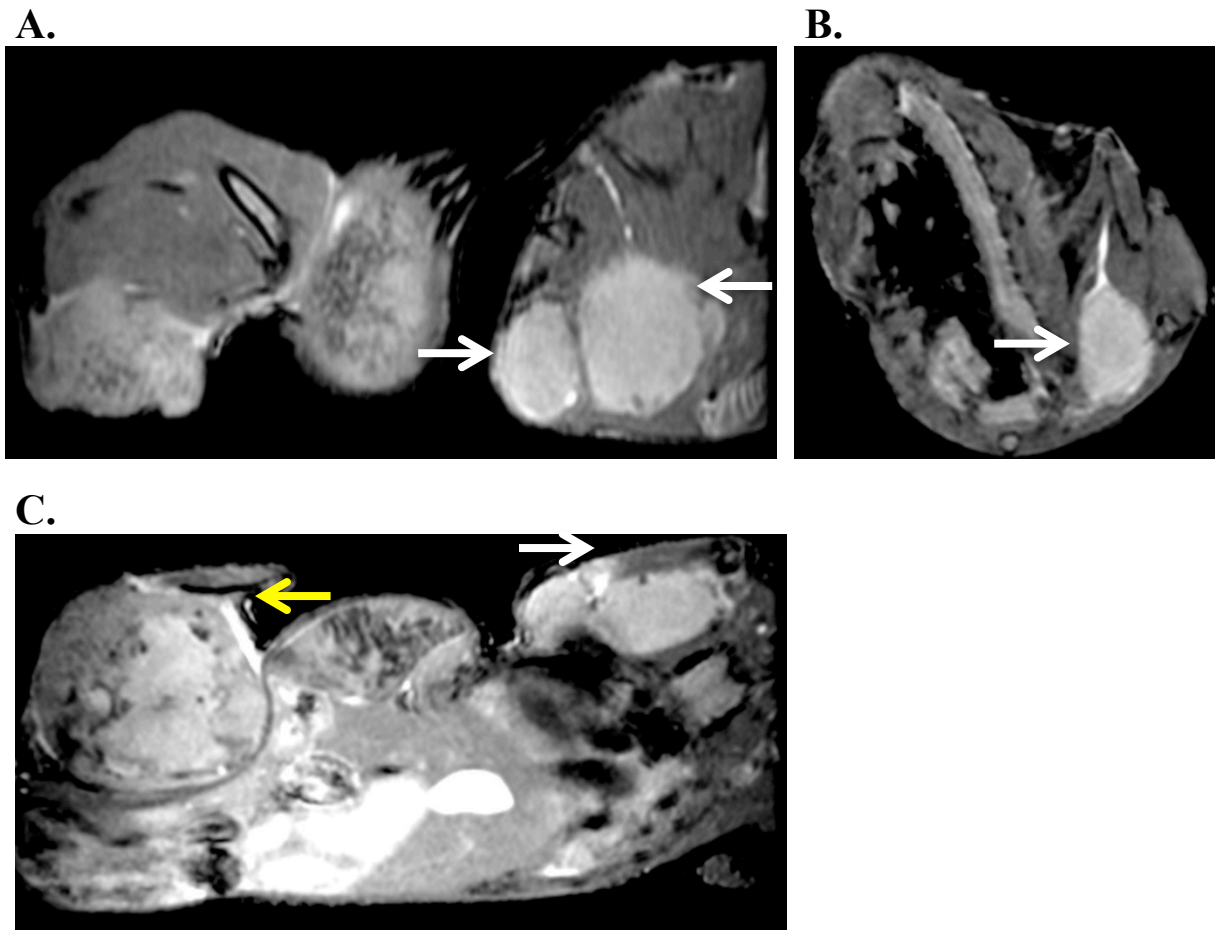

Figure 2.18 MR Images of Ipsilateral Axillary Lymph Node in 4T1 Y5R-KD Mouse at Day 28. (A. Coronal view) Enlarged axillary lymph node with two lobes (white arrows) **(B. Axial view)** Enlarge axillary lymph node (white arrow) **(C. Sagittal view)** Enlarged ipsilateral axillary lymph node (white arrow) with heterogeneous mammary fat pad 4T1 Y5R-KD primary tumour (yellow arrow) with speckled signal voids and necrotic core.

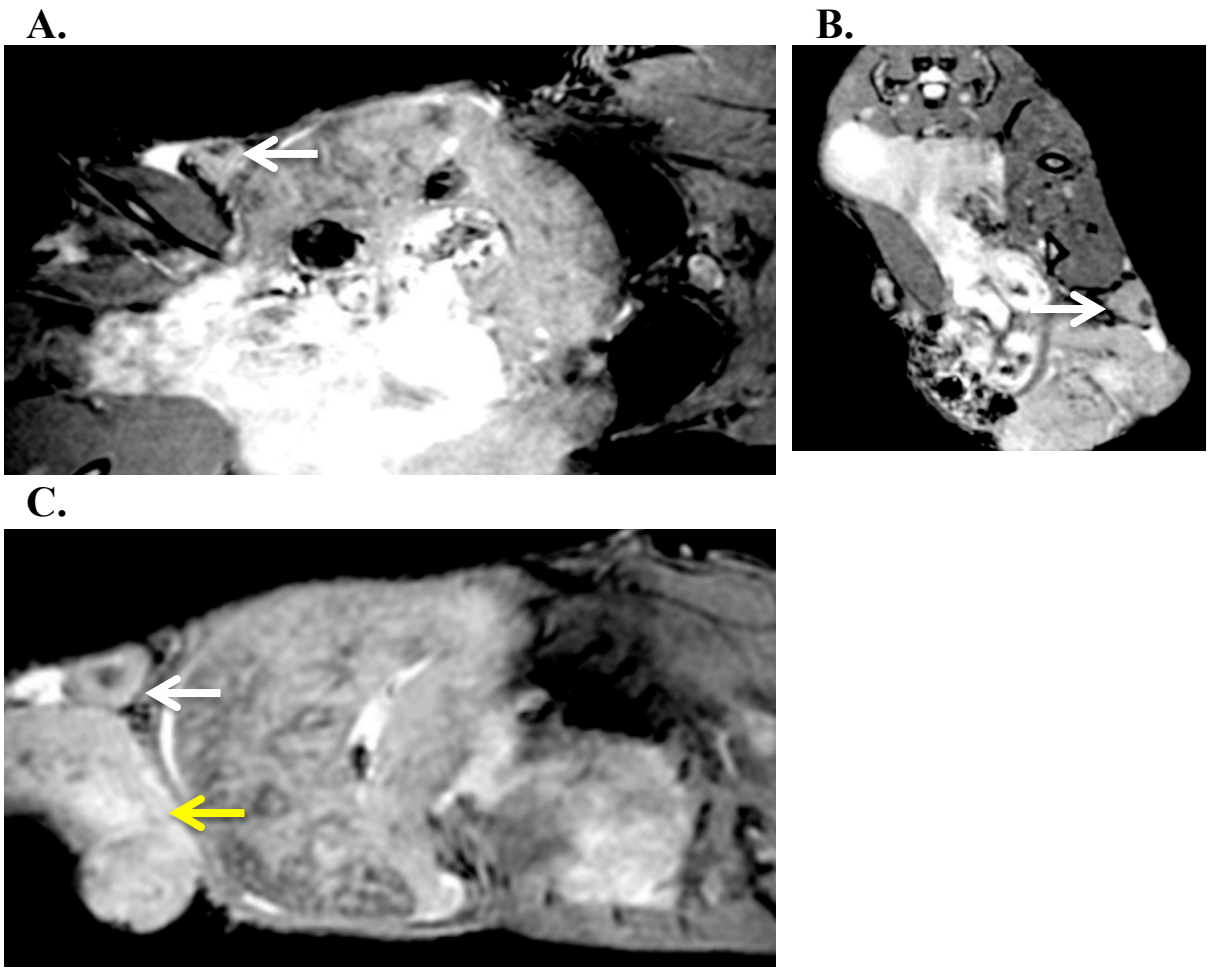

Figure 2.19 MR Images of Inguinal Lymph Node in 4T1 Y5R-KD Mouse at Day 28. (A. Coronal view) Inguinal lymph node with distinct signal void (white arrow) **(B. Axial view)** Inguinal lymph node with distinct signal void (white arrow) **(C. Sagittal view)** Inguinal lymph node with distinct signal void (white arrow) neighbouring heterogeneous mammary fat pad 4T1 Y5R-KD primary tumour (yellow arrow) with hypointense ulceration.

2.3.13 Histology of primary tumours

Primary mammary fat pad tumours were sectioned and stained with H&E and PPB&NFR to visualize tumour morphology and identify iron oxide nanoparticle localization, respectively. Tumors from both cell lines had similar histological appearances. Figure 2.20 shows representative H&E stained sections of 4T1 and 4T1 Y5R-KD tumors at Day 28. Examination of the tumors revealed that they frequently contained regions of low cell density, consistent with the heterogeneous signal in MR images. Signal hyperintensity in bSSFP images represents the presence of fluid or fat accumulation, as previously shown in Figure 2.13. Examination of H&E revealed necrotic zones in both tumour types.

Figure 2.21 shows representative PPB stained sections of 4T1 and 4T1 Y5R-KD tumors at Day 28. Figures 2.21A-C shows the PPB-positive cells in a section from a 4T1 tumour and the corresponding mouse MRI. PPB-positive cells were typically located centrally within the tumour section, which agreed well with observations from MRI (2.21C). Figure 2.21D&E show PPB staining in a section from a 4T1 Y5R-KD tumour at day 14 and the corresponding MRI. PPB staining was rarely observed in the small sample of day 28 4T1 Y5R-KD tumour sections we examined.

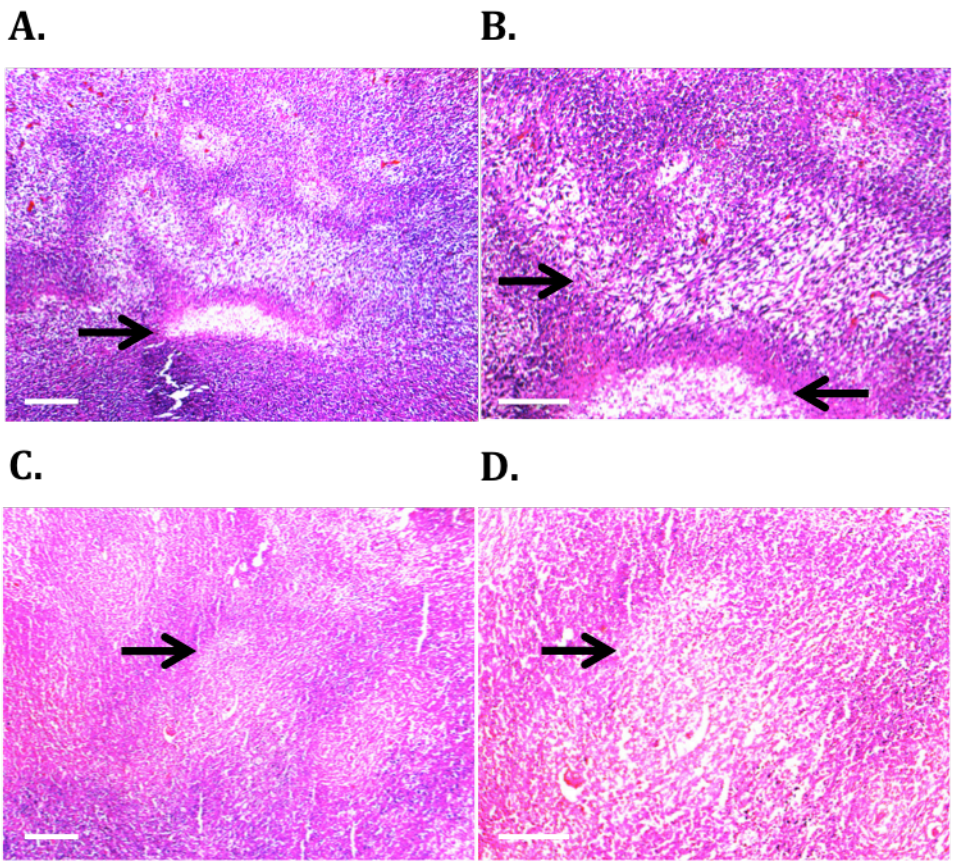

Figure 2.20 Representative H&E of 4T1 and 4T1 Y5R-KD primary tumours with necrosis at Day 28. Necrosis (denoted by black arrows) was found in both 4T1 and 4T1 Y5R-KD tumours at Day 28. **(A and B.)** H&E of 4T1 tumour. Scale bar for A= 300µm. Scale bar for B= 200µm **(C and D.)** H& E of 4T1 Y5R-KD tumour. Scale bar for C= 300µm. Scale bar for D= 200µm

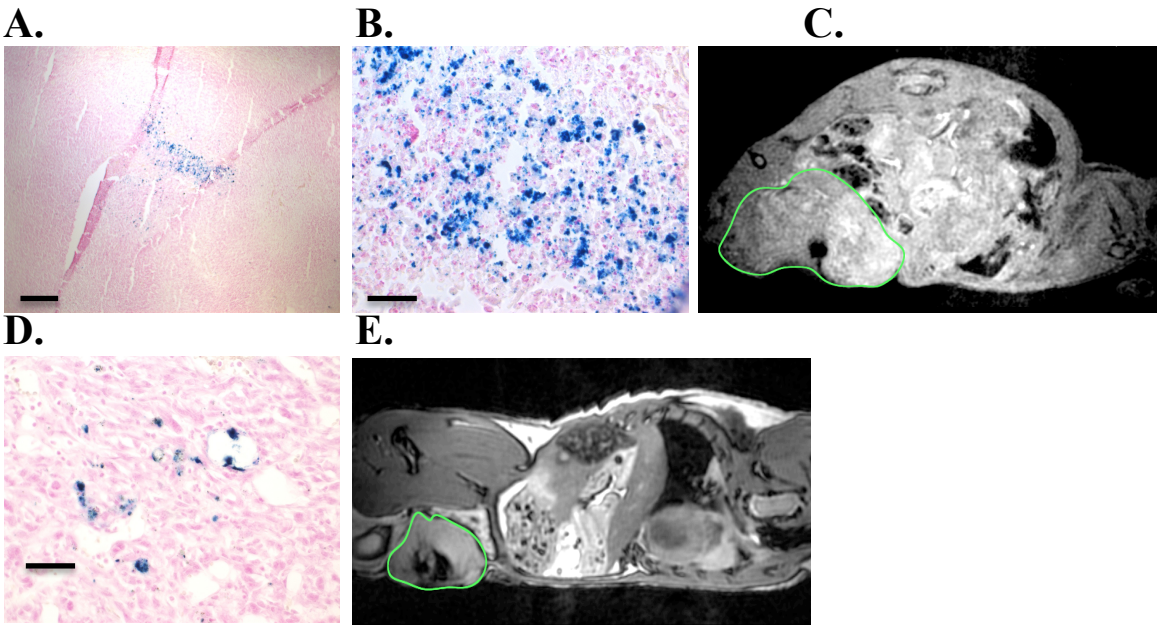

Figure 2.21 Representative PPB and NFR of 4T1 and 4T1 Y5R-KD Primary Tumours with Corresponding MR images. (A and B. 4T1 PPB&NFR) Iron appears blue with PPB staining. A&B show positive PPB staining in a 4T1 tumour at Day 28 which is concentrated at the core of the tumour. Scale bar for A= 50μm. Scale bar for B= 200μm **(C.4T1 MR)** Sagittal MR image depicting hypointensity concentrated at the core of the tumour. Tumour is outlined in green. **(D. 4T1 Y5R-KD PPB&NFR)** Positive PPB staining in a 4T1 Y5R-KD tumour at Day 14. Scale bar for C= 200μm. **(E. 4T1 Y5R-KD MR)** Sagittal MR image depicting hypointensity distributed throughout the tumour. Tumour is outlined in green.

2.3.14 Y5R Immunohistochemistry of primary tumour

Immunohistochemistry (IHC) was conducted on tumours resected at days 14, 21, and 28 in the 4T1 Y5R-KD model and at day 28 in the 4T1 model to evaluate the contribution of Y5R to tumour development. Optimization IHC was conducted on control BALB/c brains and the negative control, without the Y5R primary antibody, displayed no observable fluorescence (Appendix B). Figure 2.22A shows subtle Y5R expression at the edge of the tumour in the 4T1 Y5R-KD model at day 14, there is no observable Y5R expression in the core of the tumour at this time point. Figure 2.22B shows a diffuse distribution of Y5R in the 4T1 Y5R-KD model at day 21 throughout the tumour with enhancement at the edge of the tumour. Figure 2.22C shows a homogeneous distribution of Y5R in the 4T1 Y5R-KD tumour at day 28 with subtle enhancement at the edge of the tumour. Figure 2.20C Y5R in the 4T1 Y5R-KD model at day 28 is comparable to the Y5R expression in the 4T1 model at day 28 in Figure 2.22D. The 4T1 tumour at day 28 has high Y5R expression throughout the tumour and is enhanced at the tumour edge.

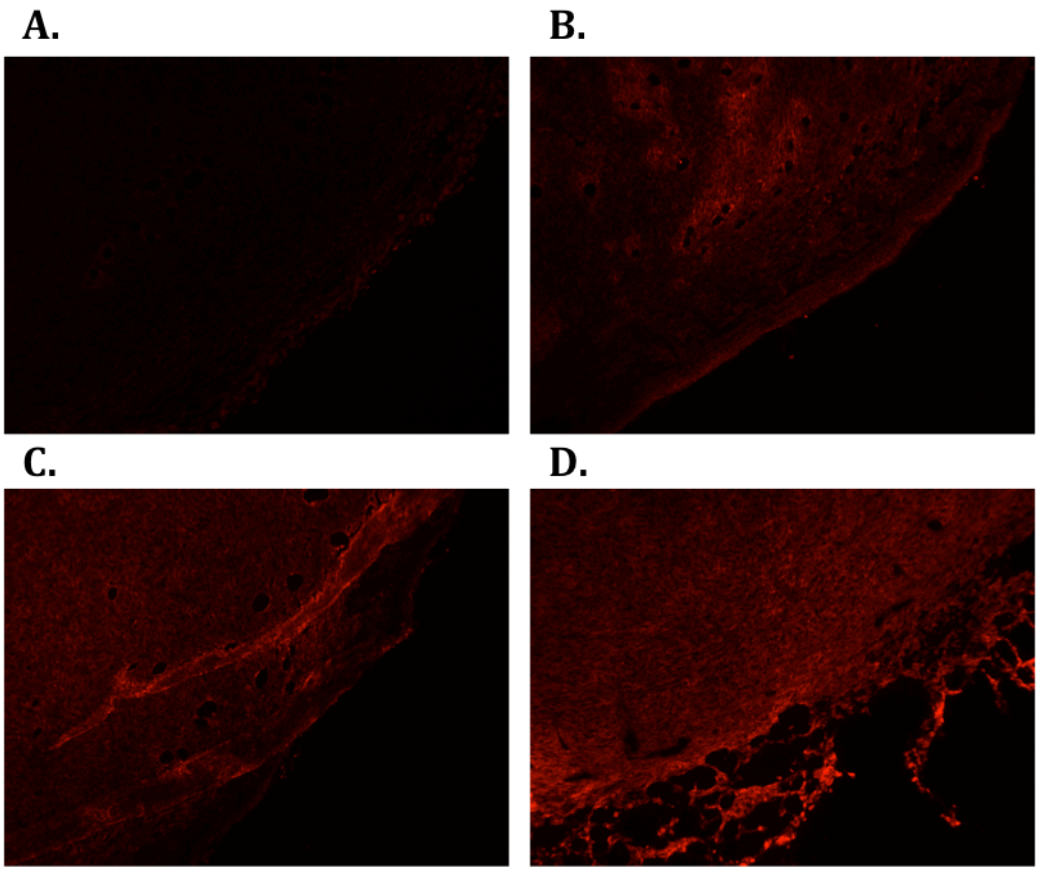

Figure 2.22 Y5R-IHC of primary MFP tumour. (A. 4T1 Y5R-KD day 14) Subtle fluorescence at edge of tumour. **(B. 4T1 Y5R-KD day 21)** Diffuse fluorescence throughout the tumour compared to the edge. **(C. 4T1 Y5R-KD day 28)** Enhanced Y5R fluorescence distributed throughout the tumour. **(D. 4T1 day 28)** Y5R fluorescence present throughout the tumour and emphasized at the edge of the tumour.

2.3.15 Histology of Lung Metastases

Lungs were stained with Hematoxylin and Eosin (H&E) to evaluate metastatic burden from the primary MFP tumour. Fluorescent immunohistochemitry, targeting Y5R, was conducted to qualitatively assess the expression of Y5R in lung metastases. Figure 2.23 shows matched H&E and Y5R IHC of a metastasis in the 4T1 model. In figure 2.23A, Y5R IHC revealed less Y5R fluorescence in the metastasis, compared to surrounding Y5R fluorescence of lung parenchyma. Figure 2.23C reveals that the Y5R fluorescence of this metastasis is comparable to the Y5R fluorescence to the surrounding lung parenchyma.

Figure 2.24A and B show matched H&E and Y5R IHC of a metastasis in the 4T1 Y5R-KD model. Similar to the 4T1 model, Y5R IHC revealed some metastases, which possessed less Y5R fluorescence, compared to surrounding Y5R fluorescence of lung parenchyma (2.24A). The MRI of this lung is shown in Figure 2.24C. Figure 2.24D depicts a metastasis situated near a vessel. The matched Y5R IHC reveals in Figure 2.24E that this metastasis has similar fluorescence to surrounding Y5R fluorescence of the lung parenchyma. As qualitatively assessed by immunohistochemistry, metastases from both 4T1 and 4T1 Y5R-KD tumours had less or similar Y5R expression in comparison to the high expression of Y5R in lung parenchyma.

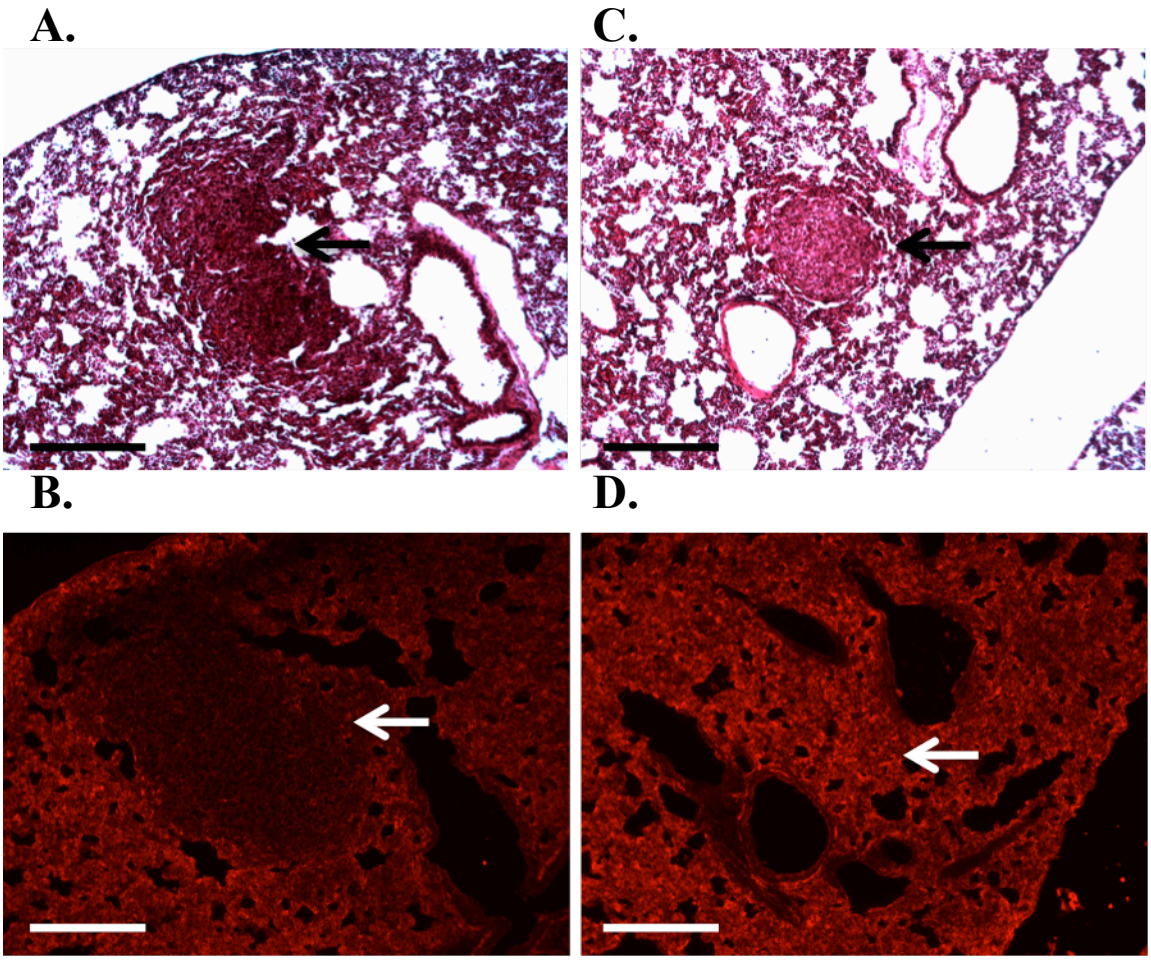

Figure 2.23 4T1 Lung Metastases at Day 28. All metastases are denoted by arrows. Representative H&E and matched Y5R IHC of metastases in lungs (Scale bars=200μm) **(A.)** H&E displays lung metastases **(B.)** Matched Y5R IHC to A. demonstrates less Y5R expression in the metastases in contrast with surrounding high Y5R expression in lung parenchyma. **(C.)** H&E displays lung metastases and **(D.)** Matched Y5R IHC to C. demonstrates equal Y5R expression in the metastases in contrast with surrounding high Y5R expression in lung parenchyma.

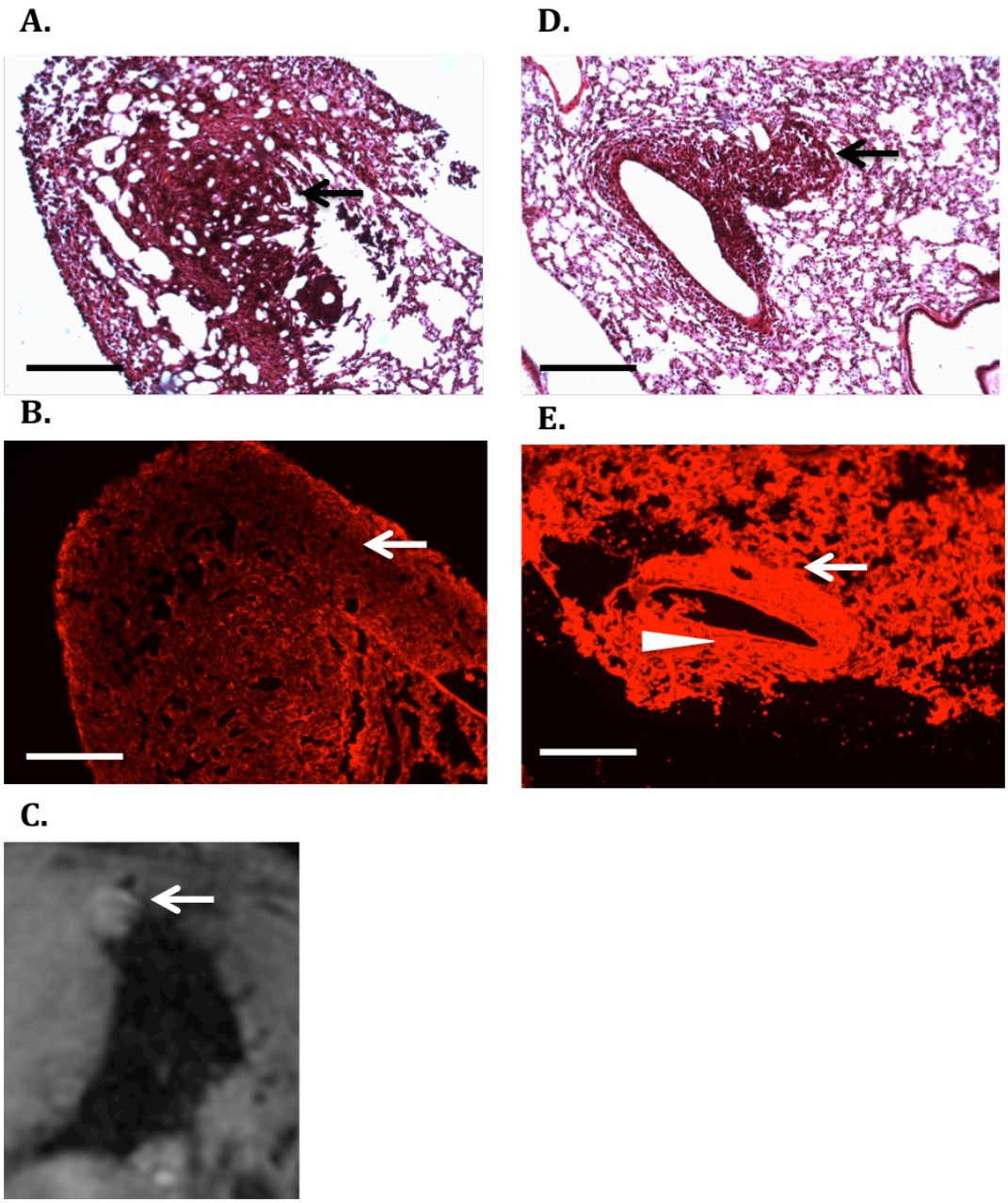

Figure 2.24 4T1 Y5R-KD Lung Metastases at Day 28. All metastases are denoted by arrows. (Scale bars=200μm) **(A.)** H&E stained lung tissue **(B.)** Matched Y5R IHC to A. demonstrates less Y5R expression in the metastases in contrast with surrounding high Y5R expression in lung parenchyma. **(C.)** Representative MRI of lung metastases. **(D.)** H&E displays lung metastases adjacent to a vessel (arrowhead) and **(E.)** Matched Y5R IHC to D. demonstrates enhanced Y5R expression in the metastases in contrast with surrounding Y5R expression in lungs.

2.3.16 Recovery of Y5R in 4T1 Y5R-KD *in vitro*

4T1 and 4T1 Y5R-KD cells were grown for 28 days *in vitro* to evaluate the stability of the 4T1 Y5R-KD. Western blotting was conducted on 4T1 and 4T1 Y5R-KD cell lysates. Cells were analyzed after their seventh passage for Y5R expression. Band intensity was evaluated using densitometry and was normalized to the average lane intensity with Coomassie blue membrane staining. Figure 2.24 demonstrates that 4T1 and 4T1 Y5R-KD cells did not have significantly different Y5R expression after 28 days of growth *in vitro* ($p>0.05$, Unpaired t-test).

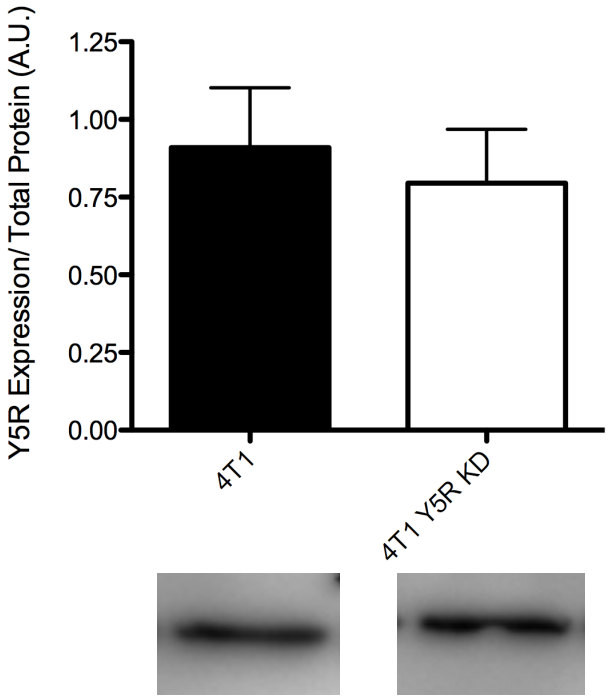

Figure 2.25 Western Blot densitometry quantification of 4T1 and 4T1 Y5R KD cell lysates normalized to total protein depicting the no significant difference in Y5R expression between the 4T1 and 4T1 Y5R-KD cell line. Densitometric data are presented as Y5R expression normalized to total protein expression discerned from Coomassie blue staining average lane intensity. Data are presented as mean± SE (n=3).

2.3.4 Discussion

Understanding the interactions between tumour cells and their microenvironment that enhance carcinogenesis and metastases is key to new paradigms for treating cancer. This study is the first to our knowledge that has illustrated the variable expression of the Neuropeptide Y5 Receptor (Y5R) to coordinate with the varying metastatic potential of different breast cancer models. Furthermore, this is the first study to reveal the potential role of cytoplasmic localization of Y5R in a breast cancer cell strain with the propensity to metastasize. Using cellular MRI, this study has shown the contribution of Y5R *in vivo* on tumourigenicity and metastasis in an immune competent model.

The 4T1-derived murine mammary carcinoma cell lines are syngeneic immune competent models and thereby permit a biologically relevant evaluation of cancer. Identification of specific biomarkers indicative of metastatic ability would be ideal to determine the fate and risk potential of cancer cells. The Jackson lab has previously confirmed the presence of Y5R in the 4T1 cell line.[22] In this study, immunocytochemistry confirmed that Y5R is expressed in the 67NR, 168FARN, and 4T1 cell lines, providing the impetus to quantify the expression of Y5R in the respective strains with Western blot analysis. As hypothesized, metastatic 4T1 breast cancer cells expressed significantly more Y5R than non-metastasizing 67NR and 168FARN cell lines. This finding suggests that the expression of Y5R coordinates with metastatic potential of breast cancer strains. Sheriff et al. have also found Y5R in estrogen receptor positive and negative human breast carcinoma cell lines, demonstrating the potential role of Y5R in both estrogen receptor positive and negative models.[27]

Despite variable expression of Y5R in each of the cell strains, Neuropeptide Y significantly stimulated proliferation of all three studied breast cancer cell lines. This finding

demonstrates the robust mitogenic properties of Neuropeptide Y. Stressful conditions, such as cold or restraint stress, significantly enhance the circulating plasma levels in mice from basal levels of the order 10^{-11} M to approaching 10^{-10} M in stress conditions.[28] Additionally, the Jackson lab has demonstrated robust NPY expression in sympathetically innervated 4T1 mammary fat pad tumours.[29] Further studies should be conducted *in vivo,* to elucidate if NPY is sufficient to accelerate proliferation of the slowly proliferating 67NR cell strain in basal and stressed conditions.

Previous experiments have demonstrated that Neuropeptide Y in conjunction with Y1R or Y2R antagonism does not inhibit proliferation in 4T1 cells, in contrast to Y5R antagonism, which abolishes Neuropeptide Y stimulated proliferation.[22] Y5R antagonism has also been shown to abolish the proliferative effect of NPY in triple negative human breast carcinoma BT-549, estrogen positive human breast carcinoma MCF-7, and SK-N-BE2 neuroblastoma.[27,30] Similarly, this study demonstrated that Y5R antagonism eliminated the proliferative effects of Neuropeptide Y of the 67NR, 168FARN and 4T1 cell line.

In a previous study by the Jackson lab examining the pro-angiogenic effects of NPY on the 4T1 breast cancer cells, twenty four hours of NPY treatment caused a marked increase in VEGF expression in 4T1 cells compared to non- treated controls, as a negative control, scrambled NPY treatment had no effect on VEGF expression.[21] As well, in a study of various human breast carcinoma cell lines *in vitro*, no NPY mRNA could be detected.[27] These findings suggest that 4T1 cells require the stimulation of NPY released from sympathetic nerves to induce Y5R-mediated cancerous properties.

Traditionally, GPCRs were considered to reside solely in the cell membrane and elicit their effect downstream through secondary effectors, however this notion has been dismissed with effects and localization in the nucleus. In fetal and embryonic endothelial cells, active Y1R has been found predominantly in the nucleus and nuclear envelope compared to the cytoplasm, with the capacity to induce an increase in nuclear Ca2+ upon NPY stimulation, suggesting a potential nuclear role in gene expression modulation.[31] In a study by Czarnecka et al., brain-derived neurotrophic factor (BDNF) increased Y5R expression and triggered internalization of Y5R in neuroblastoma cells as a pro-survival technique against cellular stress such as chemotherapy. Y5R antagonism inhibited chemo-resistance and sensitized the cells to apoptosis-induced chemotherapy.[18]

As shown with immunocytochemistry, we found Y5R is expressed predominantly in the cytoplasm and membrane in the aggressively metastasizing 4T1 breast cancer strain. In contrast, we found that non-metastasizing 67NR and 168FARN breast cancer strains express Y5R predominantly in the nucleus. The significance of nuclear Y5R localization requires further investigation. The nuclear Y5R localization of 67NR and 168FARN cells could support chemoresistance of breast cancer cells, similar to neuroblastoma.[18] If basal nuclear receptor internalization of the non-metastatic strains mediates inhibition of pro-cancerous genes, therapeutic monoclonal Y5R antibodies that induce internalization could be therapeutic for metastatic strains. Anti- EGFR and anti- HER2 antibodies that induce receptor internalization have been approved for clinical use in oncology.[32] Receptor localization of the 67NR and 168FARN strains post NPY stimulation should be further investigated to understand the role of receptor localization. The nuclear Y5R localization of 67NR and 168FARN cells could support chemoresistance of breast cancer cells, similar to neuroblastoma.[18] Additionally, the capacity of

67NR cells to proliferate under certain concentrations of NPY may modulate tumour- supporting mitogenic genes to enhance proliferation via nuclear Y5R activation. It should be noted that in human breast carcinoma cell line, BT-549 and rat aortic vascular smooth muscle cells, Y5R activation was found not be coupled with a change in intracellular Ca^{2+}.[27,33] However, NPY and Y5R specific agonism inhibits intracellular cAMP accumulation and correlates with proliferation of BT-549 cells.[27]

MRI has been widely used to study preclinical mouse models of cancer and provides excellent 3D anatomic detail and sensitivity to permit tumour size quantification and location, in addition to edema, hemorrhage, and necrosis.[24] The analysis of volumes over time can provide information about growth rates for individual tumors. Cellular MRI can be achieved by pre-labeling cells with iron oxide nanoparticles prior to their administration. In this study, we pre-labelled 4T1 and 4T1 Y5R-KD cells with MPIOs. Labeling with MPIOs has been previously shown to have no discernable effect on viability, *in vitro* proliferation, cell apoptosis, necrosis, or *in vivo* metastasis compared to unlabeled cells.[23–25]

Few groups have used cellular MRI to study cancer cells because the iron label is diluted over time in proliferative cells. Since the detection of iron-labeled cells by MRI relies on the total iron content, eventually the cancer cells will not contain enough iron to be detected as signal voids in MRI. This property can be exploited, however, as slowly-proliferative or transiently dormant cells retain iron oxide nanoparticles for longer periods of time than highly proliferative cells.[26] The Foster lab has previously used cellular MRI to monitor the development of iron-labeled primary MDA-MB-231 mammary fat pad tumours and metastasis to the lymph nodes.[26]

Similarly, in this thesis we used cellular MRI to monitor the development of iron-labeled primary 4T1 and 4T1 Y5R-KD mammary fat pad tumours and metastasis to the lungs and lymph nodes. 4T1 Y5R-KD tumours grew significantly slower over four weeks and were significantly smaller than 4T1 tumours at day 28. It is noteworthy that the significant difference in tumour growth was under the influence of basally released NPY in non- stressed conditions. This significant finding highlights the ability of NPY to activate Y5R, resulting in the acceleration of *in vivo* tumour development, independent of chronic or traumatic stress.

The Foster lab has previously shown that proliferative status of cancer cells can be evaluated through MRI through the retention of iron oxide nanoparticles.[23,26] In this study, pre-labeling 4T1 and 4T1- Y5R KD cells prior to implantation permitted evaluation of signal void volume and distribution. We found 4T1 Y5R-KD tumours had a significantly smaller signal void volume than 4T1 tumours at day 7. The presence of iron-labeled cells causes signal loss in MR images and what is known as a blooming artefact, where the signal void volume is greater than the actual volume occupied by iron oxide labeled cells.[24] The size of the blooming artefact depends on several factors including the total iron content, spatial resolution, magnetic field strength, cell type and cell density. The larger void volume measured for 4T1 tumours compared to 4T1 Y5R-KD tumours may be due to higher iron content in the tumour.

The distribution of iron- retaining cells also differed between the two cell lines. The 4T1 Y5R-KD tumours have a speckled or diffuse distribution of signal voids throughout the tumour, in contrast to the centralized signal void in the core of 4T1 tumours. Cells with similar properties tend to remain clustered within tumours.[34] This property could account for the centralized cluster of slowly proliferating cells in the core of the 4T1 tumour. Furthermore, this

property could account for the diffuse clustered aggregation of slowly proliferating iron-retaining 4T1 Y5R-KD cells that have maintained the knockdown.

Using MR imaging, we were able to detect metastases and enlargement of the axillary and inguinal lymph nodes in only the 4T1 Y5R-KD mice. The presence of metastases in lymph nodes is supported by distinct hypointensity in the inguinal lymph node due to the presence of iron oxide nanoparticles disseminated from the primary tumour. Despite the presence of lymph node metastases, lung metastases were detected in more 4T1 mice and at an earlier imaging time point compared to 4T1 Y5R-KD mice. 4T1 cells metastasize primarily hematogenously and to a lesser extent via draining lymph nodes.[20] The non-metastatic 168FARN cell line spreads to the lymphatics with occasional lung metastases.[20] This finding suggests the knockdown of Y5R in the 4T1 cell line has the capacity to diminish its aggressive metastatic phenotype to resemble the non-metastatic 168FARN cell line.

Lungs are the most common site of breast cancer metastasis.[35] NPY is released directly to lungs and has the capacity to elevate pulmonary vascular permeability.[36,37] The molecular transduction of stress via NPY as a result of enhanced tumour burden should be further explored as it may prime the microenvironment for targeted metastasis. This avenue is worth investigation due to the high expression of Y5R in the lungs shown with immunohistochemistry. Y5R could be an indicator of metastases onset and may play a role in metastases formation.

The tumour microenvironment at the edge differs from the hypoxic core of the tumour. Particularly, tumour associated macrophages (TAMs) play a large role at the invasive edge of tumours, to drive invasive phenotypes by stimulating cancer cell migration, metastasis, and neovascularization.[38] As we have shown with cellular MRI, 4T1 tumours possess an enhanced fraction of slowly proliferating iron- retaining cells in the core of the tumour with more

aggressively proliferative cells at the oxygenated tumour edge, permitting tumour expansion. This property corresponds with the enhanced Y5R expression at the edge of the tumour depicted in the immunohistochemistry. This finding suggests that the expansion of the primary tumour is mediated by the NPY-Y5R system. As the tumour develops, the formation of the hypoxic core supports the mitogenic properties of NPY, as hypoxia activates DPPIV driving Y2R/Y5R mediated tumourigenesis as previously established in Ewing sarcoma.[19]

The complete contribution of Y5R to tumour development and metastasis is diminished with the 4T1 Y5R-KD model due to the recovery of the receptor over time as shown with immunohistochemistry. The knockdown of Y5R, as shown with Western blot and ICC, at the initial establishment of the cell line, could contribute to the delayed tumour development, resulting in a significant decrease in the 4T1 Y5R-KD tumour volume at day 28. If the knockdown has the capacity to significantly impede proliferation of 4T1 cells, the subpopulation of Y5R+ cells has the opportunity to out-compete the knockdowns. This issue is further compounded with *in vitro* passaging of cells, where a greater fraction of highly proliferative cells would be consequently plated. Given that shRNA achieved a 51% reduction in Y5R, which was then recovered over time, this may suggest that Y5R+ positive cells in the 4T1 Y5R-KD model could have driven establishment of metastases.

Overall, we report the variable presence and expression of Y5R in the 67NR, 168FARN and 4T1 murine breast cancer cell strains for the first time. We have shown that NPY, at physiological and pathophysiological levels, can induce potent proliferation mediated through Y5R activation of cell lines of variable metastatic potentials and Y5R expression. Furthermore, we have illustrated that a transient knockdown of Y5R is sufficient to alter the metastasis of the

4T1 cell line. These findings support the role of NPY and Y5R in driving the development of breast cancer tumourigenesis and metastasis.

References

1. Canada, S. Canadian Cancer Statistics Special topic : Skin cancers. *Can. Cancer Soc.* **2014,** 1–132 (2014).

2. Institute, N. C. SEER Stat Fact Sheets: Female Breast Cancer. *SEER* Survival by Stage (2012).

3. Lee, Y. T. Breast carcinoma: pattern of metastasis at autopsy. *J. Surg. Oncol.* **23,** 175–180 (1983).

4. Fawzy, F. I. *et al.* Malignant Melanoma: Effects of an Early Structured Psychiatric Intervention, Coping, and Affective State on Recurrence and Survival 6 Years Later. *Arch. Gen. Psychiatry* **50,** 681–689 (1993).

5. Cooper, C. L. & Faragher, E. B. Psychosocial stress and breast cancer: the inter-relationship between stress events, coping strategies and personality. *Psychol. Med.* **23,** 653–662 (1993).

6. Funch, D. P. & Marshall, J. The role of stress, social support and age in survival from breast cancer. *J. Psychosom. Res.* **27,** 77–83 (1983).

7. Levy, S., Herberman, R., Lippman, M. & d'Angelo, T. Correlation of stress factors with sustained depression of natural killer cell activity and predicted prognosis in patients with breast cancer. *J. Clin. Oncol.* **5,** 348–353 (1987).

8. Chorot, P. & Sandin, B. Life events and stress reactivity as predictors of cancer, coronary heart disease and anxiety disorders. *Int. J. Psychosom.* **41,** 34–40 (1994).

9. Maunsell, E., Brisson, J. & Deschenes, L. Social support and survival among women with breast cancer. *Cancer* **76,** 631–637 (1995).

10. Marshall, J. R. & Funch, D. P. Social environment and breast cancer. A cohort analysis of patient survival. *Cancer* **52,** 1546–1550 (1983).

11. Ben-Eliyahu, S., Yirmiya, R., Liebeskind, J. C., Taylor, A. N. & Gale, R. P. Stress increases metastatic spread of a mammary tumor in rats: evidence for mediation by the immune system. *Brain. Behav. Immun.* **5,** 193–205 (1991).

12. Ben-Eliyahu, S., Page, G. G., Yirmiya, R. & Shakhar, G. Evidence that stress and surgical interventions promote tumor development by suppressing natural killer cell activity. *Int. J. cancer* **80,** 880–888 (1999).

13. Page, G. G. & Ben-Eliyahu, S. A role for NK cells in greater susceptibility of young rats to metastatic formation. *Dev. Comp. Immunol.* **23,** 87–96 (1999).

14. Page, G. G., Ben-Eliyahu, S., Yirmiya, R. & Liebeskind, J. C. Morphine attenuates surgery-induced enhancement of metastatic colonization in rats. *Pain* **54,** 21–28 (1993).

15. Hirsch, D. & Zukowska, Z. NPY and stress 30 years later: the peripheral view. *Cell. Mol. Neurobiol.* **32,** 645–659 (2012).

16. Bland, K. & Copeland, E. M. *The Breast: Comprehensive Management of Benign and Malignant Disease*. (Saunders by Elsevier Inc., 2009).

17. James, G. D., Berge-Landry Hv, H. van, Valdimarsdottir, H. B., Montgomery, G. H. & Bovbjerg, D. H. Urinary catecholamine levels in daily life are elevated in women at familial risk of breast cancer. *Psychoneuroendocrinology* **29,** 831–838 (2004).

18. Czarnecka, M. *et al.* Neuropeptide Y receptor Y5 as an inducible pro-survival factor in neuroblastoma: implications for tumor chemoresistance. *Oncogene* **34,** 3131–3143 (2015).

19. Tilan, J. U. *et al.* Hypoxia shifts activity of neuropeptide Y in Ewing sarcoma from growth-inhibitory to growth-promoting effects. *Oncotarget* **4,** 2487–2501 (2013).

20. Aslakson, C. J. & Miller, F. R. Selective Events in the Metastatic Process Defined By Analysis of the Sequential Dissemination of Subpopulations of a Mouse Mammary-Tumor. *Cancer Res.* **52,** 1399–1405 (1992).

21. Medeiros, P. J. & Jackson, D. N. Neuropeptide Y Y5-receptor activation on breast cancer cells acts as a paracrine system that stimulates VEGF expression and secretion to promote angiogenesis. *Peptides* **48,** 106–113 (2013).

22. Medeiros, P. J. *et al.* Neuropeptide Y stimulates proliferation and migration in the 4T1 breast cancer cell line. *Int. J. cancer* **131,** 276–286 (2012).

23. Heyn, C. *et al.* In vivo MRI of cancer cell fate at the single-cell level in a mouse model of breast cancer metastasis to the brain. *Magn. Reson. Med.* **56,** 1001–1010 (2006).

24. Foster, P. J. *et al.* Cellular Magnetic Resonance Imaging: In Vivo Imaging of Melanoma Cells in Lymph Nodes of Mice. *Neoplasia* **10,** 207–216 (2008).

25. Ribot, E. J. *et al.* In vivo single scan detection of both iron-labeled cells and breast cancer metastases in the mouse brain using balanced steady-state free precession imaging at 1.5 T. *J. Magn. Reson. Imaging* **34,** 231–238 (2011).

26. Economopoulos, V., Chen, Y., McFadden, C. & Foster, P. J. MRI Detection of Nonproliferative Tumor Cells in Lymph Node Metastases Using Iron Oxide Particles in a Mouse Model of Breast Cancer. *Transl. Oncol.* **6,** 347–354 (2013).

27. Sheriff, S. *et al.* Neuropeptide Y Y5 receptor promotes cell growth through extracellular signal-regulated kinase signaling and cyclic AMP inhibition in a human breast cancer cell line. *Mol. Cancer Res.* **8,** 604–614 (2010).

28. Ruohonen, S. T. *et al.* Stress-Induced Hypertension and Increased Sympathetic Activity in Mice Overexpressing Neuropeptide Y in Noradrenergic Neurons. *Neuroendocrinology* **89,** 351–360 (2009).

29. Medeiros, P. J. The Impact of the Neuropeptide Y System on the Progression of Breast Cancer. (University of Western Ontario, 2012). doi:Paper 1065

30. Kitlinska, J. *et al.* Differential Effects of Neuropeptide Y on the Growth and Vascularization of Neural Crest–Derived Tumors. *Cancer Res.* **65,** 1719–1728 (2005).

31. Jacques, D. *et al.* Presence of neuropeptide Y and the Y1 receptor in the plasma membrane and nuclear envelope of human endocardial endothelial cells: modulation of intracellular calcium. *Can. J. Physiol. Pharmacol.* **81,** 288–300 (2003).

32. Simpson, A. & Caballero, O. Monoclonal antibodies for the therapy of cancer. *BMC Proc.*

8, O6–O6 (2014).

33. Lettgen, B., Wagner, S., Hanze, J., Lang, R. E. & Rascher, W. Elevated plasma concentration of neuropeptide Y in adolescents with primary hypertension. *J. Hum. Hypertens.* **8,** 345–349 (1994).

34. Fidler, I. J. & Hart, I. R. Biological and experimental consequences of the zonal composition of solid tumors. *Cancer Res.* **41,** 3266–3267 (1981).

35. Weigelt, B., Peterse, J. L. & van't Veer, L. J. Breast cancer metastasis: markers and models. *Nat Rev Cancer* **5,** 591–602 (2005).

36. Hirabayashi, A., Nishiwaki, K., Shimada, Y. & Ishikawa, N. Role of neuropeptide Y and its receptor subtypes in neurogenic pulmonary edema. *Eur. J. Pharmacol.* **296,** 297–305 (1996).

37. Barklin, A. *et al.* Alteration of Neuropeptides in the Lung Tissue Correlates Brain Death-Induced Neurogenic Edema. *J. Hear. Lung Transplant.* **28,** 725–732 (2009).

38. Green, C. E. *et al.* Chemoattractant signaling between tumor cells and macrophages regulates cancer cell migration, metastasis and neovascularization. *PLoS One* **4,** (2009).

Chapter 3- Significance, Limitations, and Future Directions

3.1 Significance

Stress should be adequately appreciated as a supporting and mediating factor of carcinogenesis, metastasis, and recurrence. The perception of psychosocial and qualitative features of stress hinders the additional pathophysiological implications that it should hold. Studies have demonstrated a correlation between elevated stress levels and poor prognosis and survival in patients with breast cancer.[1–5] Additionally, women with a family history of breast cancer release elevated sympathetic neurotransmitters in response to daily stress.[6] Therefore, patients experiencing normal to chronically elevated stress could be affected by the clinical consequences of NPY.

The American Society of Clinical Oncology recommends therapy for women with metastatic breast cancer based on their receptor status (ER, PR, and HER2) and additional biomarkers that demonstrate clinical utility that have the potential to guide drug regimens.[7] In this respect, we believe that Y5R could be a potential biomarker for breast cancer metastatic potential. We found that expression of Neuropeptide Y5 Receptor (Y5R) is present in all tested breast cancer lines and coordinates with metastatic potential. Cytoplasmic receptor localization and quantity were both associated with enhanced metastatic capacity. This finding could hold prognostic utility in predicting the likelihood of metastasis. The role of Y5R is not restricted to triple negative breast cancers, which have the poorest diagnosis associated with a high recurrence rate.[8] The previous finding of Y5R in estrogen receptor positive and negative human breast carcinoma cell lines, demonstrates the potential role of Y5R in both estrogen receptor positive and negative models.[9]

We found that physiologically relevant levels of NPY have the potential to stimulate significant proliferation of breast cancer lines of variable levels of aggression and Y5R expression. If this finding is clinically translated to humans, this would provide the impetus to monitor individuals with a history of breast cancer or post trauma for recurrence or advancement of metastasis. Further research is required to elaborate on our studies to evaluate the potential of NPY as a sufficient trigger to induce recurrence by switching growth arrest of dormant breast cancer cells to form clinically relevant tumours.

One of the most significant findings was the alteration of the metastatic cascade via knockdown of Y5R in the 4T1 cell line. The five-year survival rate of regional lymph node breast cancer metastasis of 85.2% drops to 26.3% with distant breast cancer metastasis.[10] Breast cancer cells that metastasize haematogenously readily gain access to capillary beds in common distant sites of metastasis; lungs, liver, bone and brain. Alternatively, breast cancer cells that metastasize via the lymph nodes need to enter the blood circulation in order to gain access to these common distant sites of metastasis.[11] Y5R antagonism could have the potential to induce a similar alteration in the metastatic cascade.

Two Y5R antagonists are safe to administer to patients, MK-0557 (Merck & Co., Inc.) and S-2367 (velneperit, Shionogi & Co, Ltd). Both antagonists progressed to phase II trials for obesity, but were withdrawn given their lack of clinically meaningful effects, though each had some effect on weight loss.[12] Therefore, if the therapeutic potential of Y5R antagonism is clinically meaningful for breast cancer tumourigenesis and metastasis in humans, the drug safety has already been validated.

3.2 Limitations

3.2.1 *In vitro* MTS proliferation assay

The MTS proliferation assay is a colourimetric quantification of cell viability based on the reduction of MTS tetrazolium compound to a coloured foramazan product.[13] The absorbance is read and plotted as a gauge of mitochondrial activity and cell viability. A previous study found that the MTS assay demonstrated a two-fold underestimation of the anti- proliferative effects of polyphenols, in comparison to the direct measures of ATP and DNA methods.[14] Direct measures that evaluate ATP or DNA could mitigate the limitations of this assay. Furthermore, evaluations of doubling would provide a quantitative and translatable measure to evaluate proliferation. Therefore, the ability of stable Y5R antagonism to mitigate cancer cell proliferation could be enhanced *in vivo,* compared to our *in vitro* results. The physiological level of proliferation induced by NPY and inhibition via Y5R antagonism requires further investigation.

3.2.2 Transient Knockdown of Y5R in the 4T1 Cell Line

shRNA knockdown is achieved through successful vector transfection, transcription of shRNA, and subsequent sequestration and degradation of the target mRNA.[15] Vector transfection permits exploitation of the cellular transcription machinery to transcribe the shRNA. shRNA integrates into the endogenous miRNA pathway and induces targeting and degradation by the RNA-induced silencing complex (RISC).[16] Although shRNA has had success in suppressing target expression to inhibit carcinogenesis and metastasis in preclinical models in other studies[17–19], we established a transient knock down of the Y5R in the 4T1 cell line.

We established a 4T1 Y5R-KD with 98.7% GFP+ expression, confirming high vector transfection. We demonstrated 51% knockdown of the receptor with Western Blotting, which

was supported by immunocytochemistry of the cell line after one passage. The transient knockdown was demonstrated by immunohistochemistry of 4T1 Y5R-KD tumours, which depicted receptor recovery at Day 21 and 28. Therefore, the true contribution of Y5R and the ability of the receptor's blockade in mitigating cancerous properties was not fully studied.

3.2.3 Quantification of signal loss in MR images

The presence of iron oxide nanoparticles in a magnetic field causes signal dephasing, altering the Larmor frequency of surrounding protons and leading to signal loss.[20] Quantification of signal loss in MR images is difficult because (a) the extent of signal loss produced by iron-labeled cells is not linearly related to the iron concentration and (b) the extent of signal loss produced by iron-labeled cells is much larger than the actual area occupied by the cells; this is known as the blooming artefact. For example, Heyn et al. found a single signal void measured on average six voxels, 294μm, and spanned on average three MR slices, 300μm, both dimensions substantially larger than the size of the cell ~15μm.[21] Since cell number cannot be measured from images of signal loss many studies use measurements of the size of the region of signal loss or the degree of contrast produced by the iron-labeled cells. In this thesis we measured the signal void volume within the tumours.

Fluorine-19 (^{19}F) MRI is an alternative approach for cell tracking that circumvents many of the limitations associated with iron-labeled cell tracking. In comparison to the indirect visualization of iron oxide nanoparticles by observed image hypointensity, the spins of ^{19}F nuclei are detected directly and image contrast is proportional to the number of ^{19}F atoms per voxel. This property mitigates the quantitative concerns with blooming artefacts produced by iron oxide nanoparticles. Endogenous fluorine does not contribute to measurable tissue background signal, which prevents non-specific contrast agent identification, allowing for direct quantification of

labeled cell number. However, compared to iron-labeled cell tracking, sensitivity is low and an additional proton MR scan is required to attain anatomical context for the ^{19}F signal.

3.2.4 Challenges validating signal loss in MRI using PPB staining

Perls' Prussian Blue (PPB) was used to stain iron oxide nanoparticles in resected lung and tumour slices. Signal loss, as a result of iron oxide nanoparticles, in tissues can be readily identified in MR images due to the blooming artefact. In contrast, PPB staining is a direct representation of the iron oxide volume present in a slice. Therefore, small quantities of iron are difficult to detect with histology. In general, it is challenging to compare 10 micron tissue section with 200 micron image slices. Previous work in the Foster lab has shown that summing the PPB staining from numerous single tissue sections from a primary tumour will give a better picture of the quantity and distribution of PPB-positive cells.[22] Due to our limited tissue sampling, we did not overlay stained slices, which hindered our ability to localize iron oxide nanoparticles with histology in our study.

3.3 Future Directions

In Canada, breast cancer is the most frequently diagnosed cancer in females, with 1 in 9 females expected to develop breast cancer in their lifetime.[23] Metastasis of breast cancer is the culprit of dropping the 98.8% 5- year survival rate to 26.3%, supporting the need to further explore biomarkers indicative of cancer cell fate.[10] This thesis has explored the implications of the Neuropeptide Y-Y5R system in breast cancer tumourigenicity and metastasis, providing the impetus for further investigation of the role of Y5R cellular localization, influence of NPY and Y5R *in vitro* and *in vivo,* the NPY- mediated effects of chronic stress in cancer, and translation to humans.

3.3.1 Localization of Y5R

The prevalent nuclear localization of Y5R in the 67NR and 168FARN cell strains and cytoplasmic localization of Y5R in the 4T1 cell strain is a feature of great interest and should be further investigated. The effect of NPY at physiological and pathophysiological levels on receptor localization should be examined. Plasma levels of NPY have been measured in both stressed and non-stressed conditions, given that NPY has found highly expressed in tumours, it would be of great interest to evaluate the NPY levels in a tumour of a stressed subject and induced receptor localization at these concentrations.[24]

Additionally, further research should examine means of inducing Y5R externalization of the 67NR and 168FARN cell strains via the establishment and characterization of a Y5R knock-in of the 67NR and 168FARN cell strains. It would be of great significance to contrast the chemo-resistant properties of the cell strains in order to elucidate the benefits of basal nuclear localization of Y5R in the 67NR and 168FARN cell strains.

3.3.2 Influence of NPY in vitro

In order to support NPY- induced carcinogenesis of the 67NR, 168FARN, and 4T1 cell strains, the influence of NPY on migration and angiogenesis could also be assessed, using assays such as the modified Boyden chamber and endothelial tube assay, respectively.[25,26] These assays have been previously and effectively used in the Jackson lab to characterize the 4T1 cell strain under the influence of NPY. Additionally, the role of DPPIV, in cleaving NPY to an abbreviated Y2/Y5 target, should also be done in order to simulate conditions of the tumour milieu.

3.3.3 Blockade of Y5R in vivo

The transient reduction of Y5R with shRNA should be further expanded upon to evaluate the comprehensive contribution of the NPY-Y5R system in driving metastasis. Dr. Phil Medeiros of the Jackson lab previously administered oral gavage for 50 days of TAC557, a specific Y5R antagonist, resulting in attenuated tumour burden and lung metastasis.[27] This method ensures longitudinal blockade of the Y5R and would complement longitudinal monitoring of tumour and metastases development with cellular MRI. Alternatively, genetic knockout of the Y5R in the 4T1 cell strain using the CRISPR/cas9 system could be an avenue of further investigation. In a comparison of shRNA and CRISPR libraries targeting 93 essential and non-essential genes, CRISPR outperformed shRNA due to the presence of more functional constructs, apparent absence of off-target effects, better consistency across cell lines and most importantly sustained targeting of genes.[28]

3.3.4 Chronic stress and mice

Upon establishment of sustained Y5R blockade in 4T1 cells and/or up-regulation of Y5R in 67NR or 168FARN cells, the influence of chronic stress resulting in up-regulation of NPY in a murine model should be investigated. Baldock et al. induced chronic stress resulting in an NPY plasma levels through a weekly rotation of cold stress, restraint stress, and handling stress for six weeks that could be administered.[29] Due to the extensive tumourigencity and metastasis of the 4T1 cell line after four weeks that we observed, cell implantation should be done at an optimized time where the mouse has been chronically stressed.

3.3.5 Human tissue studies

This study has demonstrated the variable expression of Y5R of syngeneic murine strains coordinating with metastatic capacity. Evaluation of NPY and Y5R in human tumours and

metastases should be investigated. Metastases, recurrence, and survival should also be taken into account and analyzed. The implications of these studies would demonstrate the utility of Y5R status as a diagnostic marker and Y5R antagonism as a therapy.

3.4 References

1. Fawzy, F. I. *et al.* Malignant Melanoma: Effects of an Early Structured Psychiatric Intervention, Coping, and Affective State on Recurrence and Survival 6 Years Later. *Arch. Gen. Psychiatry* **50,** 681–689 (1993).

2. Cooper, C. L. & Faragher, E. B. Psychosocial stress and breast cancer: the inter-relationship between stress events, coping strategies and personality. *Psychol. Med.* **23,** 653–662 (1993).

3. Funch, D. P. & Marshall, J. The role of stress, social support and age in survival from breast cancer. *J. Psychosom. Res.* **27,** 77–83 (1983).

4. Levy, S., Herberman, R., Lippman, M. & d'Angelo, T. Correlation of stress factors with sustained depression of natural killer cell activity and predicted prognosis in patients with breast cancer. *J. Clin. Oncol.* **5,** 348–353 (1987).

5. Chorot, P. & Sandin, B. Life events and stress reactivity as predictors of cancer, coronary heart disease and anxiety disorders. *Int. J. Psychosom.* **41,** 34–40 (1994).

6. James, G. D., Berge-Landry Hv, H. van, Valdimarsdottir, H. B., Montgomery, G. H. & Bovbjerg, D. H. Urinary catecholamine levels in daily life are elevated in women at familial risk of breast cancer. *Psychoneuroendocrinology* **29,** 831–838 (2004).

7. Van Poznak, C. *et al.* Use of biomarkers to guide decisions on systemic therapy for women with metastatic breast cancer: American Society of Clinical Oncology clinical practice guideline. *J. Clin. Oncol.* **33,** 2695–2704 (2015).

8. Dent, R. *et al.* Triple-Negative Breast Cancer: Clinical Features and Patterns of Recurrence. *Clin. Cancer Res.* **13 ,** 4429–4434 (2007).

9. Sheriff, S. *et al.* Neuropeptide Y Y5 receptor promotes cell growth through extracellular signal-regulated kinase signaling and cyclic AMP inhibition in a human breast cancer cell line. *Mol. Cancer Res.* **8,** 604–614 (2010).

10. Institute, N. C. SEER Stat Fact Sheets: Female Breast Cancer. *SEER* Survival by Stage (2012).

11. Chambers, A. F., Groom, A. C. & MacDonald, I. C. Dissemination and growth of cancer cells in metastatic sites. *Nat. Rev. Cancer* **2,** 563–572 (2002).

12. Erondu, N. *et al.* Neuropeptide Y5 receptor antagonism does not induce clinically meaningful weight loss in overweight and obese adults. *Cell Metab.* **4,** 275–282 (2006).

13. Riss, T. L. *et al.* Cell viability assays. *Assay Guid. Man.* (2013).

14. Wang, P., Henning, S. M. & Heber, D. Limitations of MTT and MTS-based assays for measurement of antiproliferative activity of green tea polyphenols. *PLoS One* **5,** (2010).

15. Paddison, P. J., Caudy, A. A., Bernstein, E., Hannon, G. J. & Conklin, D. S. Short hairpin RNAs (shRNAs) induce sequence-specific silencing in mammalian cells. *Genes Dev* **16,** (2002).

16. McAnuff, M. A., Rettig, G. R. & Rice, K. G. Potency of siRNA versus shRNA mediated knockdown in vivo. *J. Pharm. Sci.* **96,** 2922–2930 (2007).

17. Jang, J.-Y., Jeon, Y.-K. & Kim, C.-W. Degradation of HER2/neu by ANT2 shRNA suppresses migration and invasiveness of breast cancer cells. *BMC Cancer* **10,** 391 (2010).

18. Nickerson, N. K. *et al.* Decreased Autocrine EGFR Signaling in Metastatic Breast Cancer Cells Inhibits Tumor Growth in Bone and Mammary Fat Pad. *PLoS One* **7,** e30255 (2012).

19. Jiang, Q., Zhang, H. & Zhang, P. ShRNA-mediated gene silencing of MTA1 influenced on protein expression of ER alpha, MMP-9, CyclinD1 and invasiveness, proliferation in breast cancer cell lines MDA-MB-231 and MCF-7 in vitro. *J. Exp. {&} Clin. Cancer Res.* **30,** 1–11 (2011).

20. Bulte, J. W. M. & Kraitchman, D. L. Iron oxide MR contrast agents for molecular and cellular imaging. *NMR Biomed.* **17,** 484–499 (2004).

21. Heyn, C. *et al.* In vivo MRI of cancer cell fate at the single-cell level in a mouse model of breast cancer metastasis to the brain. *Magn. Reson. Med.* **56,** 1001–1010 (2006).

22. Economopoulos, V., Chen, Y., McFadden, C. & Foster, P. J. MRI Detection of Nonproliferative Tumor Cells in Lymph Node Metastases Using Iron Oxide Particles in a Mouse Model of Breast Cancer. *Transl. Oncol.* **6,** 347–354 (2013).

23. Canada, S. Canadian Cancer Statistics Special topic : Skin cancers. *Can. Cancer Soc.* **2014,** 1–132 (2014).

24. Ruohonen, S. T. *et al.* Stress-Induced Hypertension and Increased Sympathetic Activity in Mice Overexpressing Neuropeptide Y in Noradrenergic Neurons. *Neuroendocrinology* **89,** 351–360 (2009).

25. Medeiros, P. J. & Jackson, D. N. Neuropeptide Y Y5-receptor activation on breast cancer cells acts as a paracrine system that stimulates VEGF expression and secretion to promote angiogenesis. *Peptides* **48,** 106–113 (2013).

26. Medeiros, P. J. *et al.* Neuropeptide Y stimulates proliferation and migration in the 4T1 breast cancer cell line. *Int. J. cancer* **131,** 276–286 (2012).

27. Medeiros, P. J. The Impact of the Neuropeptide Y System on the Progression of Breast Cancer. (University of Western Ontario, 2012). doi:Paper 1065

28. Evers, B. *et al.* CRISPR knockout screening outperforms shRNA and CRISPRi in identifying essential genes. *Nat Biotech* **34,** 631–633 (2016).

29. Baldock, P. A. *et al.* Neuropeptide Y Attenuates Stress-Induced Bone Loss Through Suppression of Noradrenaline Circuits. *J. Bone Miner. Res.* **29,** 2238–2249 (2014).

Appendices

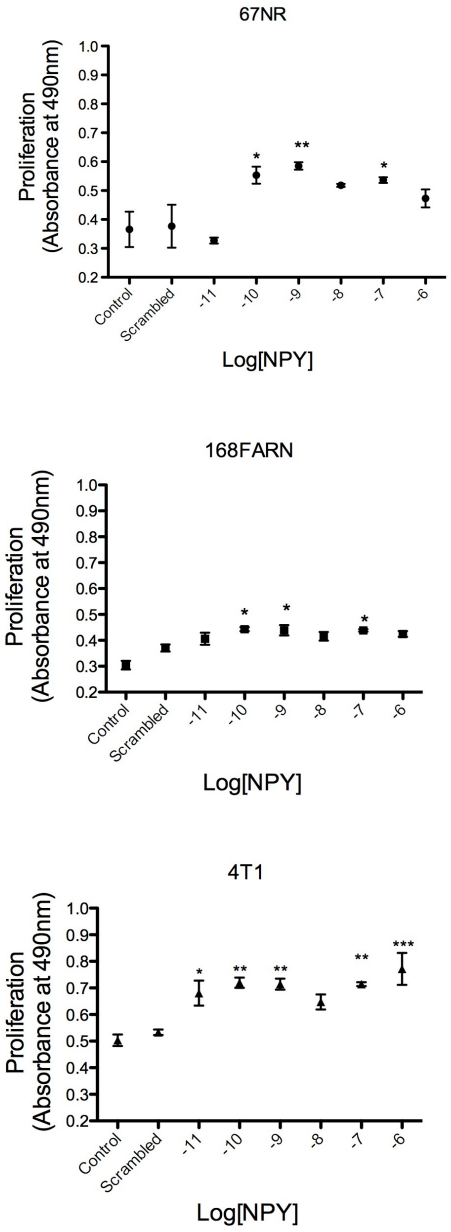

Appendix A. MTS Assay of 67NR, 168FARN and 4T1 Cell Lines with NPY stimulation (10^{-11}M-10^{-6}M) without normalization to basal growth. (A. 67NR) A proliferative effect was stimulated by NPY at 10^{-10}M, 10^{-9}, 10^{-7}M**. (B. 168 FARN)** A proliferative effect was stimulated by NPY at 10^{-10}M, 10^{-9}, 10^{-7}M**. (C. 4T1)** A proliferative effect was stimulated by NPY at 10^{-11}M, 10^{-10}M, 10^{-9}, 10^{-7}M, 10^{-6}M**.** (All values were statistically compared to respective control cell growth, * denotes $p<0.05$, ** denotes $p<0.01$, *** denotes $p<0.001$, One- way ANOVA).

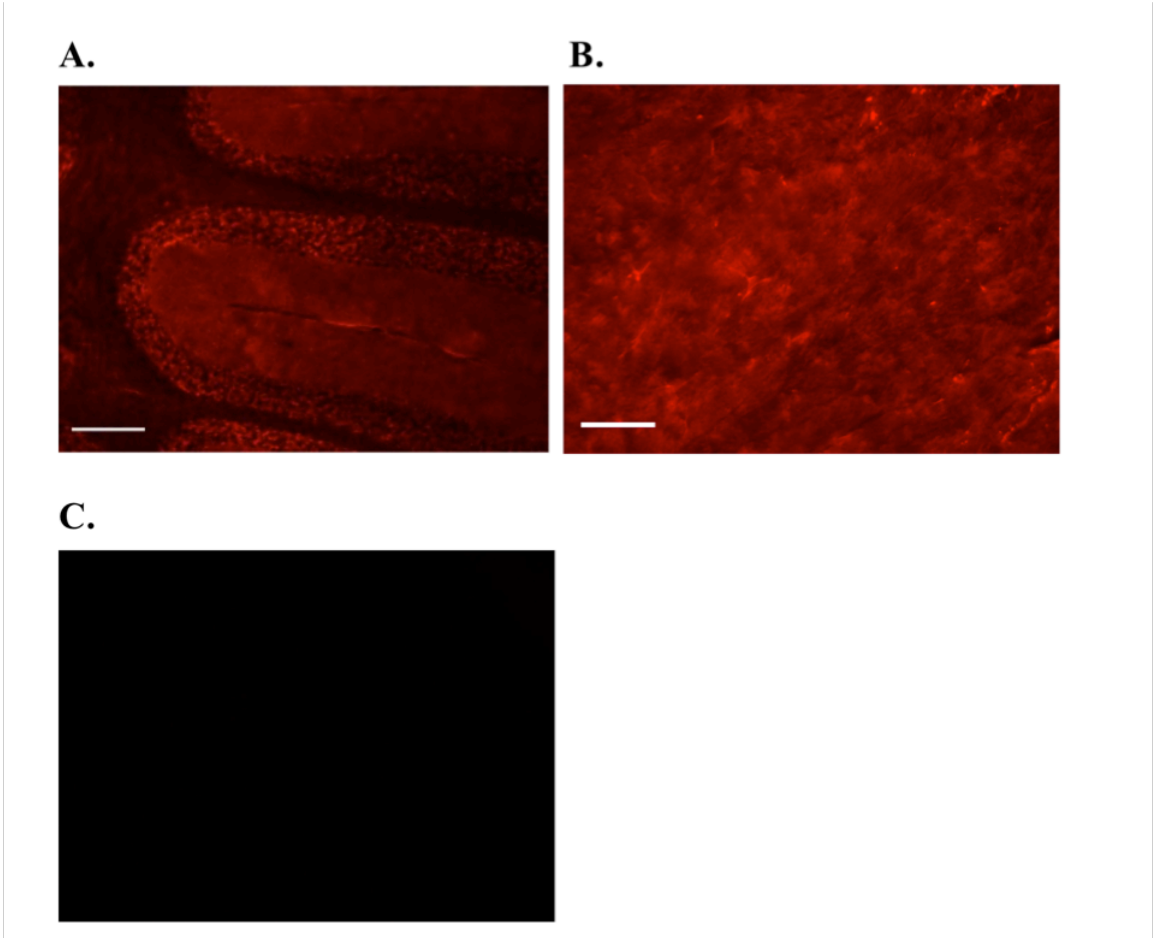

Appendix B. Control Y5R IHC of BALB/c brain. (A. Positive Control) High fluorescence in cerebellum showing high Y5R expression (Scale bars=200µm) **(A. Positive Control)** High punctate fluorescence showing high Y5R expression (Scale bars=50µm) **(C. Negative Control)**

Western

AUP Number: 2014-026
PI Name: Foster, Paula
AUP Title: Mri Analysis Of Mouse Models Of Breast Cancer Brain Metastasis
Approval Date: 10/24/2014

Official Notice of Animal Use Subcommittee (AUS) Approval: Your new Animal Use Protocol (AUP) entitled "Mri Analysis Of Mouse Models Of Breast Cancer Brain Metastasis" has been APPROVED by the Animal Use Subcommittee of the University Council on Animal Care. This approval, although valid for four years, and is subject to annual Protocol Renewal.2014-026::1

1. This AUP number must be indicated when ordering animals for this project.
2. Animals for other projects may not be ordered under this AUP number.
3. Purchases of animals other than through this system must be cleared through the ACVS office. Health certificates will be required.

The holder of this Animal Use Protocol is responsible to ensure that all associated safety components (biosafety, radiation safety, general laboratory safety) comply with institutional safety standards and have received all necessary approvals. Please consult directly with your institutional safety officers.

Submitted by: Copeman, Laura
on behalf of the Animal Use Subcommittee
University Council on Animal Care

The University *of* Western Ontario
Animal Use Subcommittee / University Council on Animal Care
Health Sciences Centre, • London, Ontario • CANADA – N6A 5C1
PH: 519-661-2111 ext. 86768 • FL 519-661-2028
Email: auspc@uwo.ca • http://www.uwo.ca/animal/website/

Appendix C: Research Ethics Approval

Western

AUP Number: 2014-026
PI Name: Foster, Paula
AUP Title: MRI analysis of mouse models of breast cancer brain metastasis

Official Notification of AUS Approval: A MODIFICATION to Animal Use Protocol 2014-026 has been approved.

The holder of this Animal Use Protocol is responsible to ensure that all associated safety components (biosafety, radiation safety, general laboratory safety) comply with institutional safety standards and have received all necessary approvals. Please consult directly with your institutional safety officers.

Submitted by: Kinchlea, Will D
on behalf of the Animal Use Subcommittee

The University *of* Western Ontario
Animal Use Subcommittee / University Council on Animal Care
Health Sciences Centre, ● London, Ontario ● CANADA – N6A 5C1
PH: 519-661-2111 ext. 86768 ● FL 519-661-2028
Email: auspc@uwo.ca ● http://www.uwo.ca/animal/website/

Appendix D: Research Ethics Modification

Curriculum Vitae, Jenna Kara

EDUCATION

09/14-08/16 (expected) **Master's Science: Medical Biophysics (Molecular Imaging)**
University of Western Ontario, London, ON, CAN
Supervisors: Dr. Paula Foster and Dr. Dwayne Jackson
Thesis: *Characterizing the Role of the NPY-Y5R System in Breast Cancer*

09/10-04/14 **Bachelor of Medical Sciences: Honours Specialization Medical Sciences**
University of Western Ontario, London, ON, CAN

SCHOLARSHIPS AND AWARDS

09/15- 08/16 **Translational Breast Cancer Research Unit Studentship funded in part by the Breast Cancer Society of Canada**
London Regional Cancer Program
Amount: $17,000

09/14-08/15 **Translational Breast Cancer Research Unit Studentship funded in part by the Breast Cancer Society of Canada**
London Regional Cancer Program
Amount: $17,000

09/14- present **Western Graduate Research Scholarship**
University of Western Ontario, Medical Biophysics
Amount: $1500 per month

RESEARCH EXPERIENCE

09/14-04/15 **Graduate Research Assistant**
University of Western Ontario, London, ON, CAN
Supervisor: Dr. Paula Foster

PUBLICATIONS

Makela A*, Murrell DH*, Parkins K, Kara J, Gaudet J, Foster PJ. "Cellular Imaging with MRI" Submitted *to Topics in Magnetic Resonance Imaging April 26, 2016.*

TEACHING EXPERIENCE

09/15- 04/16	**Teaching Assistant- Medical Biophysics 3970Z (Biophysics Laboratory)** University of Western Ontario, London, ON
09/14-12/14	**Teaching Assistant- Medical Biophysics 3501F (Biophysics of Transport Systems)** University of Western Ontario, London, ON

REGIONAL CONFERENCES

Kara J, Hrynkiewicz J, Makela A, Foster PJ, Jackson D. Stress-induced Neuropeptide Y-Y5R as a mediating factor breast cancer metastasis. *Robarts Research Retreat 2016*- London, ON, CAN (Abstract Submitted)

Kara J, Hrynkiewicz J, Makela A, Foster PJ, Jackson D. Chronic stress and Neuropeptide Y in breast cancer metastasis. *Research Oncology Day 2016*- London, ON, CAN (Abstract Submitted)

Kara J, Hrynkiewicz J, Makela A, Foster PJ, Jackson D. Characterizing the role of stress and Neuropeptide Y in breast cancer metastasis. *Imaging Network of Ontario Symposium 2016*- Toronto, ON, CAN (Poster)

Kara J, Hrynkiewicz J, Makela A, Foster PJ, Jackson D. Stress and the Neuropeptide Y-Y5R system in breast cancer metastasis and recurrence. *London Health Research Day*- London, ON, CAN (Poster)